STRUCTURAL STUDY OF THE INTERACTION BETWEEN POXVIRUS-ENCODED CC CHEMOKINE INHIBITOR VCCI AND HUMAN MIP-1β

A Dissertation

by

LI ZHANG

Submitted to the Office of Graduate Studies of
Texas A&M University
in partial fulfillment of the requirements for the degree of

DOCTOR OF PHILOSOPHY

May 2008

Major Subject: Biochemistry

STRUCTURAL STUDY OF THE INTERACTION BETWEEN POXVIRUS-ENCODED CC CHEMOKINE INHIBITOR VCCI AND HUMAN MIP-1β

A Dissertation

by

LI ZHANG

Submitted to the Office of Graduate Studies of
Texas A&M University
in partial fulfillment of the requirements for the degree of

DOCTOR OF PHILOSOPHY

Approved by:

Chair of Committee,	Patricia J. LiWang
Committee Members,	Mary Bryk
	C. Nick Pace
	J. Martin Scholtz
Head of Department,	Gregory D. Reinhart

May 2008

Major Subject: Biochemistry

ABSTRACT

Structural Study of the Interaction between Poxvirus-encoded CC Chemokine Inhibitor vCCI and Human MIP-1β.

(May 2008)

LI Zhang, B.S., Sichuan University, Chengdu, China

Chair of Advisory Committee: Dr. Patricia J. LiWang

Chemokines (chemotactic cytokines) comprise a large family of proteins that recruit and activate leukocytes, giving chemokines a major role in both immune response and inflammation-related diseases. Viral CC chemokine inhibitor (vCCI) is a poxvirus encoded protein that has been shown to bind tightly and inhibit the action of many CC chemokines. This function suggests that vCCI could be explored as an anti-inflammatory therapeutic, a possibility that has been supported in mouse studies. The structure of vCCI in unbound form was determined by others, but to date no structure has been reported of bound vCCI. We report the NMR structure of vCCI in complex with the human CC chemokine MIP-1β. The non-aggregating MIP-1β variant MIP-1β ^{45}AASA^{48} was used in this complex to allow sufficiently high concentration at pH 7 to carry out the solution structure determination. A combination of NOE distance restraints, torsion angle restraints, and residual dipolar coupling were used to determine the structure of the complex, which also required protein deuteration due to its relatively large size (34kDa). The structure shows that MIP-1β binds to vCCI with 1:1

stoichiometry, forming a complex of 311 amino acids. vCCI uses residues from its β-sheet II to interact with a surface of MIP-1β that includes residues adjacent to its N-terminus, as well as residues in the 20's region, and the 40's loop. The structure of the MIP-1β:vCCI complex reveals for the first time the regions of each protein involved in the interaction, and allows a greater understanding of the strategy used by vCCI to tightly bind numerous chemokines, while retaining selectivity for the CC chemokine subfamily.

DEDICATION

I dedicate this work to my dear parents. Being deprived of their own chances of pursuing higher education and academic degrees, they have never given up their enthusiastic seeking of self-improvement. It is their examples that I have followed to get where I am. I love you, Mom and Dad.

Sincere gratitude also goes to my advisor Dr. Patricia J. LiWang. Without her guidance and advice, as well as the constant instillation of a true passion about science, none of this would have been possible. It has been a real pleasure, Patti.

ACKNOWLEDGEMENTS

I would like to thank my current and previous committee members, Drs. Mary Bryk, J. Martin Scholtz, C. Nick Pace, and David Giedroc, for their guidance and support throughout the course of this research.

Special thanks for Drs. Andy C. LiWang and Ioannis Vakonakis, for all the things I have learned from them. I also had helpful discussions with Drs. Karl Koshlap, Melissa McCornack, and Xiangming Kong.

Thanks also go to my friends and colleagues and the department faculty and staff for making my time at Texas A&M University a memorable experience. Funding for this work was provided by National Institution of Health Grants AI47832 and AI070993, and Robert A. Welch Foundation Grant A1472.

TABLE OF CONTENTS

Page

ABSTRACT iii

DEDICATION v

ACKNOWLEDGEMENTS vi

TABLE OF CONTENTS vii

LIST OF FIGURES ix

LIST OF TABLES xi

CHAPTER

I INTRODUCTION 1

Chemokines and their receptors 1
Viral CC chemokine inhibitors 10

II FORMATION AND ANALYSIS OF VCCI:MIP-1β COMPLEX AND NMR RESONANCE ASSIGNMENTS 19

Introduction 19
Materials and methods 22
Results 26
Discussion 38

III NMR STRUCTURE OF THE VCCI:MIP-1β COMPLEX 43

Introduction 43
Materials and methods 47
Results 52
Discussion 63

IV FORMATION OF OTHER VCCI:CHEMOKINE COMPLEXES AND PRODUCTION OF VCCI VARIANTS 72

CHAPTER Page

Introduction 72
Materials and methods 73
Results 75
Discussion 77

V SUMMARY AND CONCLUSION 80

REFERENCES 83

APPENDIX A 97

APPENDIX B 119

VITA 156

LIST OF FIGURES

FIGURE		Page
1.1	An overview of the process of leukocytes chemotaxis following a chemokine gradient	4
1.2	An ensemble of several human chemokine structures	6
1.3	Sequence alignment of five members of the orthopox vCCI family	13
1.4	Two views of the X-ray structure of the cowpox encoded CC chemokine binding protein vCCI	15
1.5	The surface representation of MCP-1	17
1.6	Sequence alignment of the human CC chemokines with high affinity towards vCCI	18
2.1	Observation of vCCI:MIP-1β interaction by NMR	28
2.2	Spectral quality comparison between regular and side-chain deuterated samples	30
2.3	Assigned ^{15}N HSQC spectra for both proteins in their liganded form	31
2.4	NMR relaxation studies of ^{15}N MIP-1β bound with ^{14}N vCCI	35
2.5	NMR relaxation studies of ^{15}N vCCI bound with ^{14}N MIP-1β	36
2.6	Chemical shift perturbation mapping of vCCI upon binding to MIP-1β-^{45}AASA^{48}	37
2.7	^{15}N-^{1}H NOE comparison of wild-type MIP-1β, MIP-1β F13A, and vCCI bound MIP-1β ^{45}AASA^{48}	42
3.1	A portion of the ^{15}N-IPAP spectra of labeled vCCI in complex with unlabeled MIP-1β	53
3.2	A portion of the 4-dimensional ^{15}N, ^{13}C-edited NOESY spectrum	55

FIGURE Page

3.3 Solution structure of the vCCI:MIP-1β complex 58

3.4 Three close-up views of the structure of the MIP-1β:vCCI complex 59

3.5 ELISA binding results for the interaction of vCCI with wild-type MIP-1β and MIP-1β-^{45}AASA^{48} 61

3.6 The heparin chromatography result of MIP-1β with vCCI 62

3.7 Conserved pattern observed in the sequences of human CC chemokines with high affinity to vCCI 71

4.1 Superposition of several ^{15}N heteronuclear single quantum correlation spectra of ^{15}N-labeled vCCI in complex with different CC chemokines ... 76

4.2 A diagram illustrating the setup for acquisition of fluorescence anisotropy data 79

LIST OF TABLES

TABLE Page

3.1 NMR and refinement statistics for the vCCI:MIP-1β complex 56

CHAPTER I

INTRODUCTION

Chemokines and their receptors

The proceedings of modern immunology have been revealing more and more of the extraordinary beauty as well as perplexing complexity of the immune system. One key property of the immune system that has been extensively studied in the past two decades is the migration of leukocytes throughout the organism as surveillance against infectious microbes, tissue damage, and sensitizing foreign substances. This process is regulated by a family of proteins called chemokines (Chemotactic cytokines), and their cognate receptors on the surface of leukocytes (*1-4*).

Ever since the discovery of the first chemokine Interleukin 8 (IL-8) in 1987 (*5, 6*), a wealth of information has been obtained about this large family of proteins and their receptors. To date, about 50 chemokines and 20 receptors have been identified and characterized in human (*7, 8*). All the chemokines are 7- to 14-kD polypeptides, and are systematically classified into four subfamilies according to the relative position of the conserved cysteine residues close to the N-termini. The two largest subfamilies are CC chemokines and CXC chemokines. For CC chemokines, the first two cysteine residues

---

This dissertation follows the style of *Biochemistry*.

are contiguous, and the family has at least 24 members such as MCP-1, MIP-1α, MIP-1β and RANTES. The CXC chemokines have an intervening residue between the first two cysteines, with at least 15 members such as IL-8, SDF-1α, and SDF-1β. Two minor subfamilies, namely CX3C and C subfamilies have also been identified. A systematic nomenclature system first developed by A. Zlotnik and O. Yoshie in 1999 was gradually adopted for human chemokines and chemokine receptors (*9-11*). In this system, all the chemokine names are composed of the subfamily type followed by a "L" for "ligand" and a number, such as MIP-1β being CCL4, IL-8 being CXCL8, etc. Similarly, all the chemokine receptors are named as CCR or CXCR etc., with "R" indicating "receptor", and followed by a serial number.

The CC and CXC chemokines are produced by leukocytes as well as several types of tissue cells, including endothelial cells, epithelial cells and fibroblasts. Depending on their function in immunity and inflammation, chemokines can be classified into two groups: homing chemokines and inflammatory chemokines (*7, 12, 13*). The homing chemokines such as CXCL13, CCL19 and CCL21, are expressed constitutively in lymphoid tissues, and are responsible for the physiologic traffic and homing of lymphocytes and dendritic cells inside the lymphoid organs. These chemokines also contribute to the immune system development by regulating the maturation, differentiation, and activation of lymphocytes (*14, 15*). By contrast, secretion of inflammatory chemokines is induced mostly in response to external stimuli.

In the event of injury/microbe infection, pro-inflammatory cytokines such as tumor necrosis factor (TNF) and Interleukin-1 (IL-1) are produced mainly by

mononuclear phagocytes to stimulate the early inflammatory reactions. These cytokines then induce vascular endothelial cells to express adhesion molecules that can facilitate leukocytes to attach to the endothelial surface (*16, 17*), and also stimulate endothelial cells and macrophages to secrete chemokine (*18, 19*). Retention and presentation of secreted chemokines on the endothelial cell surface are then mediated by the relatively low affinity, non-specific binding of chemokines to glycosaminoglycans (GAGs) expressed as proteoglycans on the surface of these cells (*20*). The interaction of chemokines with GAGs is likely to localize and concentrate the chemokines, allowing the formation of a chemokine concentration gradient which disseminates from the infection site. This chemokine gradient can then be detected by chemokine receptors on the surface of leukocytes through the high affinity binding interaction (*12, 21-23*).

Chemokine receptors are seven-transmembrane α-helical domain G-protein coupled receptors (GPCRs). Upon binding by cognate chemokines on the extracellular side, these receptors are activated and undergo conformational changes, consequently activating the coupled G-proteins on the intracellular side to trigger sophisticated signal transduction cascades (*24*). As a result, a variety of cellular enzymes that modulate integrin affinity and cytoskeletal protein configuration are activated, causing leukocyte adhesion to the endothelial surface prior to migration (*25*), and morphological changes due to polymerization and de-polymerization of actin (*26*), allowing leukocytes to migrate across the endothelial layer towards sublumenal chemokines at the infected tissue region -- the process known as chemotaxis (Figure 1.1).

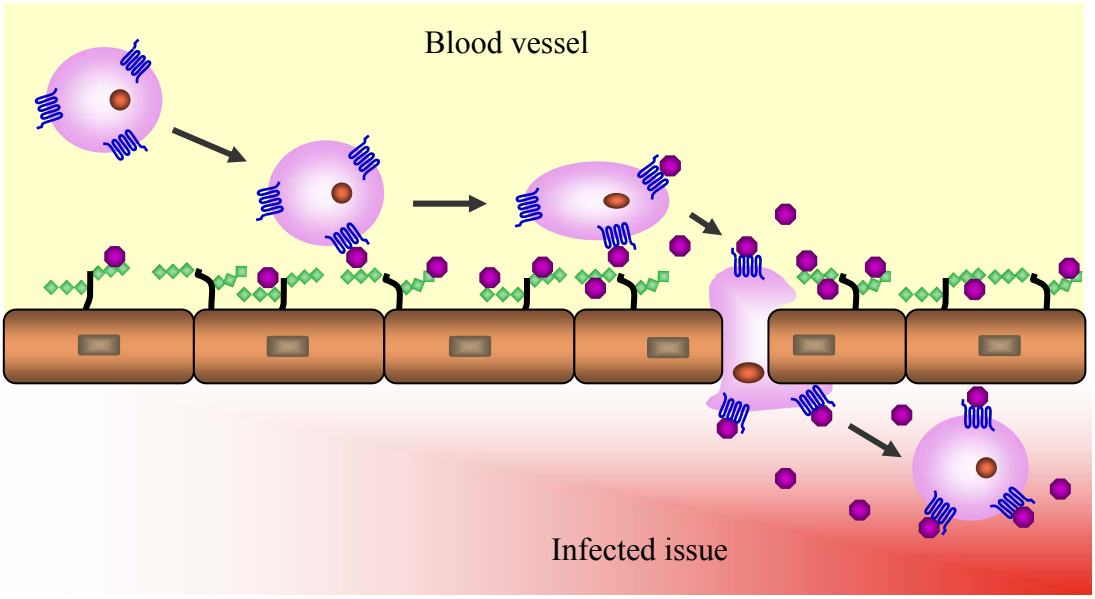

Figure 1.1. An overview of the process of leukocyte chemotaxis following a chemokine gradient. Chemokines (deep purple octagons) are secreted by tissues from the infection region (red area) and form a concentration gradient by binding to glycosaminoglycans (green diamonds) on the endothelium. Leukocytes patrolling in the blood vessel detect the gradient through the high affinity binding of chemokines using seven transmembrane chemokine receptors on the cell surface. The activated leukocytes then adhere to the endothelial surface, and subsequently undergo morphological changes, achieving migration along the endothelium and extravasation into the infected area.

It has been well recognized that chemokines from different subfamilies target different sets of receptors and thus have effects on different subset of leukocytes. For example, CC chemokines mostly activate monocytes, eosinophils, basophils and T cells, while CXC chemokines mainly target neutrophils (*22*). However, things could get rather convoluted when one takes the pleiotropic and redundant nature of chemokines and their receptors into account. It is not uncommon for one chemokine to be able to interact with multiple receptors and *vice versa*, which leads to a rather complicated and fascinating chemokine network system that requires further investigation.

Structures of chemokines from different subfamilies have been solved by NMR and X-ray crystallography (*27-34*). Despite the differences in amino acid composition and functionalities among many chemokines, their structures reveal a remarkably conserved tertiary fold, with an often extended N-terminus, followed by three strands in a Greek key arrangement and a C-terminal alpha-helix (Fig 1.2.). Another noticeable phenomenon is that many chemokine structures indicate self-oligomerization. For example, MCP-1, MIP-1β and IL-8 were solved as homodimers by NMR, and CXCL-4 was shown to be a tetramer by crystallography. The presence of oligomerization in solution has also been confirmed by other biochemical method such as ultracentrifugation, with most oligomer dissociation constants (Kd) determined in the high nanomolar to low micromolar range, such as MIP-1β with Kd of ~0.73 uM (*35*). These findings prompted the question of which form of the chemokine is responsible for the native function. To investigate this matter, monomeric variants and mandatory dimeric variants were tested for their function. In one study, a monomeric variant of the

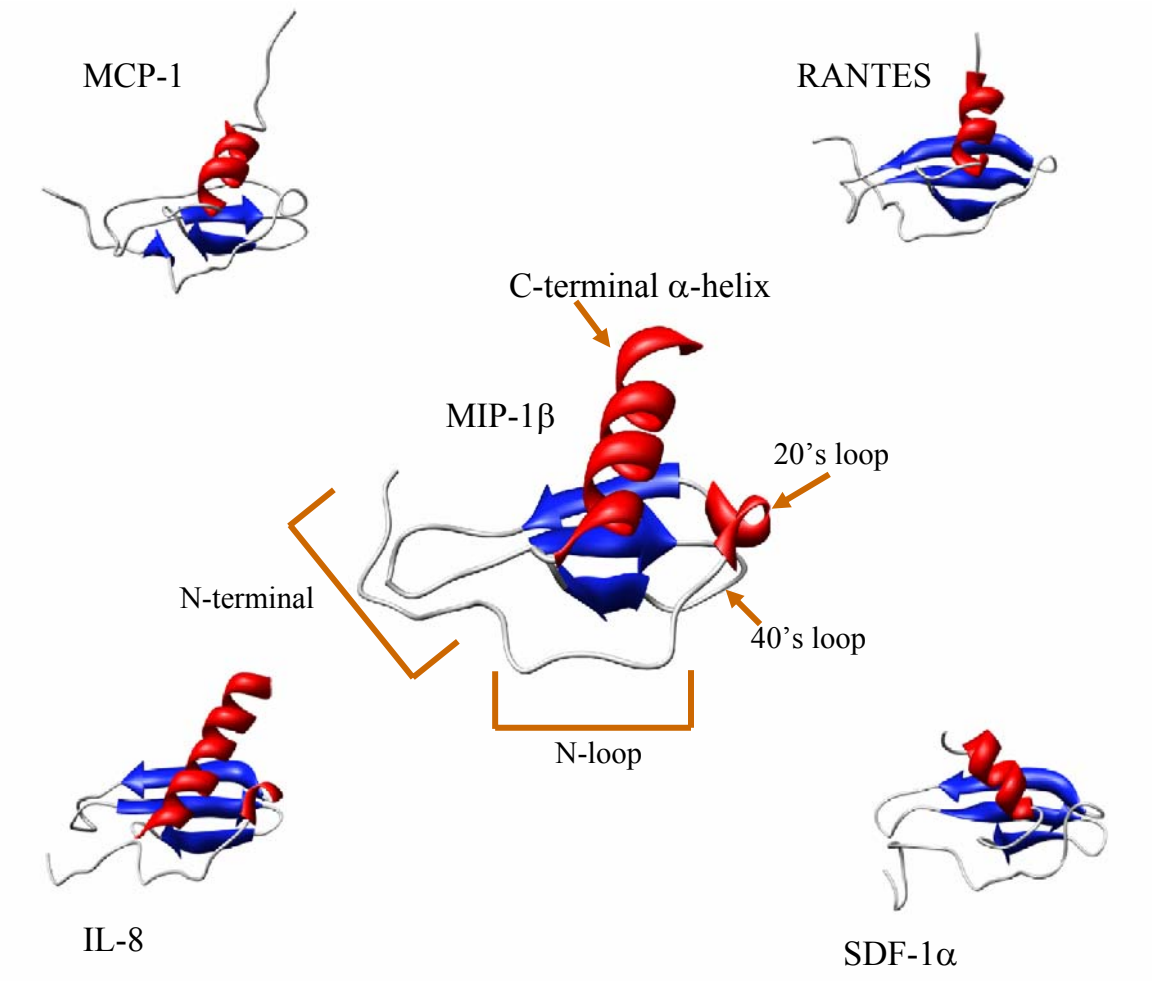

Figure 1.2. An ensemble of several human chemokine structures. Structures included are MCP-1 (PDB code 1DOM), RANTES (PDB code 1RTO), MIP-1β (PDB code 1HUM), IL-8 (PDB code 1IL8) and SDF-1α (PDB code 1SDF). Despite being classified into different subfamilies and exhibiting different functionalities, all these chemokines adopt a very similar tertiary fold, often with an extended N-terminus, followed by three strands in a Greek key arrangement and a C-terminal alpha-helix.

CXC chemokine IL-8 was reported to retain activity on neutrophils *in vitro* (*36*). Similar results were also obtained for CC chemokines using monomeric MCP-1 and MIP-1β (*35, 37*). On the other hand, a trapped dimeric MIP-1β was found to be incapable of binding and activating its receptor (*38*). These results strongly support the model that monomeric chemokines are responsible for binding and activation of cognate receptors.

Thorough understanding of the chemokine-receptor interaction from direct structural information would undoubtedly advance our comprehension of the diversity and specificity displayed by the chemokine network. However, given the fact that all chemokine receptors are large, membrane-bound insoluble proteins, obtaining a structure of any chemokine receptor turns out to be a major obstacle, and not a single chemokine receptor structure has yet been solved to date. To bypass this hurdle, mutagenesis studies in combination with biochemical assays were used to probe this interaction from both the chemokine side and the receptor side. A large number of studies have defined the receptor-binding epitopes on individual chemokines (*39-43*). The N-termini of chemokines were shown to be universally indispensable for receptor activation, with truncation or mutation at this region abolishing the receptor activation ability. In terms of receptor binding ability, while some chemokines tolerate the N-terminal variation well (such as a MIP-1β variant that with the first eight residues removed can still bind the CCR5 receptor with affinity comparable to that of the wild-type protein), some chemokines such as IL-8 showed a significant decrease in receptor binding affinity when several N-terminal residues were removed or mutated (*39, 44*). Residues outside the very N-termini have not been linked to receptor activation. Instead, some residues were

found to be crucial for receptor binding. A good example is that in human MIP-1β, mutating the Phe13 residue to an alanine resulted in a ~1000 fold affinity decrease (*35*).

Much less is known from the receptor side, due to the difficulties of studying large membrane-bound proteins. Several approaches were attempted to gain insight into these mysterious molecules, including creating receptor chimeras, grafting the extracellular loops of a receptor onto a soluble scaffold to obtain a receptor mimic, or using soluble fragments from some receptors to study their interaction with chemokines, or large scale point mutation and truncation on the receptors (*34, 41, 45-57*). However, the picture of chemokine receptors still stays rather vague. Nevertheless, a current model proposes that the N-terminal loops of chemokine receptors are likely to be negatively charged by tyrosine sulfation (*58-60*), and these negative charged residues in combination with other epitopes from the extracellular loops, contribute to the binding of the normally positively charged chemokines. When bound, the chemokine N-termini probably interact with the region inside the receptor transmembrane helical bundle, causing conformational changes that will cause receptor activation and down-stream signal transduction (*57, 61*).

While the monomeric chemokines have been established as the active form that is responsible for receptor binding and activation, the importance of chemokine oligomerization has yet to be studied in detail. It has been demonstrated that for chemokines that naturally oligomerize, their monomeric variants fail to recruit leukocytes *in vivo*, despite having the ability to bind and activate their receptors *in vitro* (*62*). This observation coincides with the finding that chemokines with their GAGs

(glycosaminoglycans) binding ability impaired are also incapable of leukocyte recruitment *in vivo* while maintaining their receptor binding and activation ability *in vitro (62)*. Further investigation found that binding to GAGs helps tighten the chemokine oligomer, and in reverse, oligomerization enhances the GAG binding ability of chemokines (*63*). A model consistent with these observations is that the oligomerization ability helps chemokines to bind to the GAGs better, allowing retention and correct presentation of chemokines on the surface of endothelial cells to form a chemokine gradient which is essential for leukocytes recruitment. The loss of oligomerization ability may impair GAG binding by chemokines thus causing disruption to the formation of chemokine gradient. These findings demonstrate a new level of fine regulation of chemokines in the immune system in which manipulation of quaternary structures achieves the correct spatial and temporal presentation of these proteins, which subsequently affect their function.

The surveillance function of chemokines is crucial for host protection in healthy human beings; however, malfunction of chemokines can cause various diseases and undesired effects by inappropriate inflammation and subsequent tissue damage. Inappropriate expression of multiple chemokines and chemokine receptors has been reported in a large number of inflammation-related tissues, including rheumatoid arthritis, autoimmune lesions in multiple sclerosis, ulcerative colitis and Crohn's disease, lung inflammation in chronic bronchitis, asthma and sarcoidosis, vascular inflammation in arteriosclerosis, and allograft rejection (*7, 64*).

Given the critical role of chemokines in the immune response process, it is natural for pharmaceutical design to choose chemokines as inhibition targets to treat inflammation-related diseases. For example, several anti-chemokine antibodies have been shown to significantly reduce eosinophilia and airway hyperactivity in ovalbumin challenged mice (*65-68*). However, given the extensive list of inflammation-related chemokines, and the highly specific interaction of each individual chemokine antibody to its target chemokine, it is likely that a comprehensive chemokine antibody cocktail mix is needed to achieve satisfactory inflammation inhibition. A better alternative could be the use of a broad spectrum chemokine inhibitor which can target multiple targets at once. The vCCI protein discussed in this dissertation presents a promising candidate for this purpose.

Viral CC chemokine inhibitors

Large DNA viruses such as poxviruses and herpesviruses possess sophisticated machinery to modulate the host immune system (*69-72*). These viruses encode a number of proteins that target the chemotaxis process either by interfering with the high affinity interactions between chemokines and their receptors, or by disrupting the low affinity interactions between chemokines and GAGs. Three major strategies used by these viruses include production of viral chemokine analogs, viral chemokine receptor mimics, and a group of chemokine-binding proteins (CKBPs) that competitively inhibit chemokines from interacting with their cognate receptors and/or GAGs (*72-76*). Among

those, the CKBPs are of most interest, due to the fact that they are soluble, secreted proteins with little or no sequence similarity to any known mammalian proteins, yet are capable of binding to multiple chemokines.

Currently the CKBPs are classified into three families: poxvirus CKBP-I, poxvirus CKBP-II and herpesvirus CKBP-III (*75*). The CKBP-I family includes M-T7 protein expressed by myxoma virus (*77*), showing low affinity interaction with members of CC, CXC and C-chemokines without apparent species restriction. This protein is believed to bind to the GAG-binding domains of chemokines, thus interrupting correct chemokine gradient formation, resulting in reduced inflammatory cell influx. The CKBP-III family includes the M3 protein produced by γ-MHV68 virus, which was found to be able to bind chemokines from all the four chemokine subfamilies, this time with very high affinity in the nanomolar range (*78, 79*). This protein was found not to mask the GAG-binding sites on the chemokines; instead, it occludes the high affinity receptor binding regions on chemokines to block receptor binding and signaling (*80*).

The CKBP-II family consists of viral encoded proteins from myxoma virus, ectromelia virus and several poxviruses (*81-89*). These proteins share one attribute in that they preferentially bind to some chemokines from the CC subfamily with very high affinity, and show little or no affinity for chemokines from other subfamilies (*81, 90*). One CKBP-II protein that is of special interest of this dissertation is the poxviruses encoded 26 kDa secreted soluble protein called vCCI. Being presumed as one of the virulence factors from poxvirus since the early 1990's (*88*), the function of this protein was unveiled in 1997 by Craig A. Smith and co-workers (*85*). These researchers used an

epitope-tagged soluble form of vCCI from variola virus (the causative agent of human small pox) and cowpox virus, and discovered that this protein promiscuously binds multiple CC chemokines with high affinity, resulting in complete inhibition of the proinflammatory activity of these chemokines. Later, an extensive binding study with vaccinia vCCI using more than 80 chemokines from several organisms revealed 26 CC chemokines that bind with high affinity, including 13 human chemokines such as MCP-1, MIP-1α, MIP-1β and RANTES (*90*). To date homologs of this protein have been identified in leporipoxvirus and orthopoxvirus strains such as cowpox, rabbitpox, raccoonpox, vaccina and variola pox, and were named vCCI for viral CC Chemokine Inhibitor. Sequence alignment reveals that vCCIs from different origins share at least 80% sequence identity, with some pairwise comparisons showing as much as 99% identity, indicating highly conserved characteristics in structure and function (Figure 1.3).

The ability of vCCI to selectively bind many CC chemokines is a valuable property to be explored. Thorough understanding of the structural foundation which allows vCCI to bind so many chemokines can lead to promising therapeutic design to block a broad range of inflammation-related diseases, such as allergic asthma and rheumatoid arthritis. Several *in vivo* studies have indeed shown supportive results in this regard. One study using a guinea pig model showed that vCCI could prevent inflammation caused by eosinophil accumulation in animals challenged with the CC chemokine Eotaxin (*86*). In a mouse model of allergic asthma, intra-nasally injected

Figure 1.3. Sequence alignment of five members of the orthopox vCCI family. Alignments were made by using ClustalW. RPV, rabbit poxvirus; VAR, variola virus; VVL, vaccinia virus Lister strain; VVC, vaccinia virus Copenhagen strain; CPV, cowpox virus. Conserved residues are highlighted in yellow. Secondary structure elements obtained from cowpox vCCI (PDB code 1CQ3) were labeled above the alignment.

vCCI-Fc fusion protein was shown to significantly reduce the local inflammatory effect and allergic airway hyperreactivity of ovalbumin-challenged mice (*87*).

In 1999 the structure of vCCI from cowpox was solved by X-ray crystallography and revealed a unique β-sandwich fold (Figure 1.4) with no topology similarity to any known mammalian receptors (*91*). The β-sandwich consists of a seven-stranded antiparallel β-sheet I oriented parallel to a five-stranded β-sheet II. There are also a couple of α-helices and several long loops connecting these elements of secondary structure. While β-sheet I was shown to be effectively shielded from solvent by two extended loops, β-sheet II is quite accessible. β-sheet II also contains a patch of conserved acidic residues without obvious structural importance. The analysis of the structure led the researchers to hypothesize that vCCI binds chemokines using its more accessible β-sheet II; also, given the fact that most chemokines are basic proteins and positively charged at neutral pH, those conserved negatively charged residues displayed on the surface of β-sheet II, such as Glu46, Asp49 and Glu125, are given special attention as potential binding residues.

Given the importance of understanding the interaction between vCCI and its chemokine partners, considerable effort has been made to study the binding interaction by a range of techniques (*90, 92, 93*). However, there has been no report about structure determination of vCCI in complex with any chemokine, or the information about which amino acid residues were used by vCCI to interact with chemokines. Instead, several groups approached this problem from another angle by using chemokines and chemokine variants to gain insight into the specific interaction used by these proteins in

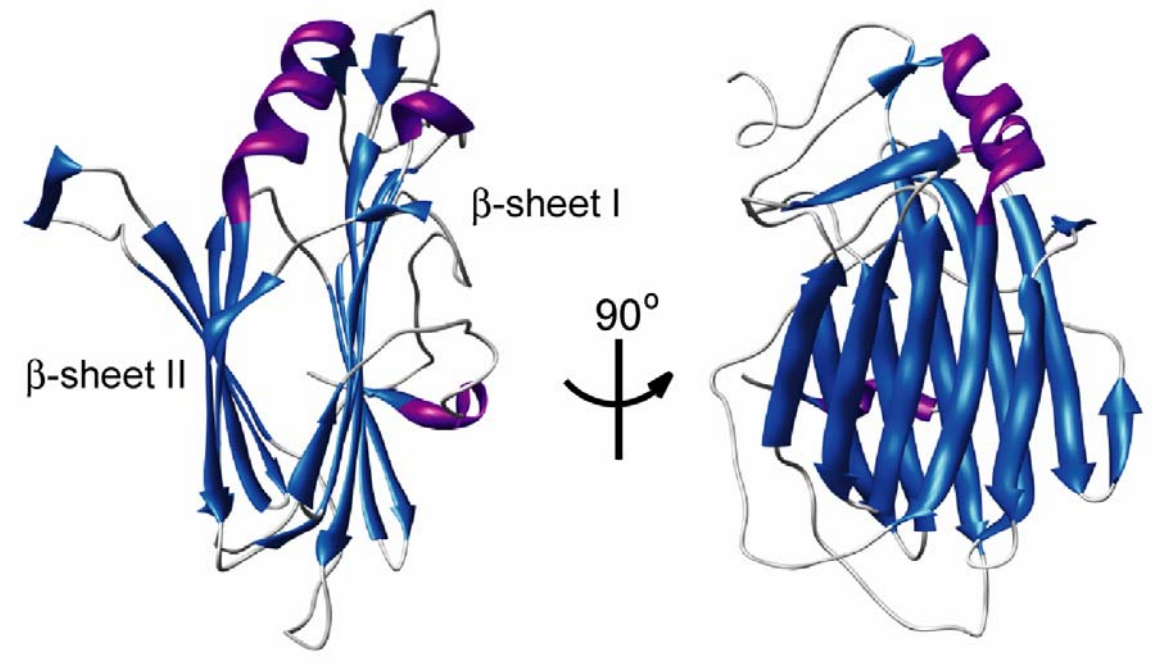

Figure 1.4. Two views of the X-ray structure of the cowpox encoded CC chemokine binding protein vCCI (PDB code 1CQ3). The structure reveals a unique β-sandwich tertiary fold of vCCI. The β-sheet II in this structure is noticed to be largely exposed to solvent, likely confers a chemokine binding surface.

complex formation with vCCI. Recently, more than 60 mutants of the CC chemokine MCP-1 have been tested for their ability to bind vCCI by both enzyme-linked immunosorbent assay (ELISA) and surface plasmon resonance (*92*, *93*). These studies indicate that MCP-1 residues Tyr13, Arg18, and Arg24 are very important in the binding interaction, since mutations on these residues caused a significant affinity decrease; a moderate affinity decrease was also observed upon changes at Lys19 and Lys38 (Figure 1.5). Combined with previous studies on residues used by MCP-1 to bind to the receptor CCR2b, these results suggest that vCCI inhibits MCP-1 activity by at least partially masking its CCR2b binding site. Also, given the relatively high conservation of residue types at these positions for CC chemokines (Figure 1.6), positioning of these residues on chemokine surfaces may outline a general vCCI binding site.

This dissertation presents the first structure-based study of vCCI in complex with a human CC chemokine. Chapter II of this dissertation addresses the production of the complex formed by recombinant rabbitpox vCCI and a variant of human CC chemokine MIP-1β, and NMR resonance assignments for both proteins in their bound conformation. Chapter III describes the solution structure determination of this vCCI:MIP-1β complex, and analysis of the basis for the selective binding of vCCI towards multiple CC chemokines. Chapter IV describes the formation of protein complexes by vCCI with several other chemokines, and also the production of several vCCI variants.

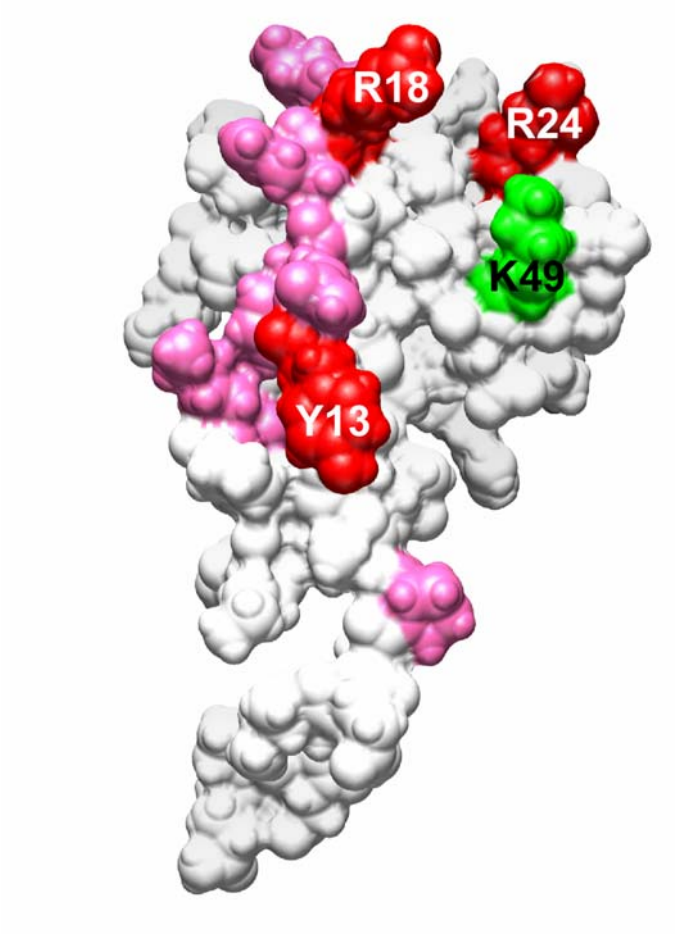

Figure 1.5. The surface representation of MCP-1. The color labeled residues are those have been implicated by mutation studies to be important in binding vCCI (Red, mutation strongly impairs binding; pink, mutation moderately impairs binding; green, mutation to Ala improves binding).

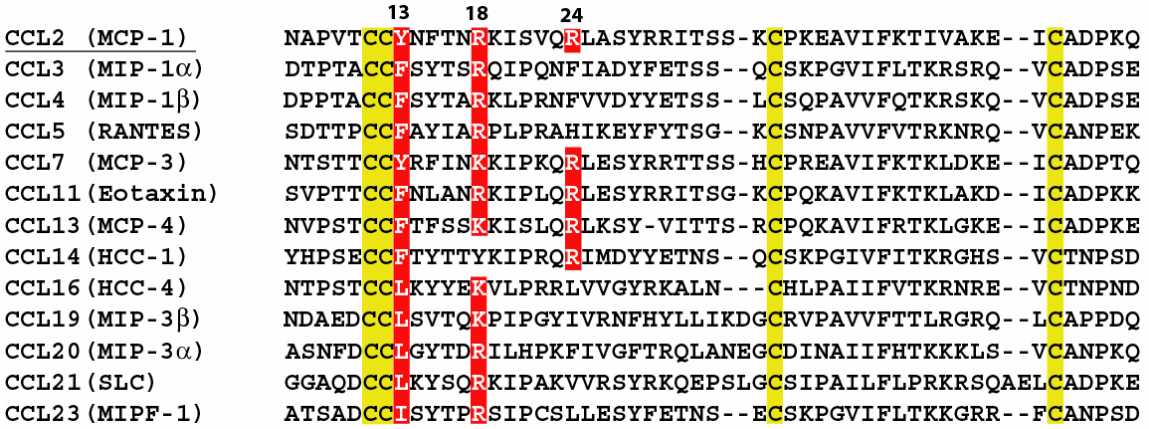

Figure 1.6. Sequence alignment of the human CC chemokines with high affinity towards vCCI. Conserved cysteine residues are highlighted in yellow. Positions highlighted with red indicate residues that likely confer high-affinity binding to vCCI. The numbering is according to the MCP-1 sequence.

CHAPTER II

FORMATION AND ANALYSIS OF VCCI:MIP-1β COMPLEX AND NMR RESONANCE ASSIGNMENTS

Introduction

Chemokines (Chemotactic cytokines) play critical roles in the immune system, causing chemotaxis of a variety of cells to sites of infection and inflammation, as well as mediating cell homing and immune system development (*7*). To date, about 50 chemokines have been identified, and these small proteins (7-14 kDa) are believed to function by binding with endothelial or matrix glycosaminoglycans (GAGs) to form a concentration gradient that is then sensed by high affinity, 7-transmembrane domain G-protein coupled chemokine receptors on the surface of immune cells, leading to activation and chemotaxis. The chemokine system is critical for host defense in healthy individuals, but can also lead to diseases including asthma, arthritis, and atherosclerosis in the case of malfunction, often due to inappropriate inflammation and subsequent tissue damage (*8*). There are four subfamilies of chemokines, CC, CXC, C, and CX_3C, named for the position of conserved N-terminal cysteine residues. Members of the same subfamily often have overlapping receptor binding and cell activation ability while different subfamilies tend to function on different cell subsets (*7*).

Structures of chemokines from different subfamilies have been solved by NMR and X-ray crystallography (*27-34*). Despite the differences in amino acid composition

and functionalities, most chemokines share a remarkably conserved tertiary structure, with an extended N-terminus, followed by three β strands in a Greek key arrangement and a C-terminal α-helix. The solution structure of the human CC chemokine MIP-1β revealed a homodimer (*27*), and subsequently the dimer dissociation constant was determined to be ~0.73 μM (*35*). Dimerization and even oligomerization of many other chemokines have been observed under *in vitro* conditions, and the ability to form quaternary structure is necessary for some chemokines to function *in vivo* (*62*).

Given the importance of understanding the interaction between chemokines and their binding partners, considerable effort has been made to study the binding of chemokines to both glycosaminoglycans (GAGs) and chemokine receptors by a range of techniques (*12, 94*). However, structure determinations of chemokines in complex with any biological molecule are rare and include only a chemokine:GAG complex (*95*), a chemokine:protein complex (*80*) and a chemokine:receptor fragment peptide complex (*54*).

All known pox and herpes viruses encode proteins that interfere with the host chemokine network, likely as part of a strategy to manipulate and subvert the immune system (*76*). Such virally encoded proteins include chemokine mimics, chemokine receptor analogs and a group of secreted, soluble chemokine binding proteins (CKBPs) which exhibit little similarity to any mammalian protein (*75*). CKBPs competitively bind to chemokines and disrupt chemokine interactions with the host cell surface receptors or GAGs. Although some CKBPs interact with a very broad spectrum of chemokines across several chemokine subfamilies, the vCCI proteins (viral CC

chemokine inhibitor, previously called T1/35 kDa, also classified as type II CKBPs) produced by leporipoxviruses and orthopoxviruses bind selectively to members of the CC subfamily (*75, 82*). vCCI proteins have been shown to be potent inhibitors of chemokine action *in vitro* and effective anti-inflammatory agents *in vivo* (*82, 87*). Sequence alignment of vCCI proteins from five orthopoxvirus members including rabbitpox, cowpox, vaccinia-Lister, vaccinia-Copenhagen and variola poxvirus (the causative agent of human smallpox) shows at least 80% identity, with some pairwise comparisons showing as much as 99% sequence identity, indicating that they have essentially identical structures, and very likely share characteristics of chemokine binding. The X-ray crystal structure of unliganded cowpox vCCI by Carfi *et al.* revealed a unique β-sandwich structure with no topological resemblance to any mammalian receptors (*91*). While β-sheet I in this sandwich has two extended loops that effectively shield it from solvent, β-sheet II is exposed to solvent, and was hypothesized by these authors to include a chemokine binding surface.

Here, we report the formation of a complex between rabbitpox-encoded vCCI and a non-aggregating variant of the human CC chemokine MIP-1β, and biochemical and biophysical analyses of this protein complex. Due to the relatively large size of vCCI (26 kDa) for NMR study, sidechain deuteration was used for better spectral resolution. Like many other CC chemokines, MIP-1β prefers acidic conditions *in vitro* and aggregates near pH 7 at concentrations required for NMR experiments. Therefore, a non-aggregating human MIP-1β variant in which three positively charged amino acid residues in the so-called 40's loop (^{45}KRSK^{48}) were replaced by Ala was chosen for the

current study. The resulting protein, MIP-1β-^{45}AASA^{48}, has been found to be soluble at neutral pH while maintaining most spectral and functional characteristics of the wild-type protein with the exception of loss of GAG binding ability (*96*). (For the purpose of simplicity when discussing the complex, MIP-1β-^{45}AASA^{48} will hereafter be referred to as MIP-1β.)

Materials and methods

Sample Preparation. The gene encoding the human MIP-1β non-aggregating mutant K45A/R46A/K48A (MIP-1β ^{45}AASA^{48}) was subcloned into a modified (with the Thioredoxin fusion protein gene removed) pET-32 Xa/LIC vector. The resulting plasmid was then transformed into BL21-(DE3) *E. coli* cells. For NMR sample preparation, bacteria were grown at 37°C in Luria broth medium for unlabeled protein, or in M9 minimal medium containing $^{15}NH_4Cl$ as the sole nitrogen source, and $^{13}C_6$-glucose or $^{12}C_6$-glucose as the only carbon source for labeled protein. Addition of IPTG to 1 mM induced over-production of the protein into inclusion bodies. Cells were harvested by centrifugation after 4~6 hours of induction. Pelleted cells containing MIP-1β ^{45}AASA^{48} were then resuspended in aqueous 20 mM Tris-HCl at pH 8.0 with 500 mM NaCl. Benzamidine was added to a final concentration of ~1 mg/ml to inhibit protease activity. Cell suspensions were passed twice through a French Press cell at 17,000 psi. The lysate was centrifuged at 20,000 × g at 4°C for 45 minutes. The pellet fraction containing the tagged protein was re-dissolved in aqueous 50 mM Tris-HCl at

pH 7.0 with 7 M Guanidine-HCl, 50 mM NaCl, 3 mM EDTA and 10 mM 2-mercaptoethanol. For thorough dissolving, material was allowed to stand at room temperature for 2 hours with constant agitation, and then centrifuged at 20,000 × g at 4°C for 60 minutes. The supernatant fraction containing MIP-1β was added drop-wise into aqueous 50 mM Tris-HCl pH 8.0, 50 mM NaCl, and 5 mM 2-mercaptoethanol with gentle stirring for a 10-fold quick dilution of Guanidine-HCl, so that the unfolded protein can refold. The solution was allowed to stand at room temperature for 4 hours before centrifuging at 16,000 × g at 4°C for 30 minutes. The supernatant fraction was subsequently dialyzed twice against 20 mM Tris-HCl at pH 8.0 with 50 mM NaCl, and then centrifuged at 16,000 × g at 4°C for 30 minutes to remove any precipitated material. The clarified supernatant containing tagged MIP-1β ^{45}AASA^{48} was then prepared for reverse-phase chromatography by addition of trifluoroacetic acid to adjust the pH to about 2, and acetonitrile to a final concentration of 10% (v/v). The sample was loaded onto a C4 reverse-phase column and eluted by an acetonitrile gradient. The fractions that contain the tagged protein were confirmed by sodium dodecyl sulfate polyacrylamide gel electrophoresis (SDS-PAGE) and pooled together. These fractions were lyophilized to remove the solvents for the following enzymatic cutting reaction. The lyophilized protein was then dissolved into sterile Factor Xa protease cleavage buffer containing 50 mM Tris-HCl at pH 8.0, 100 mM NaCl, 5 mM $CaCl_2$. The progress of cleavage was monitored by SDS-PAGE to make sure complete removal of the fusion tag was achieved. After Factor Xa cleavage, the tag-free MIP-1β ^{45}AASA^{48} was purified by reverse-phase chromatography again, quantified using its extinction coefficient at 280

nm, and lyophilized for storage. Unlabeled, ^{15}N-labeled, $^{13}C/^{14}N$-labeled and $^{13}C/^{15}N$-labeled MIP-1β ^{45}AASA^{48} were produced and purified following this protocol.

The gene encoding rabbit poxvirus vCCI was provided by Professor Richard Moyer of University of Florida. The DNA was subcloned into the pPIC9K plasmid, then transformed into *Pichia pastoris* strain SMD1168 following the manufacturer's manual (Multi-Copy *Pichia* Expression kit, Invitrogen, Carlsbad, CA). Unlabeled, ^{15}N-labeled, $^{2}H/^{15}N$-labeled and $^{2}H/^{13}C/^{15}N$-labeled protein samples were prepared by growing cells at 28°C in buffered minimal glucose media for initial biomass accumulation, then shifting cells into buffered minimal methanol media with ^{15}N (or ^{14}N for unlabeled) ammonium sulfate and ^{13}C (or ^{12}C for unlabeled) methanol as the sole nitrogen and carbon sources for induction. For deuterated samples, the media were prepared with 95% (final concentration) D_2O. Throughout the induction stage, methanol was supplied to ~0.4% (v/v) to maintain induction. The production of vCCI was monitored by sampling the medium supernatant containing the secreted vCCI for SDS-PAGE. After satisfactory expression level was achieved (normally after 48-72 hours of induction), the medium supernatant was harvested by centrifugation and sterile filtration to remove yeast cells. The supernatant was slowly diluted with H_2O by two-fold to reduce its conductivity, and then purified by anion exchange chromatography. The fractions that contain vCCI were concentrated using the Amicon concentrators (Millipore, Billerica, Massachusetts), and then further purified by size exclusion chromatography. To fully exchange amide protons in the deuterated samples, the $^{2}H/^{13}C/^{15}N$-labeled vCCI protein was partially unfolded in H_2O-based buffer with 2 M urea at 30°C for 2 hours, followed by a 10-fold

quick dilution. After allowing the protein to fully refold, the protein was exchanged into the final NMR buffer.

It was discovered that the easiest way to form the vCCI:MIP-1β complex with accurate quantification and well controlled sample condition is to quantify both proteins according to their extinction coefficient values, then use the vCCI solution in the final NMR buffer to directly dissolve the lyophilized MIP-1β protein powder. The samples were then re-checked for pH value. Normally a small amount of the unlabeled protein was added to assure fully saturation of the labeled protein. In the circumstance where strict 1:1 ratio of both proteins is required, extra amount of MIP-1β was added and the protein complex was purified by size exclusion chromatography. The final NMR samples contained 0.5-2.0 mM protein(s) (concentration determined in monomeric subunits) in 93% H_2O/7% D_2O containing 100 mM NaCl, 20 mM sodium phosphate pH 7.0, 0.1 mM DSS, 0.01% sodium azide, and Complete Protease Inhibitor (Roche Applied Science, Indianapolis, IN).

NMR Spectroscopy. To obtain the backbone and sidechain assignments for the bound form of MIP-1β, samples containing $^{13}C/^{15}N$-labeled MIP-1β bound with unlabeled vCCI were used for ^{13}C-HSQC, CBCANH, CBCA(CO)NH, HBHA(CO)NH and HCCH-COSY experiments (*97*). For vCCI, the suite of experiments HNCA, HN(CO)CA, HNCACB, HN(CO)CACB, and HNCO were performed on the bound and free $^{2}H/^{15}N/^{13}C$-labeled vCCI to obtain backbone and C^{β} assignments (*98*). Spectra were recorded at 37 °C on Varian Inova 600, 750 and 800 spectrometers. NMR data were

processed using NMRPipe (*99*) and analyzed with PIPP (*100*) and SPARKY version 3.110 (Goddard & Kneller, University of California, San Francisco). Proton chemical shifts were directly referenced to the methyl resonance of DSS, while the carbon and nitrogen chemical shifts were referenced indirectly (*101*).

For chemical shift perturbation mapping, the observed chemical shift change ($\Delta\delta_{obs}$) for each backbone amide between bound and free vCCI was measured as the weighted average of the proton and nitrogen chemical shift changes using the equation $\Delta\delta_{obs} = [(\Delta\delta^2_{HN} + \Delta\delta^2_{N}/25)/2]^{1/2}$ (*102*).

^{15}N T_1, T_2 and ^{15}N-H^N NOE values were measured for both components of the complex following similar procedures as previously described (*103*). Data were excluded from the correlation time calculation if the corresponding ^{15}N-H^N NOE was lower than 0.65, or if either T_1 or T_2 differed from the average value by more than one standard deviation.

Results

The first hurdle in this project is to obtain folded, soluble proteins. For MIP-1β, an unfolding-refolding protocol was successfully applied to produce this protein. In contrast, vCCI posed a greater challenge, as expression of vCCI using bacteria only produced unfolded protein. And possibly due to the relatively large size of this protein, refolding attempts turned out to be fruitless. For NMR studies, the bacterial production of proteins is mostly preferred, both for the large quantity that can be obtained, and the

isotopic labeling methods which are well-established for bacteria but currently unavailable for insect or mammalian cell lines. Eventually, successful production of folded vCCI was accomplished using the yeast *Pichia pastoris* with high yield (normally 30~50 mg/Liter), and different isotopic labeling schemes were applied to obtain a variety of samples.

Formation of protein:protein complex was demonstrated by the ^{15}N heteronuclear single quantum correlation (HSQC) spectra. This type of spectrum shows a peak for each directly bonded N-H pair, and as such provides the fingerprint of a protein. Addition of unlabeled MIP-1β into ^{15}N-labeled vCCI caused noticeable changes in the spectrum, indicating interaction between these two proteins (Figure 2.1). Upon titration of ^{15}N-labeled vCCI with ^{14}N MIP-1β, two sets of vCCI peaks in the ^{15}N HSQC spectra were evident when less than one equivalent of MIP-1β subunits was added, indicating slow exchange between two conformations on an NMR timescale. The spectrum resolved into only one peak per vCCI ^{15}N-^{1}H resonance after addition of one full equivalent of MIP-1β subunits, with additional amounts of MIP-1β causing no further spectral change, consistent with a 1:1 ratio of proteins in the complex. More drastic spectral changes were observed when adding unlabeled vCCI into ^{15}N-labeled MIP-1β (Figure 2.1), clearly indicating interaction between these two proteins, as well as the effect of breaking of the MIP-1β dimer by vCCI.

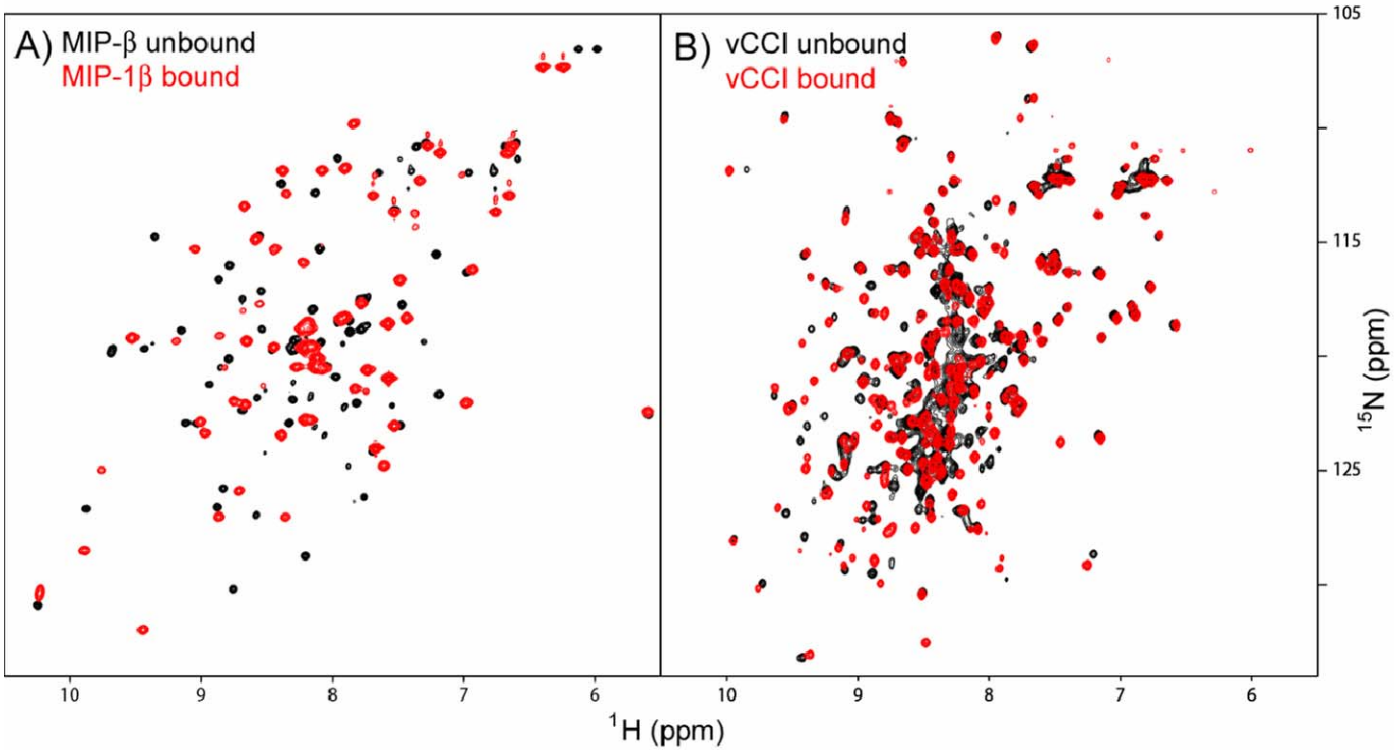

Figure 2.1. Observation of vCCI:MIP-1β interaction by NMR. (A) Overlay of the ^{15}N heteronuclear single quantum correlation (HSQC) spectra of unbound (black) and bound (red) ^{15}N-labeled MIP-1β-^{45}AASA^{48} (in these spectra vCCI is not isotopically labeled and so not visible). (B**)** Overlay of the ^{15}N HSQC spectra of unbound (black) and bound (red) ^{15}N-labeled vCCI (in these spectra MIP-1β is unlabeled so not visible). All spectra were collected at 310K, pH 7.

Larger proteins have more crowded spectra because they contain more amino acid residues, and have lower signal-to-noise ratio due to their faster relaxation rates. The combination of these facts gives rise to the difficulty of studying larger proteins effectively by NMR. Deuteration techniques have been developed in the last several years to overcome this hurdle (*104*). It has been demonstrated that deuteration of a protein larger than 20 kDa can significantly improve the relaxation properties of the remaining subset of protons for NMR experiments. In this study, vCCI contains 242 amino acid residues, with its spectra being not only crowded but also quite heterogeneous in terms of peak intensity (likely caused by the conformationally flexible residues in this protein). Indeed, attempts following traditional protocols by using regular samples allowed only ~50% of the peaks to be unambiguously assigned, which necessitated the use of side-chain deuteration. With the vCCI side-chains being uniformly deuterated and the amide protons recovered using partial unfolding exchange technique, the vCCI spectral resolution was significantly improved by providing greater signal-to-noise ratio, as well as narrower linewidths (Figure 2.2). These improvements made possible the high percentage resonance assignments for vCCI in both free and liganded forms.

For investigation of proteins by NMR methods, sequence specific resonance assignment is the first step, in which NMR data from several different spectra are used to identify the chemical shift value of each $^{1}H^{N}$, ^{15}N, $^{13}C\alpha$, $^{13}C\beta$, ^{13}CO and sidechain atoms in both proteins. The complete assignment results were reported elsewhere (*105, 106*). The assigned ^{15}N HSQC spectra of both proteins in liganded form are shown in Fig 2.3.

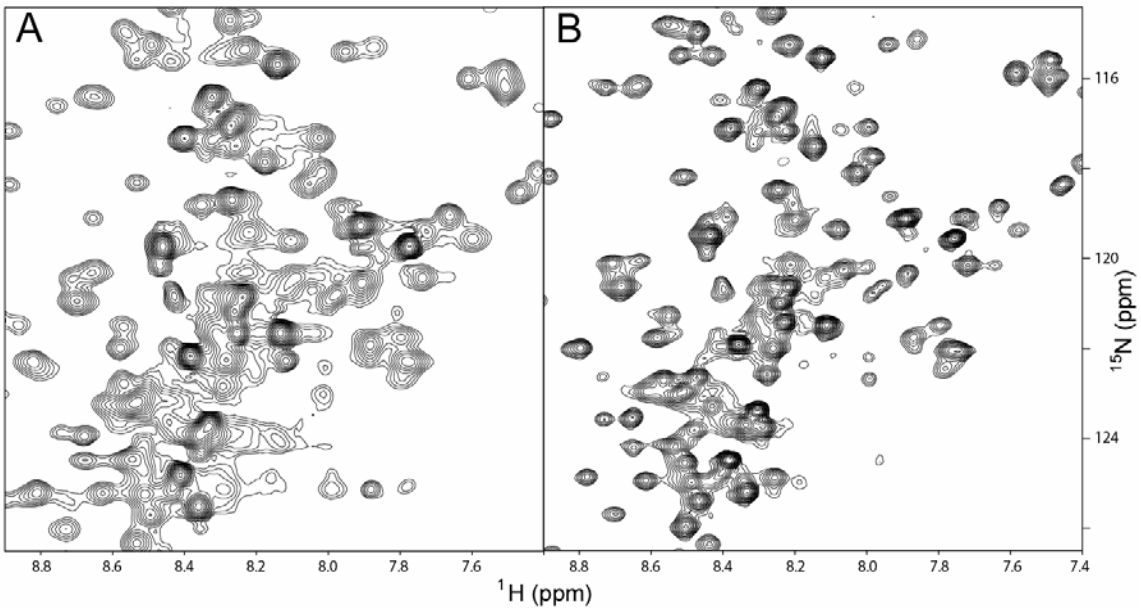

Figure 2.2. Spectral quality comparison between regular and side-chain deuterated samples. (A) Selected section of ^{15}N heteronuclear single quantum correlation (HSQC) spectrum of ^{13}C/^{15}N-labeled vCCI. (B) Corresponding spectrum of uniformly side-chain deuterated ^{2}H/^{13}C/^{15}N-labeled vCCI. The latter spectrum shows significantly improved signal-to-noise ratio, and sharper peaks due to narrower linewidths.

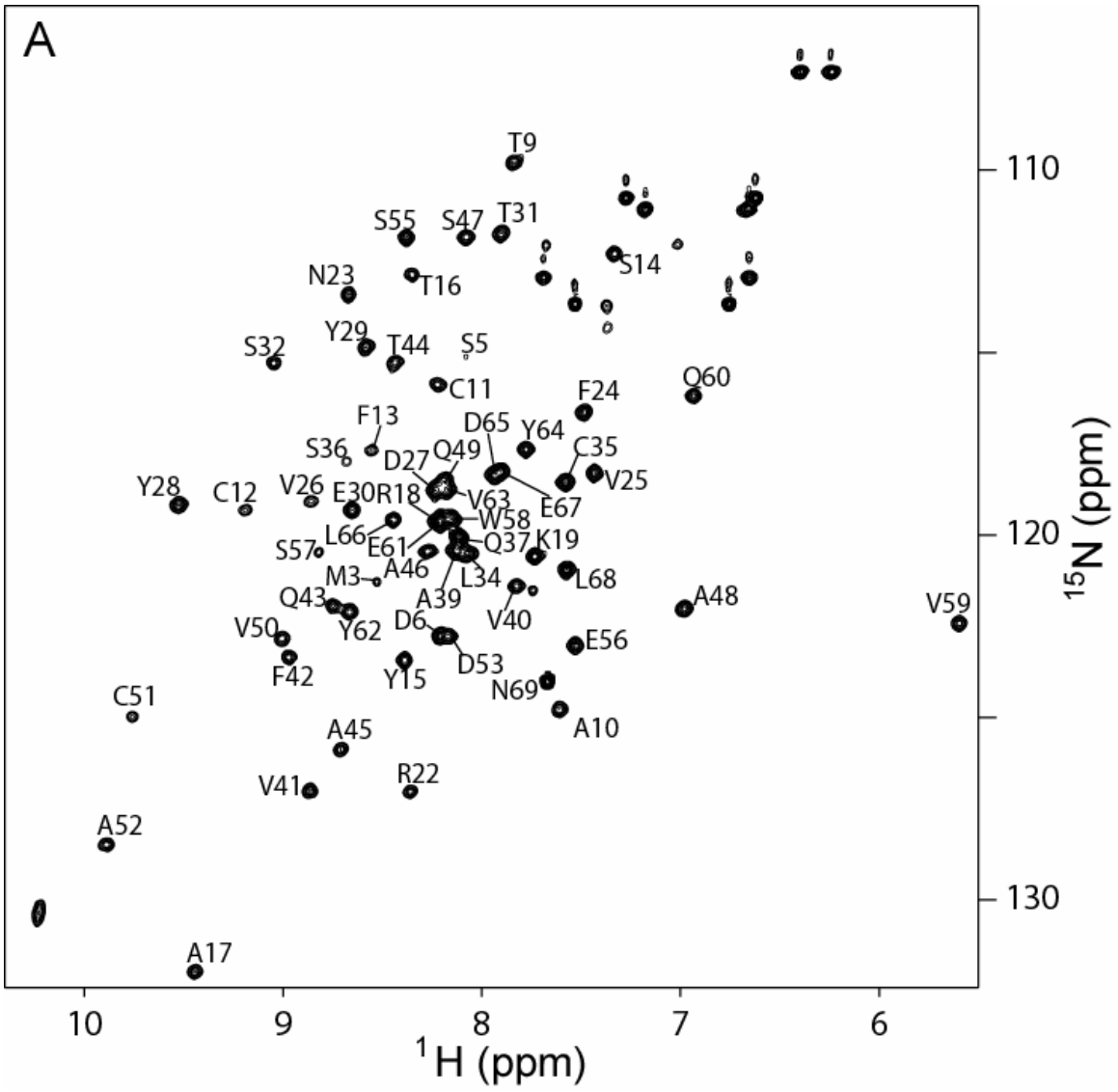

Figure 2.3. Assigned ^{15}N HSQC spectra for both proteins in their liganded form. (A) The MIP-1β ^{45}AASA^{48} spectrum. (B) The vCCI spectrum. (C) The close-up of the crowded central region of the same spectrum as in (B).

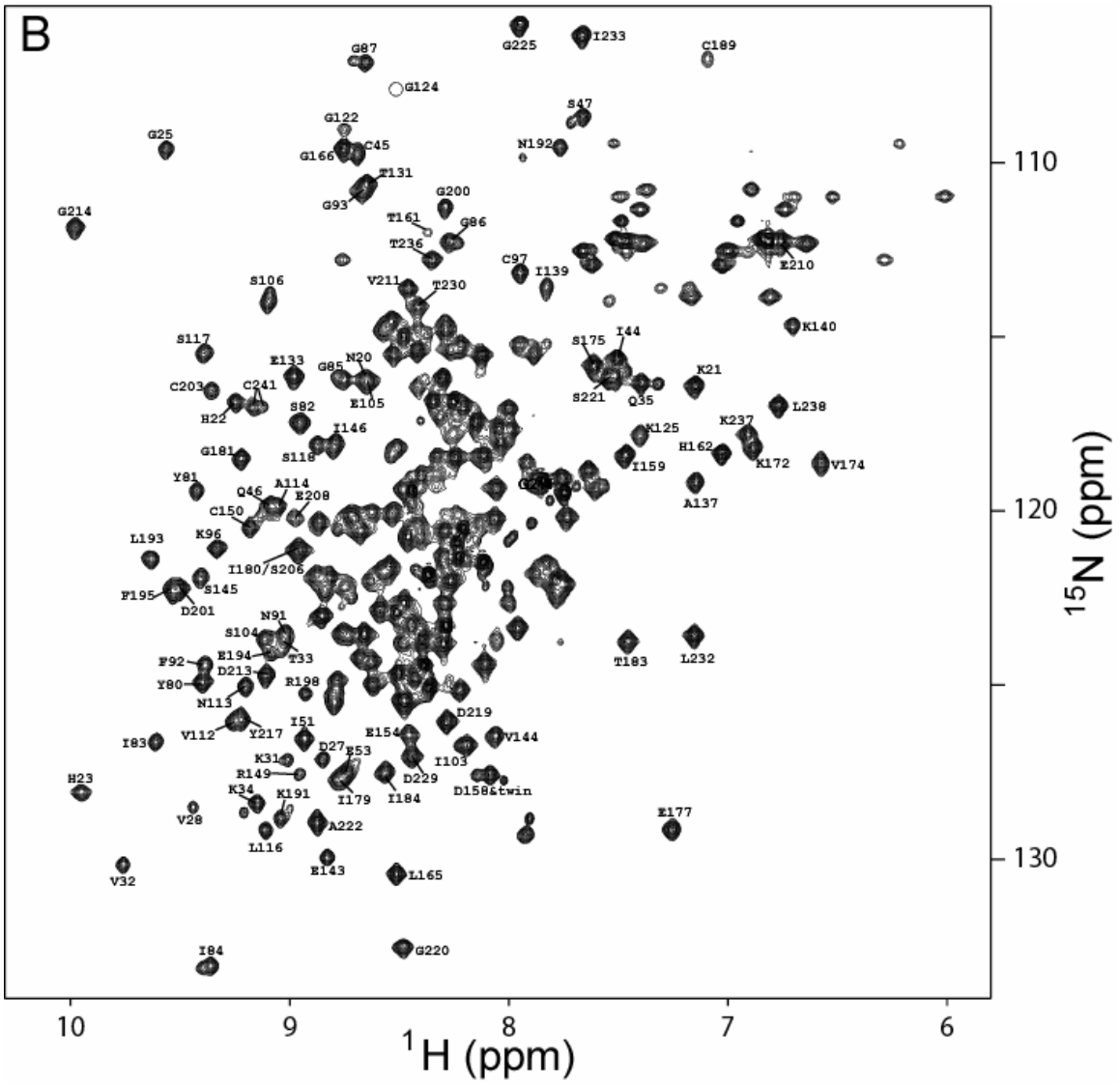

Figure 2.3. Continued

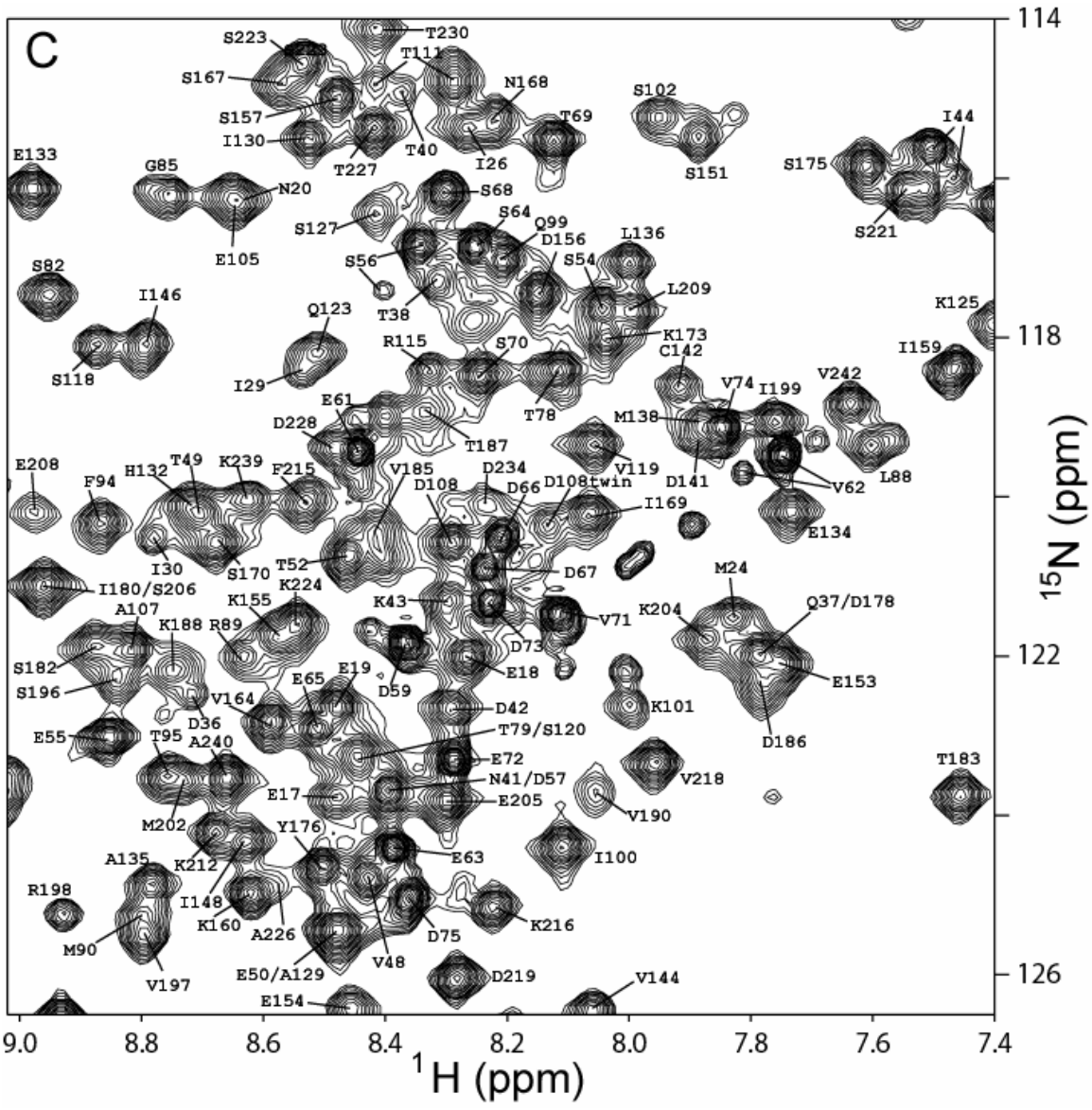

Figure 2.3. Continued

After the completion of resonance assignments, NMR relaxation measurements were carried out on the complex by using both ^{14}N vCCI:^{15}N MIP-1β (Figure 2.4) and ^{15}N vCCI:^{14}N MIP-1β (Figure 2.5). From these data, the overall rotational correlation time was calculated to be 13.2 ± 0.7 ns for ^{15}N vCCI in complex and 13.1 ± 0.6 ns for ^{15}N MIP-1β in complex. These values are both consistent with a molecular weight of around 34 kDa, confirming a complex with 1:1 stoichiometry.

The relaxation data also reveal some noticeable properties of individual residues on both proteins. Even when bound with MIP-1β, vCCI still contains a region with conformationally flexible residues, expanding from Glu55 to Thr78, with ^{15}N-H^{N} NOE values much lower than 0.6 (Figure 2.5). These residues are identified to be responsible for the peaks with anomalously strong signal intensity in the spectra. Close examination links this region to the loop between β-strand 2 and 3 of vCCI. On the MIP-1β side, it is also worth noticing that the first several residues at the N-terminus appear to be relatively flexible even when bound with vCCI.

Protein-protein complex formation is often accompanied by changes in ^{15}N-^{1}H chemical shifts of residues in regions that are affected by the binding interaction. Chemical shift perturbation mapping can be used to reveal the likely interacting sites on proteins. For vCCI, the vast majority of chemical shift perturbations upon association with MIP-1β occur on β-sheet II and the nearby loops, with a few additional changes directly across the β sandwich in β-sheet I, likely due to propagation of changes from β-sheet II (Figure 2.6). The MIP-1β spectra show significant change upon binding vCCI, particularly in the regions associated with the chemokine dimer interface.

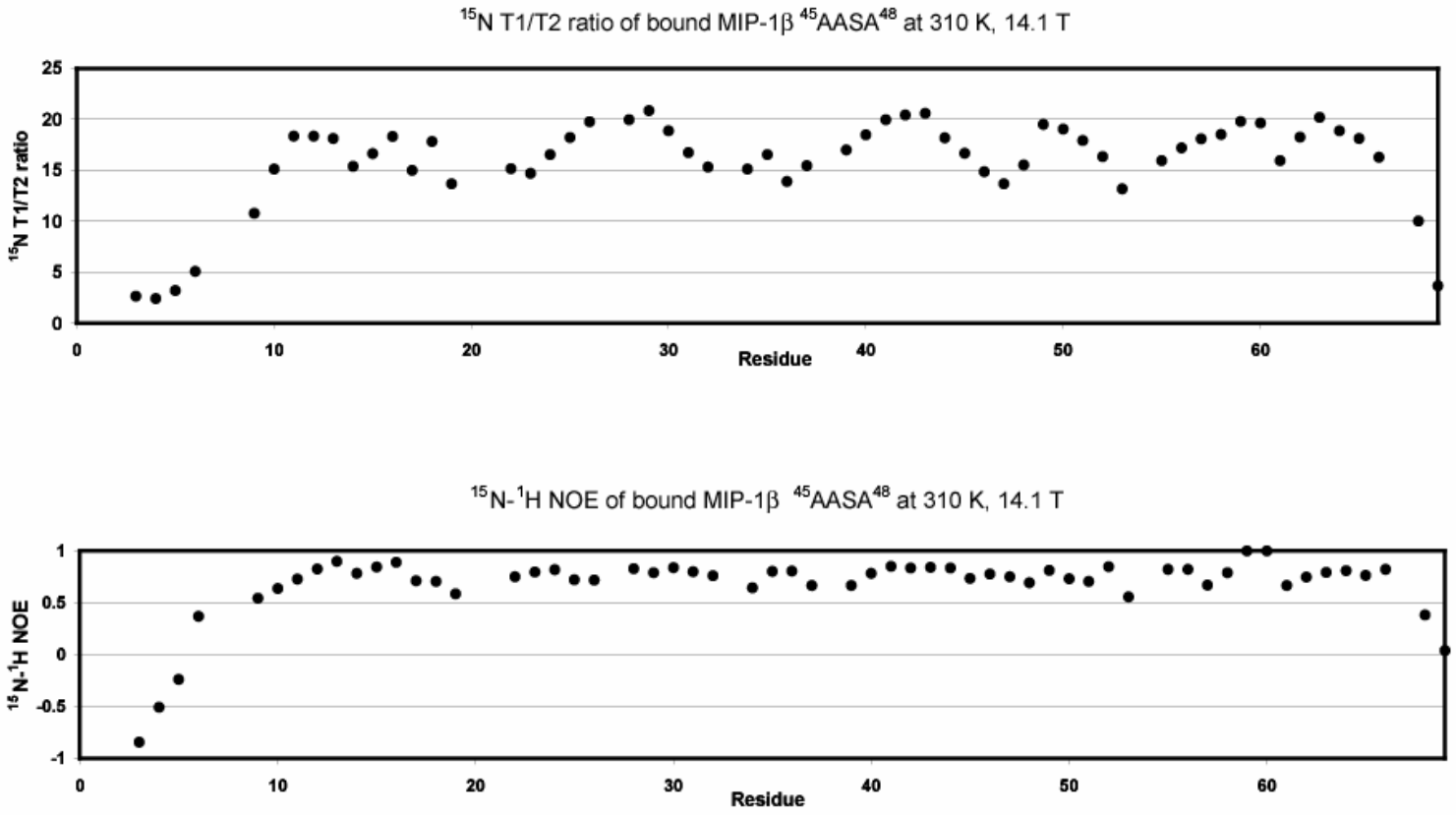

Figure 2.4. NMR relaxation studies of ^{15}N MIP-1β bound with ^{14}N vCCI. Experiments were carried out at 310 K and 14.1 T.

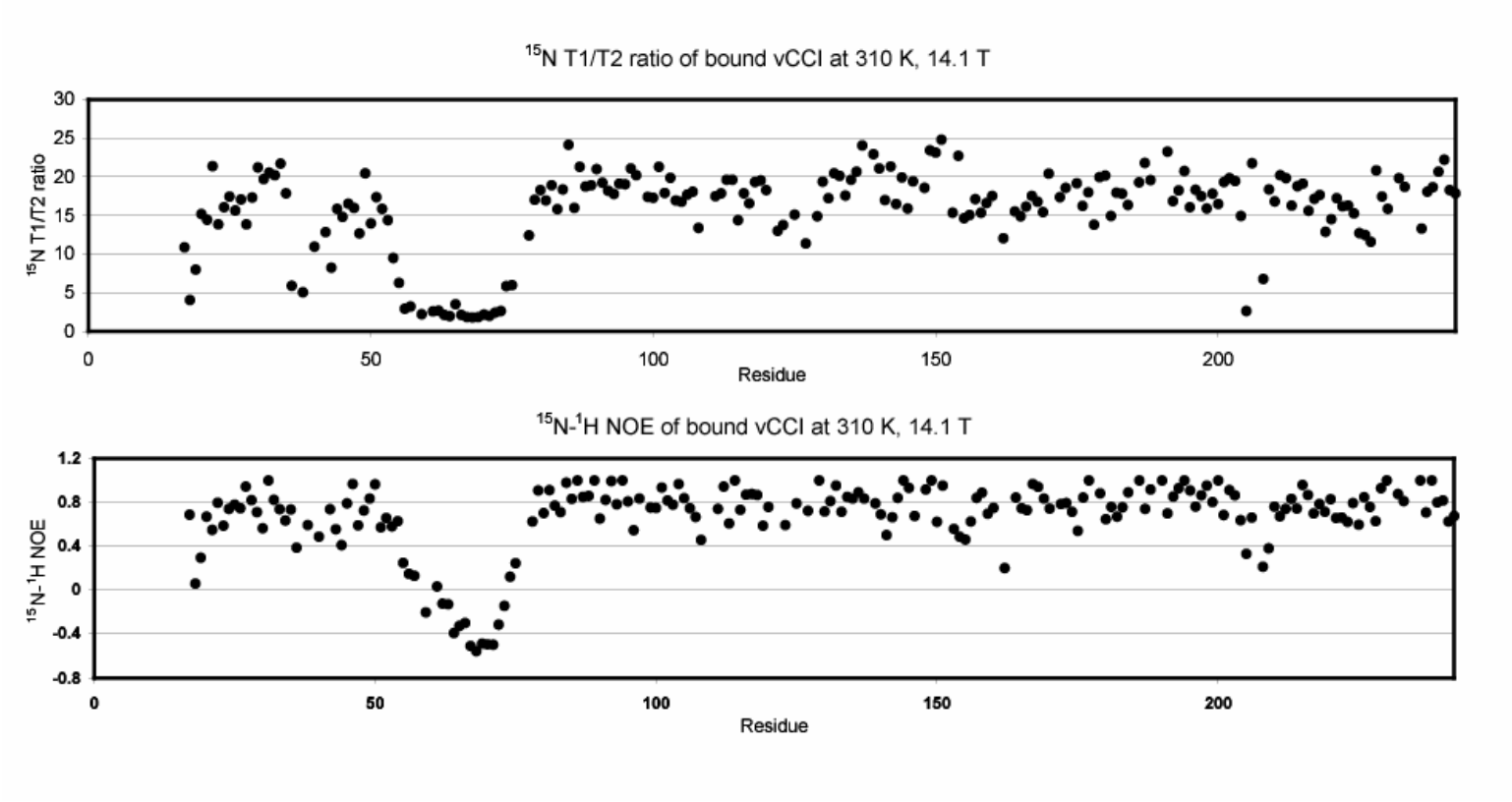

Figure 2.5. NMR relaxation studies of ^{15}N vCCI bound with ^{14}N MIP-1β. Experiments were carried out at 310 K and 14.1 T.

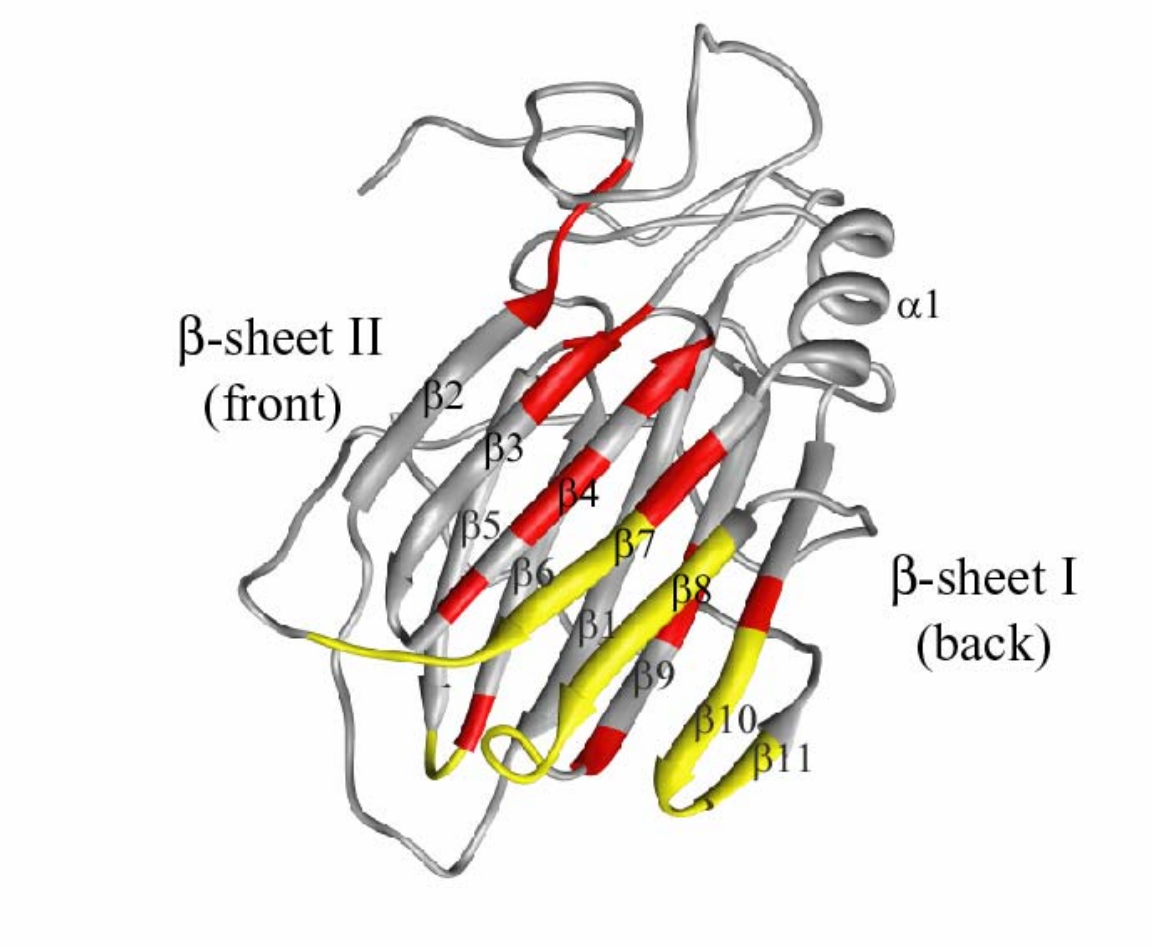

Figure 2.6. Chemical shift perturbation mapping of vCCI upon binding to MIP-1β-^{45}AASA^{48}. Residues with weighted average H^N and N chemical shift perturbation bigger than one standard deviation from the mean value are shown in red. Residues that are missing from the HSQC because of chemical exchange line broadening are shown in yellow.

Discussion

The complex between rabbitpox vCCI and human MIP-1β was formed successfully *in vitro*, as demonstrated by the ^{15}N HSQC spectra. Using the strategy of isotope labeling one protein, and titrating in the unlabeled binding partner, it was clear that these two proteins bind with 1:1 stoichiometry under NMR sample conditions. This conclusion was also supported by subsequent NMR relaxation studies of both proteins when they are in the bound form. When bound with each other, both vCCI and MIP-1β give similar calculated rotational correlation time values of ~13 ns, consistent with a macromolecule of ~34 kDa. Given the known fact that MIP-1β dimerizes in solution with a Kd ~0.73 uM, the formation of a 1:1 vCCI:MIP-1β complex means unavoidable breakage of the MIP-1β homodimer. This is plausible since the vCCI:MIP-1β binding constant has been determined to be in the sub-nanomolar range, so that formation of this complex is much more favored than MIP-1β self-dimerization. This also explains the drastic changes in MIP-1β ^{15}N HSQC spectra upon addition of vCCI, since these changes include both vCCI binding and homodimer dissociation.

The vCCI:MIP-1β complex has a total molecular mass of ~34 kDa, which is relatively large for an NMR study. While the spectra from the 8 kDa MIP-1β in complex resolved well and were readily assigned using regular sample labeling, the vCCI spectra were very crowded, and have rather heterogeneous peak intensity due to different conformational flexibility exhibited by different regions in this protein. Attempts using the regular approach turned out to be fruitless and side-chain deuteration

was necessary to overcome this hurdle. With much reduced ^{1}H-^{1}H interaction, the deuterated samples produced spectra with much higher signal-to-noise ratio, as well as narrower line width. These improvements allowed high percentage resonance assignments to be achieved.

In the original publication of the cowpox vCCI structure, the authors hypothesized that the β-sheet II of vCCI to be the surface of chemokine binding, due to the presence of highly conserved non-structural acidic residues on this solvent-accessible surface. After obtaining backbone assignments for both free and bound vCCI, chemical shift perturbation mapping was used to determine the chemokine binding area on vCCI. The majority of perturbations did occur across the β-sheet II, suggesting that this side of vCCI is indeed involved in chemokine binding. The loop that connects β2 and β3 strands was discovered to be not heavily involved in MIP-1β binding, with limited chemical shift perturbation observed, and remains quite flexible even after binding with the chemokine. This loop comprises a significant number of negative charges, with ~50% being Asp and Glu residues. Given the facts that this loop is on β-sheet II and exposed to solvent, it is surprising to see that binding to a positively charged chemokine did little to its flexibility. On the other hand, it is difficult to use chemical shift perturbation to pinpoint which MIP-1β residues are important for vCCI binding, because the changes on spectra reflect the combined effects of both vCCI binding interaction and MIP-1β homodimer dissociation.

Previously a detailed comparison of the structures and dynamics of wild-type MIP-1β and a monomeric variant F13A was carried out by our group (*107*). The

superposition of F13A structure with a subunit from the MIP-1β homodimer revealed that although the F13A point mutation abolished dimerization, the core structure was not significantly altered. When the entire structures are compared, the largest deviations were found in the F13A N-terminal and other loop regions, with the N-terminus being particularly poorly defined, likely the direct result of the loss of dimerization. ^{15}N relaxation parameters (T1, T2, and NOE) were used to distinguish between ordered and flexible backbone conformations, and revealed greater mobility in the N-terminus of F13A extends up to residue 10.

In the current study, MIP-1β ^{45}AASA^{48} forms a homodimer in solution with a similar dissociation constant as the wild-type protein; however, upon addition of the tighter binding ligand vCCI, it is discovered that the homodimer was broken and a complex with 1:1 stoichiometry was formed. Therefore, it would be interesting to compare the vCCI bound MIP-1β ^{45}AASA^{48} with the wild-type and monomeric counterparts to inspect the effect of vCCI binding on dynamics of MIP-1β. By comparing the ^{15}N-H^N NOE values of these proteins (Figure 2.7), it is clear that the core structures of the three proteins exhibit similar conformational rigidity in solution, illustrated by the similar NOE values from residue 15 and beyond. The major difference is observed in the stretch of the first ten N-terminal residues, where the NOE values gradually decrease towards the N-termini. F13A has consistently lower values than the other two proteins, with the first several detectable residues from Met3 to Asp6 having NOE values less than -2, indicating very high conformational flexibility. In contrast, the corresponding stretch of residues in wild type MIP-1β has generally higher NOE values,

showing the restraining effect by the interaction between subunits in the homodimer. The N-terminal region up to the 10^{th} residue in the vCCI bound MIP-1β ^{45}AASA^{48} shows NOE values in a range between the other two proteins, indicating that these residues definitely do not have as much freedom to adopt various conformations as F13A; instead, the interaction of vCCI only allows restricted motions of this region. On the other hand, these NOE values are smaller than those of the wild-type MIP-1β, so it is reasonable to infer that these residues are not involved in very strong binding interactions. In particular, the first six residues have NOE values close to or below zero, indicating they are largely free to move even after binding with vCCI. Given the current knowledge that the N-terminal residues are crucial for MIP-1β and some other chemokines to activate the cognate receptors, it is likely that the inhibitory strategy of vCCI towards chemokines does not include blocking chemokine activity at the receptor activation phase; instead, blockade at earlier stages such as preventing chemokine from binding to receptors, and disruption of the chemokine gradient may be the main tactics. This makes sense since the composition of the chemokine N-terminal regions are highly variable, so it will be more efficient for vCCI to target the much more conserved chemokine core structure region.

Research in this chapter represents the initial foundation for the structural investigation of the vCCI:chemokine interaction. Further studies providing direct structural contact information are needed to gain a more accurate view on this matter.

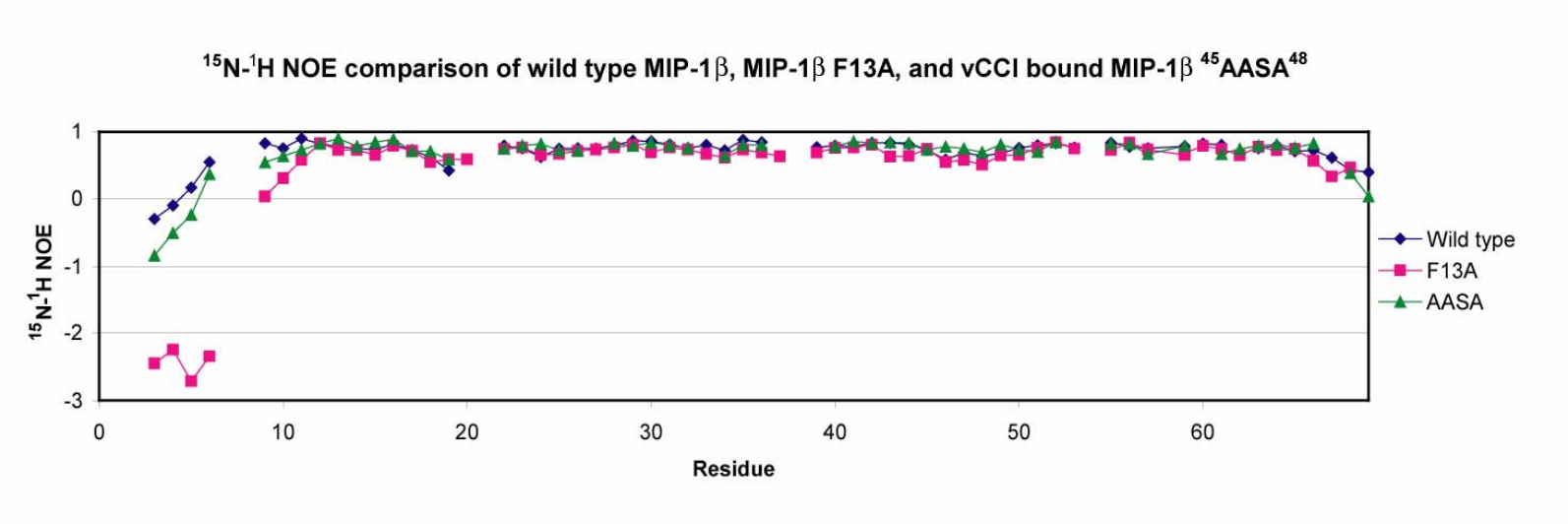

Fig. 2.7. ^{15}N-^{1}H NOE comparison of wild-type MIP-1β, MIP-1β F13A, and vCCI bound MIP-1β ^{45}AASA^{48}. Color coding: blue diamond, wild-type MIP-1β; red square, MIP-1β F13A; green triangle, vCCI bound MIP-1β ^{45}AASA^{48}. Experiments for vCCI bound MIP-1β ^{45}AASA^{48} were carried out at 310 K and 14.1 T. Experiments for wild-type MIP-1β and MIP-1β F13A were carried out carried out at 298 K and 14.1 T as previously reported (*107*).

CHAPTER III

NMR STRUCTURE OF THE VCCI:MIP-1β COMPLEX

Introduction

As crucial components of the immune system, chemokines play important roles in many physiological processes, including the maturation, differentiation and activation of lymphocytes, and chemotaxis of leukocytes as part of the immune response in the occasions of infection and inflammation (*7*). Given the importance of chemokines in the immune system, their high affinity interaction with chemokine receptors and the low affinity interaction with GAGs present two targets for manipulation and disruption by invading viruses.

Large DNA viruses, such as herpes virus and poxvirus, produce an intriguing set of proteins to modulate the host immune system, helping them to evade the host immune response assault (*72, 75*). Among these immunomodulatory proteins, the vCCI (viral CC chemokine inhibitor) encoded by poxviruses presents an interesting subject for further investigation. This secreted, soluble protein bears little sequence homology to any known mammalian proteins, yet has been found to preferentially bind to members of the CC chemokine subfamily with very high affinity, and has little or no affinity to chemokines from other subfamilies. As the first step towards exploring vCCI as a potential therapeutic agent to target certain subset of chemokines in inflammation-related diseases, efforts have been made to understand the interaction between vCCI and

its chemokine ligands. The structure of cowpox encoded vCCI has been solved by X-ray crystallography, showing a unique β-sandwich tertiary fold (*85*). Studies using the wild-type and variants of the CC chemokine MCP-1 revealed crucial residues which contribute to binding affinity on this chemokine (*92, 93*). However, little is known about how vCCI interacts with chemokines, especially how vCCI is capable of selectively binding to multiple members of CC chemokine subfamily.

As discussed in the previous chapter, vCCI and MIP-1β are found to form a complex in 1:1 stoichiometry. The total molecular mass of this complex (~34 kDa) is relatively large for NMR study, which necessitates side chain deuteration of vCCI. Comparison of the resonance assignments of bound and unbound vCCI indicates that the interaction mainly happens on the β-sheet II of this protein. Still, much more detailed information is needed for a structure determination.

After obtaining the basic NMR data sets, the next step is to collect various NOESY spectra, and then use the assignment results to identify each NOE peak in these spectra to obtain spatial distance information between individual nuclei. It is obvious that the bigger a molecule, the more NOE peaks will need to be identified. Furthermore, when it comes to a protein complex, a new challenge arises: in order to pinpoint the residue-specific interactions at the protein:protein interface, *inter*molecular NOE data is the most direct and important information to be acquired; however, with the traditional NOESY experiments, it would be extremely difficult to distinguish the valuable intermolecular NOEs from thousands of intramolecular NOEs produced by both proteins in the complex. To overcome this obstacle, special methods must be applied. One way

is to isotopically label one molecule in the complex, then use heteronuclear isotope-filtered experiments to solve the ambiguities between isotopically labeled and unlabeled species (*108-112*). However, most of this type of experiment requires extensive phase cycling in the NMR pulse sequences to suppress isotope-attached proton signals, which will significantly increase the instrument time needed for data acquisition; and more importantly, in order to achieve satisfactory filtering effect, this method requires additional time delays in the pulse sequences, and when applied to large complexes, these delays will cause significant sensitivity loss due to the fast decay of magnetization. With these considerations in mind, a better choice to study the current complex is to apply *differential* isotope labeling schemes on both proteins, and use this sample for a 4D NOESY experiment that solely detects the intermolecular NOEs. For this purpose, an enhanced-sensitivity gradient 4D $^{13}C,^{15}N$-edited NOESY experiment was selected (*113*), in which pulsed field gradient is utilized to decrease the phase cycle steps by a factor of two while achieving signal sensitivity enhancement up to a factor of square root of two, relative to its original version.

One relatively recent advance in NMR structure determination is the use of alignment media to allow measurement of net residual dipolar coupling (*114*). Dipolar coupling can be used to extract information about the orientation of internuclear vectors relative to the external magnetic field. This measurement is not affected by the actual locations of individual vectors in a molecule. Therefore, in addition to constraining local geometry, dipolar couplings can also be used to restrain the global bond orientations

relative to a common frame. This property makes dipolar coupling data a much needed complement to the NOE constraints, as the latter only determine local distances.

In isotropic solution, rotational Brownian motion of molecules cancels out all internuclear dipolar interaction so that they cannot be measured. However, if a sample is made in the presence of some type of media which applies subtle hindrance on the macromolecules (normally by very slight electrostatic interaction or steric restriction), and allows the macromolecules to have a small net alignment rather than being oriented in any direction with an equal probability, a residual amount of dipolar coupling between nuclei can be measured.

For practical consideration, it is important to find the appropriate media to obtain optimal alignment result. Several common options of media are available (*114*). One choice is the use of liquid crystal phase bicelle medium formed by a mixture of long-chain phospholipids and detergent (*115-121*), which produces highly porous bilayers that cooperatively order in the magnetic field. However, this system has a major disadvantage as the phospholipids may hydrolyze during the process of data collection, thus affecting precise measurement. Another popular option is to use the filamentous bacteriophage, Pf1, to form liquid crystalline media (*122, 123*). This system has been shown to be robust and allows adjustment of the phage concentration to achieve desired alignment. However, since Pf1 carries a substantial amount of negative surface charge, caution must be taken because it may cause aggregation of the sample due to electrostatic interaction. A relatively new and particularly useful non-liquid crystal system is the anisotropic radial compressed or stretched polyacrylamide gels (*124-127*).

This method appears to be robust and compatible with most macromolecules due to the inert nature of the acrylamide gel, and so was chosen for the study of current complex. The major parameter that requires careful optimization is the choice gel concentration, since high concentration gel can inhibit the rotational diffusion rate of molecules, thus causing resonance line broadening and low signal-to-noise ratio, while low concentration gels will not be able to introduce sufficient alignment.

In this chapter, we report the solution structure determination of the complex formed by rabbitpox-encoded vCCI and the ^{45}AASA^{48} nonaggregating variant of the human CC chemokine MIP-1β. The structure reveals that upon formation of a complex with 1:1 stoichiometry, vCCI occludes the regions in the chemokine that are important for chemokine homodimerization, receptor binding and GAG interaction. The structure also defines key interactions that form the basis for the affinity and selectivity of vCCI toward certain CC chemokines.

Materials and methods

Sample Preparation. The gene encoding the human MIP-1β non-aggregating mutant K45A/R46A/K48A (MIP-1β ^{45}AASA^{48}) was subcloned into a modified pET-32 Xa/LIC vector, and the resulting plasmid was transformed into BL21-(DE3) *E. coli* cells for protein production. Unlabeled, ^{15}N-labeled, ^{13}C/^{14}N- labeled and ^{13}C/^{15}N- labeled MIP-1β ^{45}AASA^{48} were produced and purified following the same protocol as described in Chapter II.

The gene encoding rabbit poxvirus vCCI was cloned into pPIC9K plasmid, then transformed into *Pichia pastoris* strain SMD1168 (Invitrogen). Unlabeled, $^{2}H/^{15}N$-labeled and $^{2}H/^{13}C/^{15}N$ labeled protein samples were prepared following similar protocol as described in Chapter II. For deuterated samples, the media were prepared with 95% (final concentration) D_2O. After protein purification procedures, the obtained deuterated vCCI was partially unfolded in H_2O buffer with 2 M urea to allow complete exchange of the amide protons, followed by the removal of urea for vCCI to fold back to its native conformation. After allowing the protein to fully refold, the protein was exchanged into the final NMR buffer.

The final NMR samples contained 1.0-2.0 mM protein(s) (concentration determined in monomeric subunits) in 93% H_2O/7% D_2O containing 100 mM NaCl, 20 mM sodium phosphate pH 7.0, 0.1 mM DSS, 0.01% sodium azide and Complete Protease Inhibitor (Roche Applied Science).

NMR Spectroscopy. Spectra were recorded at 37 °C on Varian Inova 600, 750 and 800 spectrometers. 3D ^{15}N-NOESY of $^{2}H/^{15}N/^{13}C$-labeled vCCI in complex with unlabeled MIP-1β and 3D ^{13}C-NOESY and ^{15}N-NOESY of $^{13}C/^{15}N$-labeled MIP-1β in the presence of unlabeled vCCI were used to obtain intramolecular NOE constraints and for verification of chemical shift assignments (*128*). To detect intermolecular restraints, a 4D $^{13}C,^{15}N$-edited NOESY (*113*) was recorded on a complex of $^{2}H/^{1}H^{N}/^{15}N$-vCCI with $^{13}C/^{14}N$-MIP-1β.

Residual dipolar coupling (RDC) constants were measured in the presence of alignment media to obtain structural restraints as well as the relative orientation of the two binding partners. The samples were prepared using the apparatus developed by Chou *et al.* (*124*) and purchased from New Era Enterprise (Vineland, NJ). In brief, polyacrymide gel solution, ammonium persulfate and N, N, N', N'-tetramethylethylenediamine were thoroughly mixed in H_2O with proper ratio and put into the cast module. The gel was allowed to stand overnight for complete polymerization, then extensively dialyzed against H_2O to remove any residual amount of un-reacted reagents. The cleaned gel was cut to 24 mm in length and fully dried at 45°C for 8 hours. The dried gel piece was then soaked in sample solution at 28°C for 48 hours to allow complete re-hydration and sample absorption. After that, the gel piece containing sample was inserted into an open-end Wilmad NMR tube with 4.2 mm internal diameter. After carefully testing gels with different percentages and original diameter sizes for an optimal alignment condition, 4.8% polyacrylamide gel with 5 mm original diameter was chosen to align the sample. The residual dipolar couplings of resolved ^{1}H-^{15}N were measured using the IPAP scheme (*114, 129*) for both components of the complex.

All spectra were processed with nmrPipe (*99*) and analyzed with PIPP (*100*). Proton chemical shifts were directly referenced to the methyl resonance of DSS, while the carbon and nitrogen chemical shifts were referenced indirectly (*101*).

Structure Calculation. Torsion angles ϕ and ψ were derived from the TALOS database (*130*). Only residues for which all the ten predictions fell in the same region of the Ramachandran plot were used. Structures were calculated using Dynamo (F. Delaglio, NIH). For MIP-1β-^{45}AASA^{48}, the high resolution NMR structure of the wild-type MIP-1β (PDB code 1HUM) was used to prepare a starting input for the calculation. For rabbitpox vCCI, the sequence was first aligned with the unliganded cowpox vCCI (PDB code 1CQ3), then threaded by Modeller 8v1 (*131*) to obtain a starting set of coordinates for calculation. As the first step, separate structural refinement of each protein was carried out. The high temperature in the annealing steps was kept at 500K so that large changes in conformation were not likely unless heavy violation of the NMR data occurred. Ten structures were chosen from a calculation of 50 structures based on adherence to experimental restraints and low overall energy. These 10 structures were then used to obtain an averaged, energy minimized structure, which was further refined with RDC restraints. The resulting refined structure of vCCI showed 0.25 Å backbone r.m.s. deviation from the 1CQ3 structure for 213 aligned residues, showing the same overall fold. Similarly, the resulting refined structure of MIP-1β ^{45}AASA^{48} showed 0.16 Å backbone r.m.s. deviation from a monomeric unit of the wild-type structure. These two initially refined protein structures were then used as inputs to calculate the complex structures. At this stage, the backbone atoms of each protein were constrained within 0.2 Å of the input coordinates without penalty, and the side chains were allowed to move freely to satisfy other restraints. The final ensemble of 15 structures was selected from an ensemble of 100 structures based on lowest energy and no violation of NOE restraints

by > 0.4 Å, or dihedral restraints by > 5°. PROCHECK analysis shows that for the ensemble of the final 15 structures, 70.2% of the residues are in the most favored region, 26.5 % in the additionally allowed region, 2.7 % in the generously allowed region and 0.6% in the disallowed region.

ELISA Assays. Ninety-six well OptiPlate-HB plates (PerkinElmer, Wellesley, MA) were coated with 100 uL of 65 nM vCCI in PBS buffer overnight at 4 °C. The plate was then washed with 0.1% Tween-20 in phosphate buffered saline (PBS-Tween), and excess binding sites were blocked with 300 uL of blocking buffer (0.5% BSA in PBS-Tween) for 2 h at room temperature with constant agitation. The wells were again washed with PBS-Tween, after which serial dilutions of chemokines in blocking buffer were added into individual wells, and incubated for 2 h at room temperature with constant agitation. After washing, 100 uL of 400 ng/mL polyclonal antibody to human MIP-1β (R&D Systems, Minneapolis, MN) was added and incubated for 1 h then washed. 100 uL of 400 ng/mL mouse anti-goat IgG conjugated with horseradish peroxidase (Pierce, Rockford, IL) was then incubated for 1 h and washed. 100 uL Amersham ECL reagent (GE Healthcare, Buckinghamshire, U.K.) was added and incubated for 10 min for stable luminescence emission, followed by detection with an Orion microplate luminometer (Berthold, Oak Ridge, TN). The EC_{50} values of wild-type MIP-1β and the ^{45}AASA^{48} variant were determined using three separate experiments, each performed in triplicate.

Heparin Chromatography. Protein concentrations were determined from the absorbance at 280 nm. Approximately 150 ug of lyophilized wild-type MIP-1β was taken up in 0.2 mL of aqueous 1 M NaCl, 50 mM Tris pH 7.4 (buffer B). After complete dissolving of MIP-1β, ~0.85 mg of vCCI in 1.4 mL of aqueous 50 mM Tris pH 7.4 (buffer A) was added so that the final solution is equivalent to 12.5% buffer B. The sample was incubated at room temperature for 2 hours, and then injected onto a 1 mL Hi-Trap heparin column (Pharmacia, Piscataway, NJ) pre-equilibrated with 12.5% buffer B. The column was rinsed with 10 mL of 12.5% buffer B, followed by a gradient towards 100% buffer B at a rate of 1 mL/min for 30 min. Buffers were degassed prior to each run to minimize the formation of bubbles during the gradient, and the elution profile was monitored by A280. Experimental results were confirmed by replicate runs.

Results

The residual dipolar coupling is often measured as a change in splitting between ^{15}N doublet components of a backbone amide N-H pair upon alignment (Figure 3.1), which gives information about the orientation of that N-H pair in relation to the overall molecule. While a single N-H orientation may not provide much information about a structure, orientations of high percentage of total available N-H pairs can be combined together to give a very accurate and self-consistent protein conformation, as well as provide critical data on the overall orientation of each protein in a complex with respect

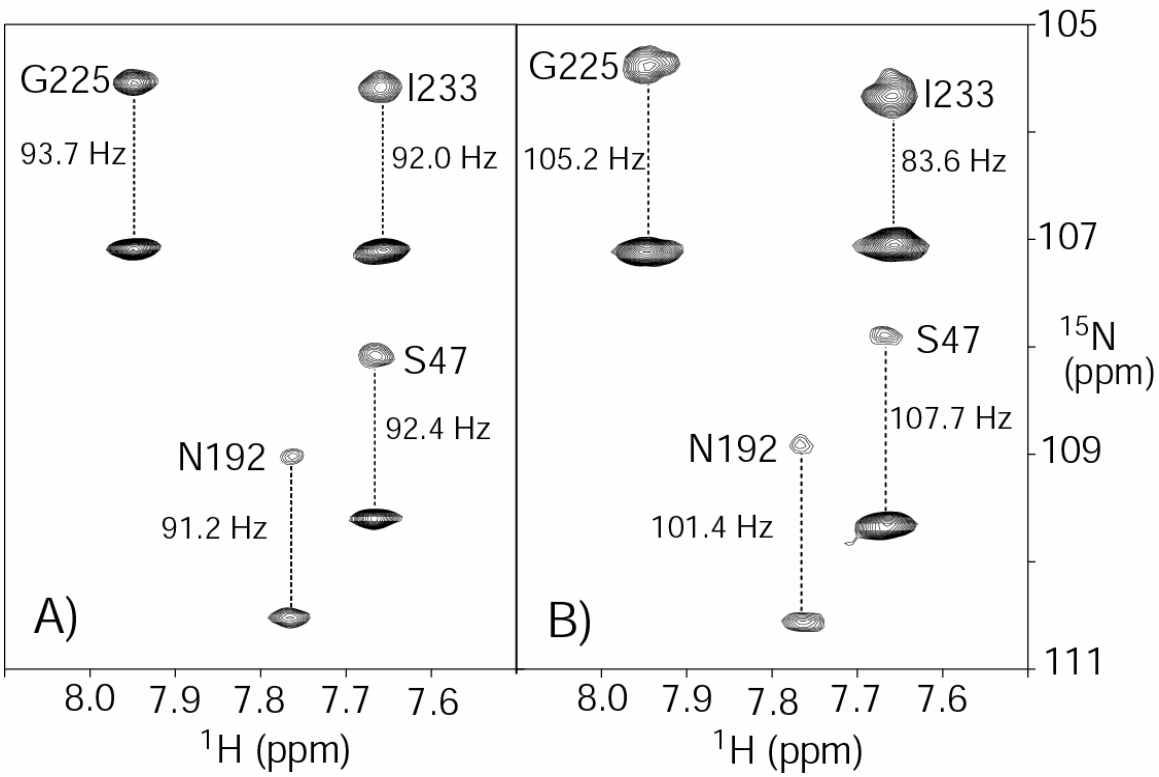

Figure 3.1. A portion of the ^{15}N-IPAP spectra of labeled vCCI in complex with unlabeled MIP-1β. (A) in isotropic solution and (B) in radial compressed 4.8% polyacrylamide gel as the alignment medium. A comparison of the splitting between ^{15}N doublet components of the two spectra yields residual dipolar coupling constants. Experiments were carried out at 310 K, 14.1 T.

to each other. An extensive set of 184 RDCs for the complex were measured, representing 59% of the total possible.

With resonance assignments obtained, the NOESY (Nuclear Overhauser Effect spectroscopy) experiments become the most useful experiments for solution structure determination, providing information about spatial distance between nuclei. In this type of spectrum, a peak is seen for each pair of ^{1}H atoms that are close in space to each other. Sets of NOE data were acquired, providing information about intramolecular distances for each protein in the liganded form, and more importantly, intermolecular distances in the vCCI:MIP-1β complex. The intramolecular NOE data were used to exam the tertiary fold for both proteins, confirming that both proteins in the complex retain the same overall tertiary fold and secondary structures as in the unbound form. The intermolecular NOEs depicting direct structural information of the binding interface were obtained using a 4D ^{15}N,^{13}C-edited NOESY experiment that was measured on a $^{2}H/^{1}H^{N}/^{15}N$ vCCI:$^{13}C/^{14}N$ MIP-1β sample. Because of the differential isotopic labeling of the proteins in the complex, this experiment shows resonances only for inter-molecular contacts, providing distance information between the amide protons of vCCI and any nearby side chain and backbone H^{C} protons of MIP-1β (Figure 3.2). A total of 32 distinct intermolecular NOE restraints were obtained from this spectrum and from the 3D NOESY experiments mentioned above. The structure of the complex was calculated to be consistent with a total of 917 constraints including RDC, dihedral angle and NOE distance restraints (Table 3.1). The final ensemble of 15 structures shows a 0.78 Å r.m.s deviation for backbone atoms. The atomic coordinates for the ensemble of 15 NMR

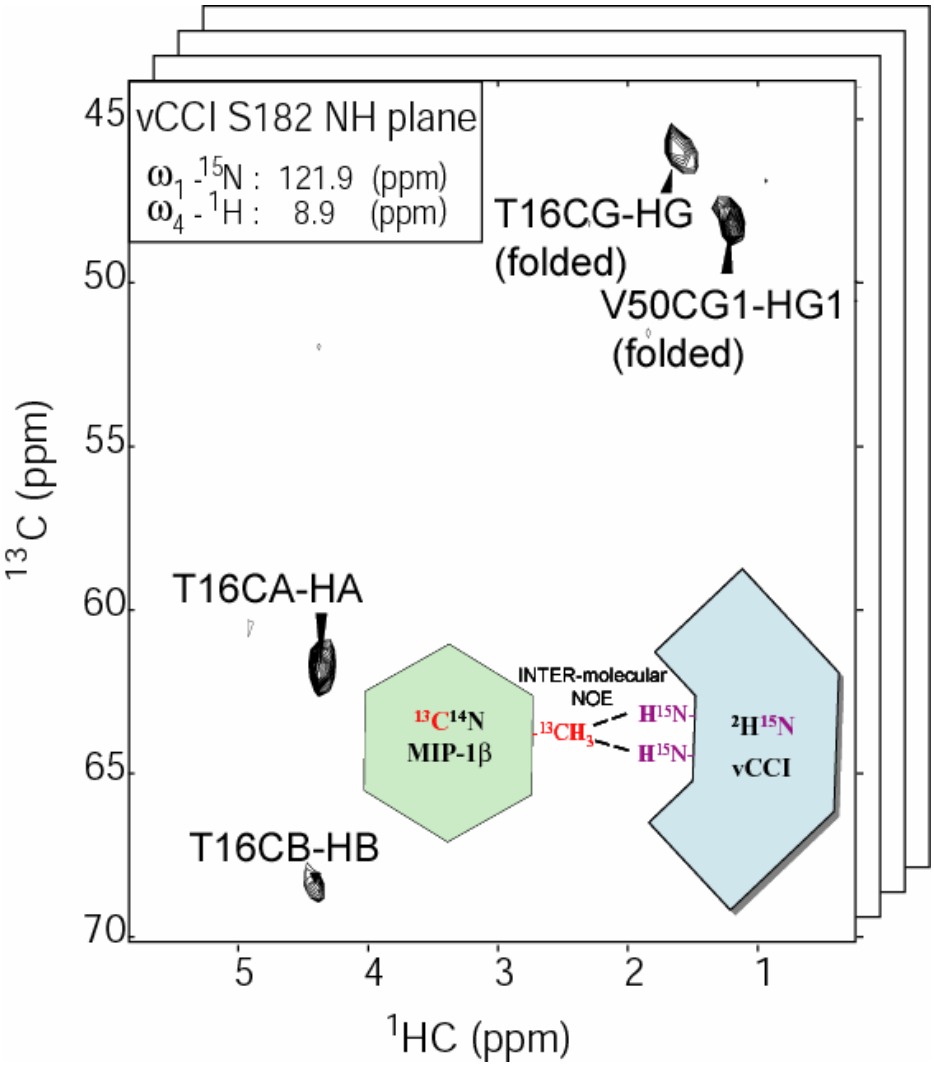

Figure 3.2. A portion of the 4-dimensional ^{15}N, ^{13}C-edited NOESY spectrum. This experiment provides intermolecular contacts between MIP-1β and vCCI. This view shows peaks for any residue of MIP-1β that is in close contact with the amide of Ser182 in vCCI. Inset: A diagram of the principle behind obtaining intermolecular distances (intermolecular NOE distance restraints). A NOESY peak is seen when ^{1}H-^{1}H distances are ≤ 5 Å apart (dashed lines).

Table 3.1 NMR and refinement statistics for the vCCI:MIP-1β complex

NMR distance & dihedral constraints	
Distance restraints	
Total NOE	599
Intra-residue	81
Inter-residue	
Sequential (|i-j| = 1)	264
Non-sequential (|i-j| > 1)	222
Protein–protein intermolecular	32
Total dihedral angle restraints	
Phi	134
Psi	134
Total RDCs	184
Q factor for average energy-minimized structure	10.1%
Structure statistics*	
Violations (mean and s.d.)	
Distance constraints (Å)	0.020 ± 0.003
Dihedral angle constraints (º)	0.54 ± 0.04
Max. distance constraint violation (Å)	0.217 ± 0.068
Max. dihedral angle violation (º)	3.83 ± 0.53
Deviations from idealized geometry	
Bond lengths (Å)	0.00457 ± 0.00014
Bond angles (º)	0.587 ± 0.015
Impropers (º)	0.427 ± 0.026
Average pairwise r.m.s.d. (Å)	
vCCI	
Heavy	1.64 ± 0.09
Backbone	0.42 ± 0.08
MIP-1β	
Heavy	1.61 ± 0.18
Backbone	0.38 ± 0.05
Complex	
Heavy	1.78 ± 0.12
Backbone	0.78 ± 0.25

*Fifteen structures from the final ensemble were included in the analysis. Residues 1-7 and 56-76 in vCCI were excluded from pairwise r.m.s deviation calculation.

The force constants used for the structure calculation are: 1,000 kcal mol^{-1} $Å^{-2}$ for bond lengths, 500 kcal mol^{-1} rad^{-2} for angles and improper torsions, 4 kcal mol^{-1} $Å^{-4}$ for quartic van der Waals repulsions, 80 kcal mol^{-1} $Å^{-2}$ for experimental interproton distances, 200 kcal mol^{-1} rad^{-2} for the TALOS- predicted torsion angle restraints, 0.1-0.5 kcal mol^{-1} Hz^{-2} for residual dipolar coupling.

structures (accession code 2FIN) and the averaged energy minimized structure (accession code 2FFK) have been deposited in the Protein Data Bank.

The vCCI:MIP-1β complex is formed by one monomer of vCCI interacting with one monomer of MIP-1β (Figure 3.3). Each component of the complex is largely similar in conformation to the proteins in their unliganded forms. MIP-1β spans the entire width of vCCI, making contacts across the vCCI β-sheet II starting with MIP-1β residue 8, through the 20's region, and including the 40's loop and the third β strand, constituting a protein:protein interface with 2200 $Å^2$ buried solvent accessible surface area (measured using a 1.4 Å probe). The extended MIP-1β N-terminal fragment from Pro8 to Ser14 is positioned almost parallel to the vCCI β strand 8, making numerous contacts with residues from Ser182 to Thr187. The residue Phe13 of MIP-1β is proximal to a hydrophobic cluster formed by highly conserved vCCI residues including Val185 and Tyr217 (Figure 3.4). The strand of MIP-1β continues across the β-sheet II face of vCCI, with the Arg18 sidechain protruding towards the vCCI residues Asp141 and Glu143, consistent with involvement in electrostatic interactions. The 20's region and 40's loop of MIP-1β fit into a binding surface formed by vCCI strands β2 and β3 and the loop connecting these two strands. The third β strand of MIP-1β is oriented roughly orthogonal to the vCCI β strands and interacts with residues from vCCI β strands 4, 7 and 8.

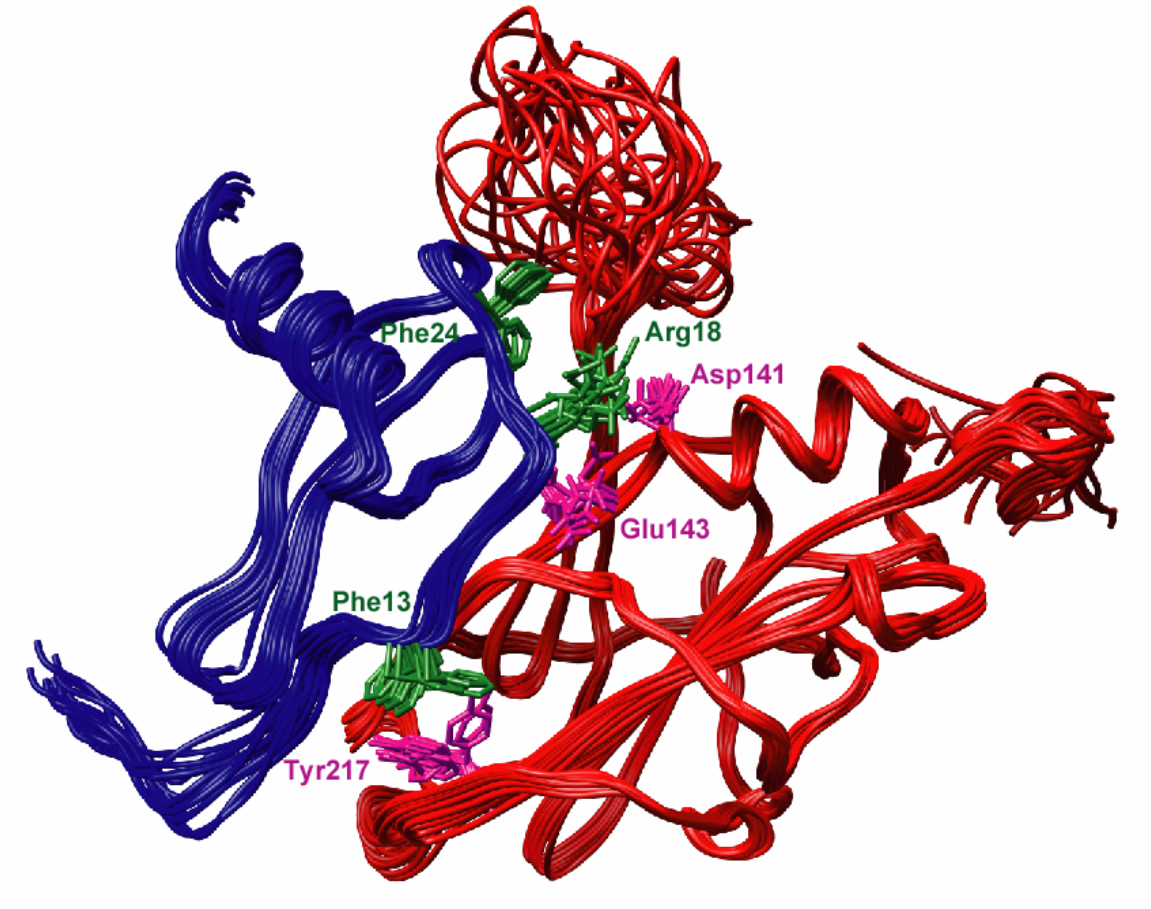

Figure 3.3. Solution structure of the vCCI:MIP-1β complex. Superposition of 15 NMR structures, with vCCI backbone in red and selected sidechains in pink; MIP-1β backbone is blue and selected sidechains are in green.

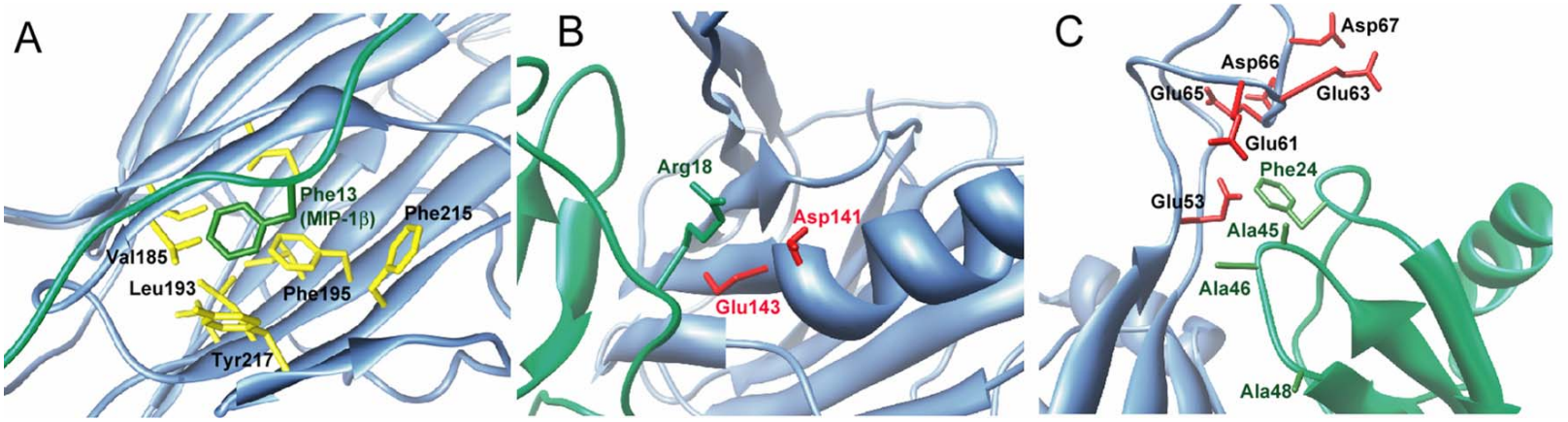

Figure 3.4. Three close-up views of the structure of the MIP-1β:vCCI complex. (A) Close-up view of MIP-1β Phe13 (green) and the surrounding hydrophobic residues (yellow) from vCCI. (B). View of MIP-1β Arg18 (green) in proximity to acidic residues from vCCI (red). (C) View of the 20's region and the 40's loop of MIP-1β (green) in proximity to vCCI acidic residues (red). In the present structure, MIP-1β residues 45 and 46, and 48 are changed to Ala to enhance solubility.

Quantitative ELISA assays were carried out to determine the relative affinity for vCCI of wild-type MIP-1β and the variant used in the present structure determination. These studies reveal an EC_{50} for wild-type MIP-1β of 0.66 ± 0.4 nM, and an EC_{50} for MIP-1β-^{45}AASA^{48} of 0.64 ± 0.6 nM (Figure 3.5).

In order to experimentally determine whether vCCI inhibits GAG binding by MIP-1β, wild-type MIP-1β was pre-incubated with the appropriate amount of vCCI, and then loaded onto a heparin sepharose column. This type of column contains heparin with various lengths, and is considered to be a relatively accurate mimic of the heparan sulfate that is generally found on the cell surface (*132*). In the absence of vCCI, MIP-1β generally binds tightly to the immobilized heparin, requiring about 500 mM NaCl to elute (*96*). However, in the presence of vCCI, MIP-1β co-elutes with vCCI without binding to the heparin column at all (Figure 3.6), indicating the loss of heparin binding ability caused by vCCI.

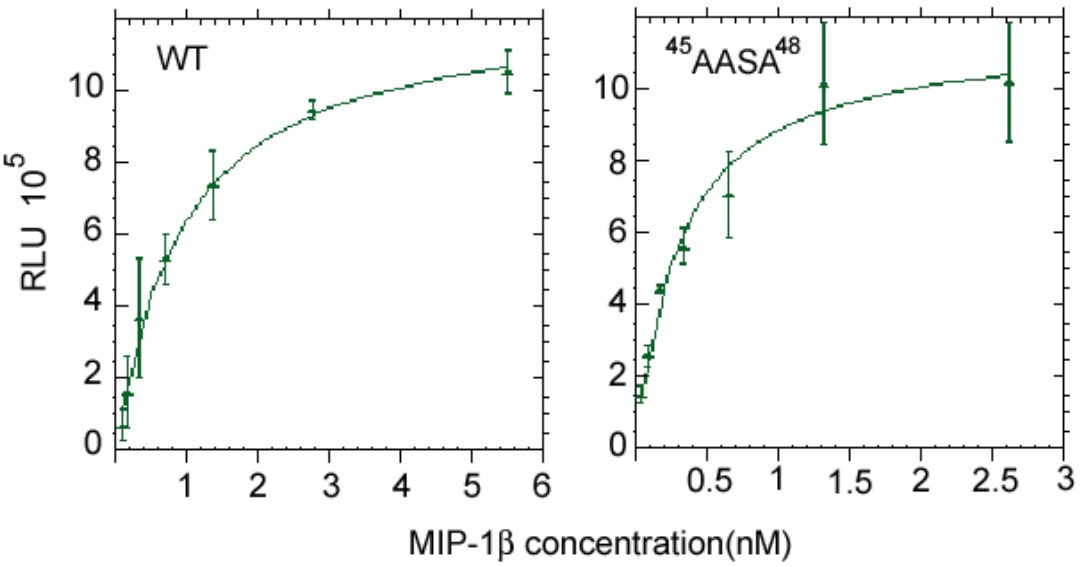

Figure 3.5. ELISA binding results for the interaction of vCCI with wild-type MIP-1β (left) and MIP-1β-^{45}AASA^{48} (right). In three independent experiments, EC_{50} for wild-type MIP-1β ranged from 0.15-0.93 nM, and that for MIP-1β-^{45}AASA^{48} ranged from 0.24-1.4 nM. RLU is Relative Light Units, a measure of luminescence signal.

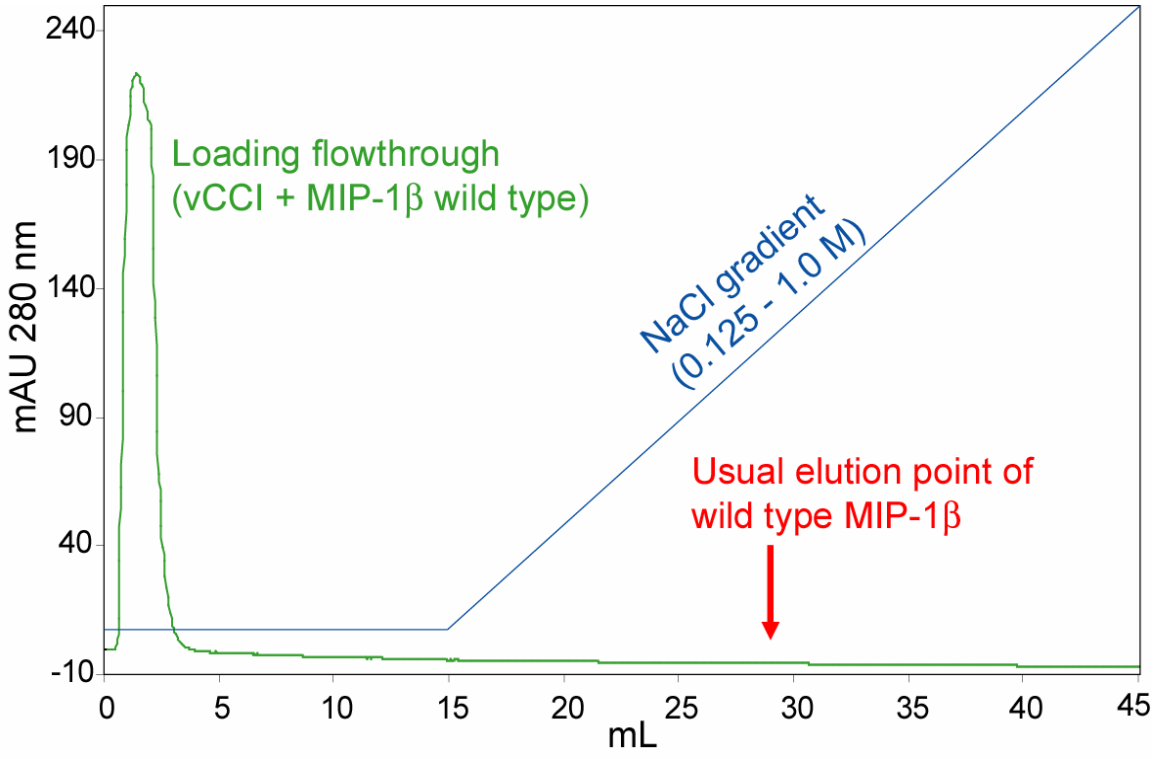

Figure 3.6. The heparin chromatography result of MIP-1β with vCCI. Blue line depicts the NaCl gradient. Green trace is the absorbance at 280 nm. The pre-incubated vCCI and wild-type MIP-1β was found in the flow-through fraction right after loading.

Discussion

vCCIs comprise a group of poxvirus encoded proteins with highly conserved sequence and unique structural topology. These proteins tightly bind and inhibit the action of CC chemokines but have low or no affinity for chemokines of other subfamilies, making them potent and specific anti-inflammatory agents with demonstrated effectiveness *in vivo* (*86, 87*). An extensive binding study with vaccinia vCCI using more than 80 chemokines from several organisms revealed 26 CC chemokines that bind with high affinity, including 13 human chemokines such as MCP-1, MIP-1α, MIP-1β, and RANTES (*90*). In order to probe the chemokine residues that are important in vCCI binding, two previous studies using vCCI and variants of human CC chemokine MCP-1 suggested that the MCP-1 monomeric subunit binds vCCI through an interface that is partially overlapping with the site that MCP-1 uses to bind its natural receptors, with residues Tyr13, Arg18 and Arg24 found to be particularly important (*92, 93*). The present work displays the structural underpinning of the high affinity between poxvirus vCCI and CC chemokines.

In the vCCI:MIP-1β structure, vCCI makes no contact with the first seven chemokine residues, which are involved in receptor activation. However, the highly conserved vCCI residues Ser182-Thr187 make extensive contact with the MIP-1β residues Pro8-Ser14. This region of MIP-1β, and in particular Phe13, has been shown to be critical to the chemokine both for receptor binding and for dimer formation, providing a clear rationale for the inhibitory capability of vCCI. The positioning of the MIP-1β N-

terminal region allows its Phe13 to make close contact with hydrophobic vCCI residues from β8 at the edge of β-sheet II, and β10 from the opposing β-sheet I (Figure 3.3). These residues are at the edge of a large hydrophobic network between the two sheets of the vCCI β-sandwich, so that Phe13 of MIP-1β makes a "cap" on the network. An amino acid with a shorter or a polar side chain would not be able to make these contacts, and would therefore lack this component of binding affinity. Indeed, detailed mutagenesis studies of the CC chemokine MCP-1 show about a 10-fold reduction in affinity when the analogous residue Tyr13 is replaced by Ala (*92, 93*). In all human chemokines that bind tightly to vCCI this position is an aromatic or a large hydrophobic amino acid (*90*), again demonstrating the importance of this residue both in the function and inhibition of CC chemokines.

Another important interaction in the complex involves a positively charged Arg18 of MIP-1β. Our structure reveals that this residue is in close proximity to the conserved negatively charged vCCI residues Asp141 and Glu143 (Figure 3.4B). In twelve of the final ensemble of fifteen structures, the MIP-1β Arg18 guanidino group is within 3.9 Å or less of the gamma carboxyl group of Asp141 of vCCI, so that Asp141 is well positioned for electrostatic interaction. Although this interaction is not shielded from water, mutagenesis experiments on MCP-1 indicate its significance, showing a more than twenty-fold reduction in affinity when Arg18 is substituted with Ala. Additionally, sequence analysis of human chemokines that bind vCCI shows a nearly universal positive charge at this position (Figure 1.6).

A particularly intriguing interaction occurs between the chemokine 20's region and the large flexible vCCI loop that connects the β2 and β3 strands. Among the CC chemokines having high affinity interaction with vCCI, some have a large hydrophobic residue at this position (such as MIP-1β with Phe24), while others have a positively charged residue instead (such as MCP-1 with Arg24). Both types of residues at this position are apparently allowed, which raises the question of whether this amino acid takes part in the binding interaction, and if so, how two completely different amino acid types are tolerated here. This is quite important from a structural standpoint, because it provides insight into the ability of vCCI to maintain selectivity and yet bind such a large number of chemokines. The structure of the vCCI:MIP-1β complex shows that the 24th position in MIP-1β faces the loop in vCCI between the β2 and β3 strands (Figure 3.4C). In all orthopox vCCI proteins, this loop region is highly acidic, with about 50% of the residues being Asp or Glu. ^{15}N relaxation studies reveal this region to be quite flexible regardless of the presence of the bound MIP-1β used in this study. The arrangement of negative charges and the conformational plasticity in this region of vCCI allow favorable interactions with positively charged residues in the chemokine and have minimal hindrance to large hydrophobic residues. A negatively charged chemokine residue at this position would be expected to be disfavored by the highly acidic loop, which explains the observation that an Arg24Glu MCP-1 mutant has no detectable binding to vCCI by surface plasmon resonance (*92*). Regarding vCCI interactions with those chemokines having a neutral rather than a basic residue at this 24th position, the high flexibility of the acidic vCCI loop region surrounding MIP-1β residue Phe24 makes it

difficult to pinpoint specific contacts, so it is possible that Phe24 itself does not contribute favorably to binding vCCI. However, the chemokine 40's loop is close in space to the 24th position and often contains basic amino acid(s) at the turn, such as Lys45 in wild-type MIP-1β (Figure 3.4.C), so productive electrostatic binding interactions are expected with the acidic flexible loop of vCCI. This interaction compensates for the absence of a basic residue at the 24th position. In MCP-1 studies, the loss of Arg24 by mutation to Ala was not compensated by a nearby positive charge (wild-type MCP-1 has Ile and Val at the 45th and 46th position respectively, using MIP-1β numbering), causing a more than 10-fold drop in affinity. An analysis of the sequences of the human chemokines that bind tightly to vCCI shows that they all have at least one positive charge in the 24th or the 45th position (with one chemokine having a positive charge at position 46 instead; Figure 1.6).

The MIP-1β variant used here has mutations K45A/R46A/K48A, which overall lead to an affinity for vCCI approximately the same as the wild-type chemokine, as determined by ELISA assay (Figure 3.5). Although neutralization of the Lys at position 45 would be expected to decrease the affinity of the mutant by the above argument, replacing the large basic Lys residue with Ala at positions 48 apparently compensates for this change. In the current structure, the 48th position is approached closely by the side chains of vCCI Tyr80 and Arg89, so substitution of Lys48 by Ala in MIP-1β could alleviate steric crowding and poor electrostatic effects of the wild-type protein. In support of this, the analogous mutation in MCP-1 Lys49Ala actually showed an increase in affinity for vCCI (*92, 93*).

Inhibition of chemokine binding with GAGs has been demonstrated for several viral proteins, likely as a strategy used by the viruses to disrupt the chemokine concentration gradient that is necessary for directed chemotaxis of leukocytes (*77, 80, 133*). However, it has been controversial whether vCCI also possesses this kind of inhibition towards chemokines. One competition experiment has been reported in which the chemokine MIP-1α (which shares 70% identity with MIP-1β) was pre-incubated with increasing amounts of short chain GAGs, followed by addition of vCCI (*86*). In this experiment, the GAGs were not able to successfully compete with vCCI, suggesting that vCCI and GAGs may not share a common binding surface on the chemokine. However, it is notable that relatively short chain GAGs were used, which would be expected to have a lower binding affinity than full-length GAGs and may not closely representing the physiological GAGs (*134*), and the experiment was carried out with very low (pico-molar) concentration of proteins. It is also noteworthy that different chemokines have somewhat different strategies for binding GAGs (*132*), possibly as a mechanism of selectivity, so it is possible that vCCI could inhibit this function to a different extent in different chemokines.

Heparin chromatography has become a valuable technique to assess the ability of a protein to interact with physiological GAGs. In this type of experiments, a protein sample is loaded into a heparin column, and the ability to interact with heparin is reflected by the salt concentration that is needed to elute this protein. It has been demonstrated that usage of a heparin sulfate column can produce analogous chemokine binding results as using the cell surface sugar heparan sulfate (*135*) or the sugars on

human umbilical vein endothelial cells (*134*). The heparin binding of wild-type MIP-1β and variants was previously studied by our group (*96*). While wild-type MIP-1β showed strong interaction with the heparin and required ~500 mM NaCl for elution, the ^{45}AASA^{48} variant with three negatively charged residues substituted by alanines lost the ability to bind to the column.

In the present structure, the GAGs binding region of MIP-1β, comprised of residues from the 40's loop as well as Arg18 (*94, 135*), interacts with vCCI. Therefore, the structure strongly suggests that vCCI may interfere with GAGS binding by MIP-1β and by chemokines that share a similar GAGs binding site. This hypothesis was supported by the heparin chromatography results, in which the presence of vCCI abolished the heparin binding by wild-type MIP-1β. This provides experimental evidence that the vCCI binding site on MIP-1β does overlap with the GAGs binding site.

An interesting question that arises from these experiments is whether vCCI occludes the GAGs binding site on the other CC chemokines with which it has high affinity binding interaction. Although CC chemokines tend to share similarity in regions of receptor binding and dimerization, there is variation in their GAGs binding sites; therefore it is likely that vCCI may not be able to interfere with the GAGs-binding ability in all these chemokines. This aspect of vCCI function requires further investigation in future studies.

The only other reported protein:protein complex involving a chemokine is the X-ray crystal structure of the γ-herpesvirus protein M3 in complex with a monomeric variant of the CC chemokine MCP-1 (*80*). M3 is a large protein that is able to bind

chemokines from all four chemokine subfamilies. While both M3 and vCCI share some properties of chemokine binding, their strategies are distinct. Most obvious, the M3:MCP-1 binding interface is unrelated to the vCCI:MIP-1β interface reported here. M3 primarily uses the loops at the edge of two different domains to contact each MCP-1 subunit (binding in a 2:2 complex), while in contrast, vCCI uses much of its β-sheet II to contact MIP-1β and forms a 1:1 complex. M3 makes close contacts to residues involved in the receptor binding surface of MCP-1, such as Tyr13 and Arg18, but only peripherally contacts the residues of the 40's loop of the chemokine, which appear to be largely solvent exposed.

Overall then, the ability of vCCI to inhibit many CC chemokines hinges on several key interactions, ranging from occlusion of the receptor binding residues as well as a likely blockade of the chemokine GAG binding site. Sequence analysis of human chemokines having high affinity to vCCI exhibits a conserved pattern (Figure 3.7): Hydrophobic residue 13 as well as positively charged residue 18 is a near-absolute requirement. Residue 24 and members of the 40's loop are close in space, and there is a requirement for at least one positive charge in the 24/45 position; the lack of a positive charge at one of these sites (e.g. 24) is always compensated by at least one positive charge at the other (e.g. 45 or in one case, 46). CC chemokines that have high affinity to vCCI (such as MIP-1β and MCP-1) show adherence to these principles, while chemokines having lower affinity to vCCI (such as TARC/CCL17) do not. CXC chemokines almost universally lack several elements of this pattern, particularly at positions 18 and 24, and so have low or no affinity to vCCI. In summary, this work

represents the first structure of a vCCI:chemokine complex, and reveals a general strategy used by vCCI for selective chemokine binding, which could provide a guideline for future therapeutic design.

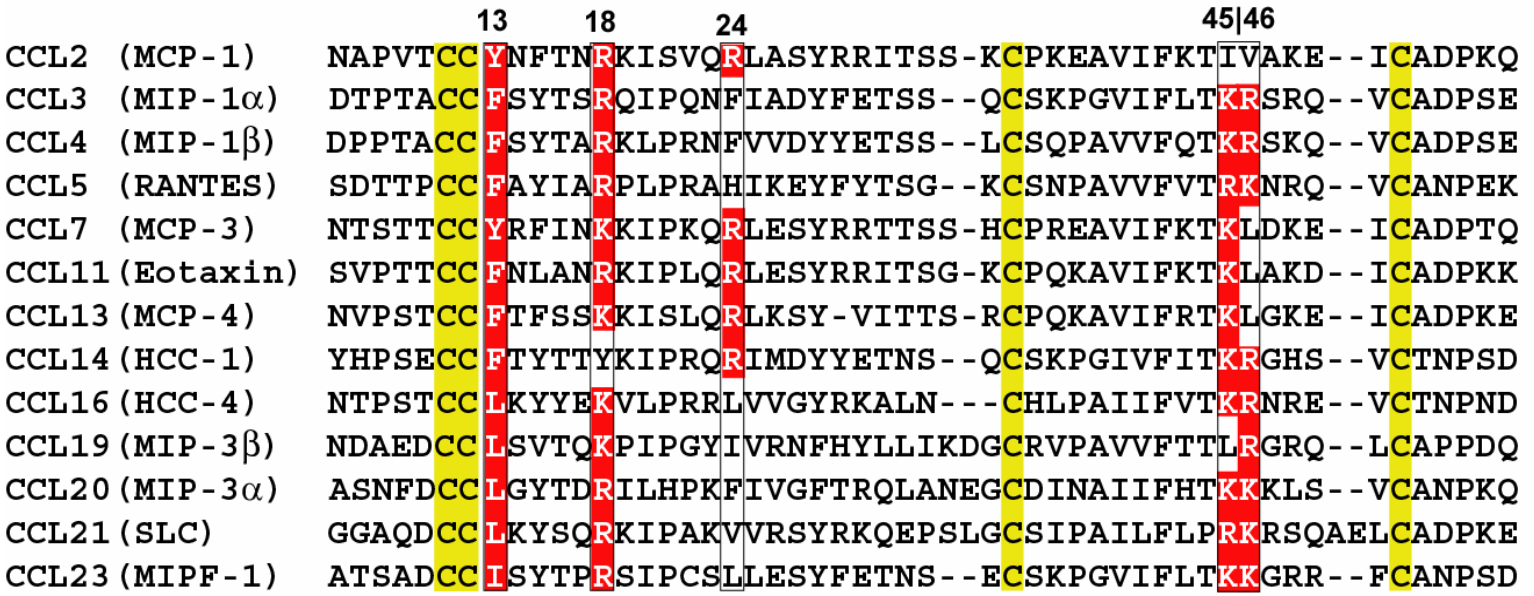

Figure 3.7. Conserved pattern observed in the sequences of human CC chemokines with high affinity to vCCI. Conserved cysteine residues are highlighted in yellow. Positions highlighted with a red background indicate residues that likely confer high affinity binding to vCCI. Residue numbering according to the MIP-1β sequence is used.

CHAPTER IV

FORMATION OF OTHER VCCI:CHEMOKINE COMPLEXES AND PRODUCTION OF VCCI VARIANTS

Introduction

The most intriguing characteristic of vCCI is its ability to bind with high affinity to many CC chemokines, while having little or no affinity for other CC chemokines or chemokines from other subfamilies. This attribute is directly related to its potential to be tailored and harnessed as a therapeutic agent to treat certain inflammation-related diseases, or to provide insightful guidance for designing drugs that possess the virtue of being both broad spectral and specific. Determination of the first vCCI:chemokine structure in the previous chapter represents a solid first step towards gaining detailed understanding of this interaction. The next move is to obtain structural details of vCCI in complex with other chemokines, including some that are similar to MIP-1β, and others that are substantially different. With the knowledge accumulated from handling vCCI and MIP-1β, we have recently gained the ability to form complexes between vCCI and several other wild-type chemokines. After further optimization of sample and experimental conditions, these complexes should also be suitable for structure determination, which will allow substantial expansion of our current understanding of this interaction.

In the current vCCI:MIP-1β structure, multiple regions on vCCI are considered to be contributing towards the high affinity binding interaction. To confirm these structural observations, a straightforward method is to use site-directed mutagenesis to study the effect produced by varying certain residues or regions in vCCI. As the first generation of structure-based vCCI variants, Asp141Ala, Asp141Lys, Glu143Ala, and Glu143Phe are designed to test the importance of these putative chemokine-binding residues. In the complex structure, these residues are discovered to be in close proximity with Arg18 from MIP-1β, so it will be interesting to test the effect caused neutralization or reverse of the original negative charges. Also a deletion variant with the conformationally flexible loop between β-strand 2 and 3 (including residues Glu53-Pro77) replaced by Gly-Gly-Ala-Gly-Gly residues will be produced, providing a starting point for the investigation of the correlation between conformational plasticity and the broad spectral binding compatibility of vCCI.

Materials and methods

Sample Preparation. The genes encoding the wild-type human MCP-1 and Eotaxin-1 were subcloned into the pET-28a vector. The genes encoding the wild-type human MIP-1α, MIP-1β and RANTES were subcloned into the pET-32a vector. All the resulting plasmids were transformed into BL21-(DE3) *E. coli* cells for protein production. These proteins were produced and purified following the same protocol as described in Chapter II. Unlabeled proteins were used to make complexes with ^{15}N-labeled wild-type vCCI.

The final NMR samples contain 0.1-0.5 mM vCCI and saturating amount of unlabeled chemokines in 93% H_2O/7% D_2O containing 100 mM NaCl, 20 mM sodium phosphate pH 7.0, 0.1 mM DSS, 0.01% sodium azide, and Complete Protease Inhibitor (Roche Applied Science, Indianapolis, IN).

The genes for vCCI variants Asp141Ala, Asp141Lys, Glu143Ala, and Glu143Phe were produced using the Quikchange™ procedure (Stratagene, La Jolla, CA) and cloned into the pPICZαA vector (Invitrogen, Carlsbad, CA). For the vCCI loop deletion variant, an overlap extension protocol was used, in which separate PCR reactions were used to obtain the DNA products corresponding to the N-terminal part and C-terminal part of vCCI, with the regions encoding residues Glu53-Pro77 replaced by DNA sequence encoding Gly-Gly-Ala-Gly-Gly. These two pieces of products were cleaned and then mixed together for a PCR reaction with 10 thermo-cycles to allow matching DNA sequence overlapping and extension to occur, so that a full length template is generated. The full length template is then amplified by regular PCR reaction. The resulting product was subsequently cloned into the pPICZαA vector. All these variant genes were transformed into *Pichia pastoris* strain SMD1168 following the manufacturer's manual (EasySelect™ *Pichia* Expression kit, Invitrogen, Carlsbad, CA). Protein production was performed following the same protocol as previously described in Chapter II.

NMR Spectroscopy. ^{15}N HSQC spectra were recorded at 37 °C on a Varian Inova 600 spectrometer. NMR data were processed using NMRPipe (*99*) and analyzed with PIPP

(*100*). Proton chemical shifts were directly referenced to the methyl resonance of DSS, while the nitrogen chemical shifts were referenced indirectly (*101*).

Results

Protein:protein complex formation by vCCI with wild-type human MCP-1, MIP-1α, MIP-1β, RANTES and Eotaxin-1 was observed by ^{15}N heteronuclear single quantum correlation (HSQC) experiment. The chemokines used in these complexes are not isotopically labeled so that they are invisible by NMR, while vCCI is ^{15}N-labeled so that each directly bonded ^{15}N-H pair is detected as a peak in the spectra. Comparison of these spectra reveals that even though the bound vCCI spectra have similar overall peak distribution patterns, there are numerous noticeable differences when different chemokines are used (Figure 4.1). This indicates subtle variation in the chemical environment experienced by vCCI upon interaction with those different chemokines.

Several vCCI variants were successfully cloned and their production was achieved by expression using *Pichia pastoris* strain SMD1168, including Asp141Ala, Asp141Lys, Glu143Ala, Glu143Phe, and a deletion mutant in which the Glu53-Pro77 region was replaced by Gly-Gly-Ala-Gly-Gly. These mutants were also successfully purified following similar protocols as used for the wild-type protein.

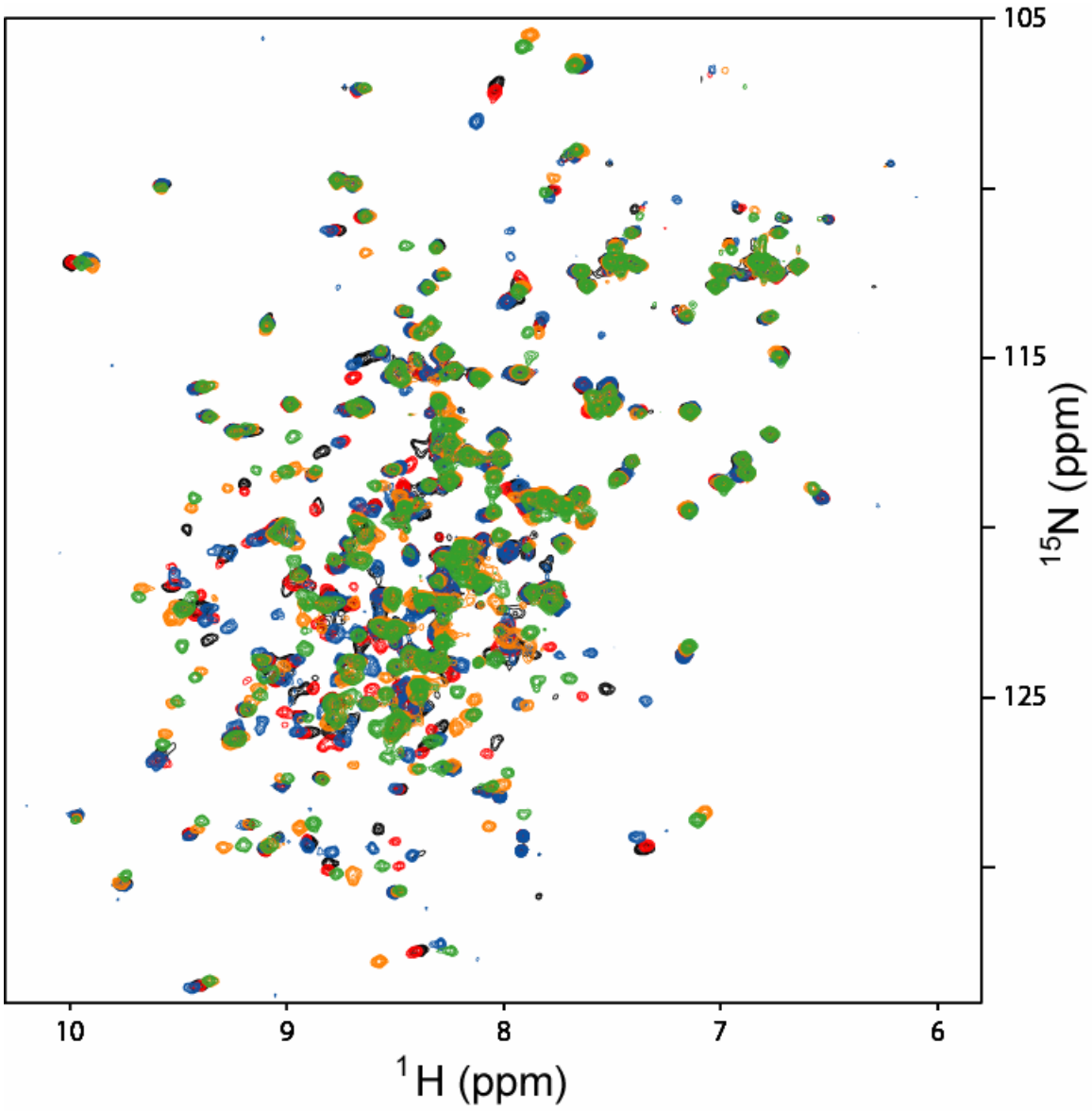

Figure 4.1. Superposition of several ^{15}N heteronuclear single quantum correlation spectra of ^{15}N-labeled vCCI in complex with different CC chemokines. Color coding: green, MCP-1; red, MIP-1a; black, MIP-1b; blue, RANTES; brown, Eotaxin-1. All spectra were collected at 310K, pH 7, 14.1 T.

Discussion

Several new vCCI:chemokine complexes were successfully formed. Although these demonstrated samples contain relatively low protein concentration (0.1-0.5 mM), given the fact that no difficulty was observed in the sample preparation process, it will likely be feasible to increase the amount of proteins used to achieve sufficiently high concentration for solution structural study by NMR. It is also worth mentioning that higher spectral quality can be obtained by carefully optimizing sample condition for each individual complex, such as testing different pH, ionic strength and addition of small amount of organic solvent in the buffer. Adjustment of the conditions for NMR data collection may also contribute to higher spectral quality. After that, similar approaches as used to solve the vCCI:MIP-1β structure can be applied to these new complexes. Therefore, production of these complexes shows a promising next step towards expanding the current understanding of vCCI:chemokine interaction.

Several vCCI variants were successfully produced. These proteins, in conjunction with the newly developed fluorophore-labeled human Eotaxin-1 (F5-maleimide Eotaxin-1 C75) in our laboratory, can be used to determine the effect of individual mutations on binding by a fluorescence anisotropy binding assay (Figure 4.2). This technique utilizes a polarized laser light source to excite of a fluorophore that is attached on Eotaxin-1, followed by subsequent monitoring of the emission of polarized fluorescence. An unliganded chemokine exhibits fast rotational Brownian motion in solution, so that the light emitted from its fluorophore has significant components in

both the parallel and perpendicular directions of the original excitation light, giving a low value of anisotropy as shown by equation in Figure 4.2. However, upon binding vCCI, the tumbling of the chemokine slows significantly, and therefore a larger portion of the emitted light stays parallel to the excitation light, because emission occurs before the fluorophore has rotated away from the original orientation. Therefore, the binding of vCCI will produce a larger value in anisotropy. With titration of vCCI or its variants into the labeled chemokine, accurate Kd values can be obtained. An integral part of the future work of this project should include binding affinity determination of various vCCI variants using fluorophore-labeled chemokines to capture a comprehensive understanding of their interaction.

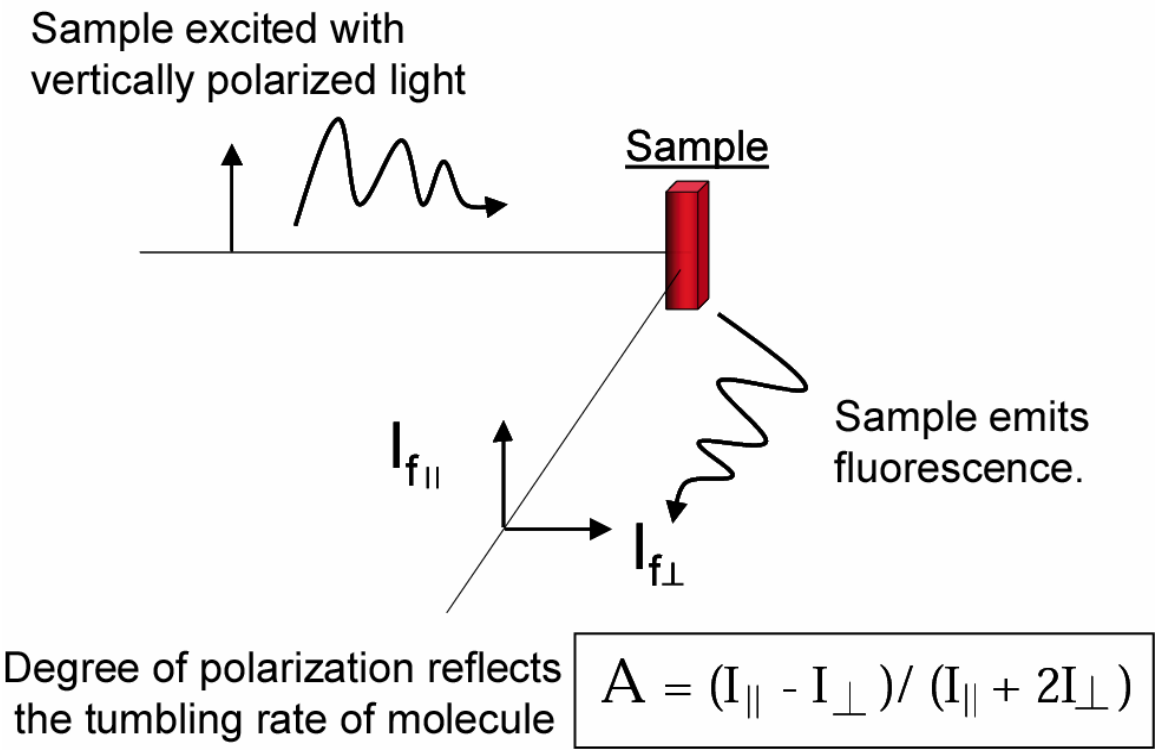

Figure 4.2. A diagram illustrating the setup for acquisition of fluorescence anisotropy data.

CHAPTER V

SUMMARY AND CONCLUSION

By determining the first solution structure of vCCI protein in complex with the chemokine MIP-1β, we are finally able to examine specific interactions between these proteins at molecular level. The structure reveals that vCCI forms a complex with MIP-1β in 1:1 stoichiometry, and interacts with the chemokine mainly through its β-sheet II. Upon binding, vCCI occludes the regions on the chemokine that are important for chemokine homodimerization, receptor binding, and GAG interaction, providing a clear explanation for the inhibitory capability of vCCI. The structure also provides plausible explanation for the previous experimental observations made by other researchers using various binding assays on wild-type and variant chemokines, and reveals the reason why certain amino acid substitutions on the chemokines significantly affected their binding affinity. When combined with chemokine sequence alignment analysis, the structural information gathered from this complex also allows us to propose that a conserved pattern of residue presentation on the chemokines is likely to confer high affinity binding towards vCCI.

This work also represents successful utilization of current technical advances in NMR structure determination. The use of side-chain deuteration greatly improved the spectral resolution to allow unambiguous assignments of nuclei resonance. The residual dipolar coupling constant measurement helped to determine the relative orientations of both proteins to each other when in complex, and provided valuable restraints for better

structure refinement. The application of differential isotope-labeling schemes on both proteins allowed direct detection of inter-molecular NOEs, providing explicit information about the binding interface. These improvements have notably alleviated the difficulty of studying a protein complex with relatively large molecular mass.

Despite the significant progress made in understanding the vCCI:chemokine interaction, important questions remain and demand further investigation. The most intriguing and therapeutic-related attribute of vCCI is the ability to bind to multiple CC chemokines with high affinity, while having little or no affinity for other CC chemokines or chemokines from other subfamily. If fully understood and successfully tailored, this specificity exhibited by vCCI has the potential be explored as treatment for various inflammatory diseases. From the insights gained from the vCCI:MIP-1β structure, we proposed a paradigm which should account for the high affinity binding from the point of view of the chemokine. However, it is almost certain that there are many relatively subtle interactions that remain to be revealed, especially from vCCI. In order to gain a detailed and complete understanding of the highly selective binding of vCCI towards CC chemokines, the next step should include obtaining structural details of vCCI in complex with other chemokines, including those are similar to MIP-1β, and others that are substantially different. Progress has been made on this front. Equipped with the current knowledge we have gained from handling vCCI and chemokines, we have recently achieved the formation of complexes between vCCI and several other wild-type chemokines, including MIP-1α, MCP-1, Exotaxin and RANTES. Similar approaches as

reported in this dissertation can be applied on these complexes to help us capture a more complete picture of vCCI:chemokine interaction.

To reveal more specific interactions by vCCI towards chemokines, another essential next step would be applying biochemical and biophysical studies on vCCI variants. Previously, little progress has been made on this front, due to the difficulty of locating meaningful regions on the relatively large vCCI for mutation design. The current structure data should be able to facilitate designing of vCCI variants aiming to make changes in the regions that are likely to contribute towards affinity and selectivity. Quantitative measurement of the effect of these changes can then be achieved by using techniques such as fluorescence anisotropy and quantitative ELISA.

REFERENCES

1. Baggiolini, M., Dewald, B., and Moser, B. (1997) Human chemokines: An update. *Annu. Rev. Immunol. 15*, 675-705.

2. Baggiolini, M. (1998) Chemokines and leukocyte traffic. *Nature 329*, 565-568.

3. Murphy, P. M. (1994) The molecular biology of leukocyte chemoattractant receptors. *Annu. Rev. Immunol. 12*, 593-633.

4. Olson, T. S., Ley, K. (2002) Chemokines and chemokine receptors in leukocyte trafficking. *Am. J. Physiol. Regul. Integr. Comp. Physiol. 283*, R7-28.

5. Walz, A., Peveri, P., Aschauer, H., and Baggiolini, M. (1987) Purification and amino acid sequencing of NAF, a novel neutrophil-activating factor produced by monocytes. *Biochem. Biophys. Res. Commun. 149*, 755—761.

6. Yoshimura, T., Matsushima, K., Tanaka, S., Robinson, E. A., Appella, E., Oppenheim, J. J., and Leonard, E. J. (1987) Purification of a human monocyte-derived neutrophil chemotactic factor that has peptide sequence similarity to other host defense cytokines. *Proc. Natl. Acad. Sci. U.S.A. 84*, 9233—9237.

7. Baggiolini, M. (2001) Chemokines in pathology and medicine. *J. Intern. Med. 250*, 91-104.

8. Gerard, C., and Rollins, B. J. (2001) Chemokines and disease. *Nat. Immunol. 2*, 108-115.

9. Murphy, P. M., Baggiolini, M., Charo, I. F., Hébert, C. A., Horuk, R., Matsushima, K., Miller, L. H., Oppenheim, J. J., Power, C. A. (2000) International union of pharmacology. XXII. Nomenclature for chemokine receptors. *Pharmacol. Rev. 52*, 145-76.

10. Bacon, K., Baggiolini, M., Broxmeyer, H., Horuk, R., Lindley, I., Mantovani, A., Maysushima, K., Murphy, P., Nomiyama, H., Oppenheim, J., Rot, A., Schall, T., Tsang, M., Thorpe, R., Van Damme, J., Wadhwa, M., Yoshie, O., Zlotnik, A., Zoon, K.; IUIS/WHO Subcommittee on chemokine nomenclature. (2002) Chemokine/chemokine receptor nomenclature. *J. Interferon Cytokine Res. 22*, 1067-8.

11. Nomenclature, I. U. o. I. S. W. H. O. S. o. C. (2001) Chemokine/chemokine receptor nomenclature. *J. Leukoc. Biol. 70*, 465-466.

12. Lau, E. K., Allen, S., Hsu, A. R., and Handel, T. M. (2004) Chemokine-receptor interactions: GPCRs, glycosaminoglycans and viral chemokine binding proteins. *Adv. Protein Chem. 68*, 351-91.

13. Ono, S. J., Nakamura, T., Miyazaki, D., Ohbayashi, M., Dawson, M., Toda, M. (2003) Chemokines: Roles in leukocyte development, trafficking, and effector function. *J. Allergy Clin. Immunol. 111*, 1185-99.

14. Butcher, E. C., Picker, L.J. (1996) Lymphocyte homing and homeostasis. *Science 272(5258)*, 60-6.

15. Kunkel, E., Butcher, E. (2002) Homeostatic chemokines and the targeting of regional immunity. *Adv. Exp. Med. Biol. 512*, 65-72.

16. Springer, T. A. (1995) Traffic signals on endothelium for lymphocyte recirculation and leukocyte emigration. *Annu. Rev. Physiol. 57*, 827-72.

17. Springer, T. A. (1994) Traffic signals for lymphocyte recirculation and leukocyte emigration: The multistep paradigm. *Cell 76(2)*, 301-14.

18. Middleton, J., Patterson, A. M., Gardner, L., Schmutz, C., and Ashton, B. A. (2002) Leukocyte extravasation: Chemokine transport and presentation by the endothelium. *Blood 100(12)*, 3853-60.

19. Weber, C. (2003) Novel mechanistic concepts for the control of leukocyte transmigration: Specialization of integrins, chemokines, and junctional molecules. *J. Mol. Med. 81(1)*, 4-19.

20. Ali, S., Palmer, A. C. V., Banerjee, B., Fritchley, S. J., and Kirby, J. A. (2000) Examination of the function of RANTES, MIP-1α, and MIP-1β following interaction with heparin-like glycosaminoglycans. *J. Biol. Chem. 275*, 11721-11727.

21. Mackay, C. R. (2001) Chemokines: Immunology's high impact factors. *Nat. Immunol. 2*, 95-101.

22. Proudfoot, A. E. (2002) Chemokine receptors: Multifaceted therapeutic targets.[erratum appears in Nature Rev Immunol 2002 Mar;2(3):215]. *Nat. Rev. Immunol. 2*, 106-15.

23. Rollins, B. J. (1997) Chemokines. *Blood 90*, 909-928.

24. Thelen, M. (2001) Dancing to the tune of chemokines. *Nat. Immunol. 2(2)*, 129-34.

25. Alon, R., Grabovsky, V., Feigelson, S. (2003) Chemokine induction of integrin adhesiveness on rolling and arrested leukocytes local signaling events or global stepwise activation? *Microcirculation 10(3-4)*, 297-311.

26. Sánchez-Madrid, F., del Pozo, M.A. (1999) Leukocyte polarization in cell migration and immune interactions. *EMBO J. 18(3)*, 501-11.

27. Lodi, P. J., Garrett, D. S., Kuszewski, J., Tsang, M. L.-S., Weatherbee, J. A., Leonard, W. J., Gronenborn, A. M., and Clore, G. M. (1994) High-resolution solution structure of the β chemokine hMIP-1β by multidimensional NMR. *Science 263*, 1762-1767.

28. Handel, T. M., and Domaille, P. J. (1996) Heteronuclear (^{1}H, ^{13}C, ^{15}N) NMR assignments and solution structure of the monocyte chemoattractant protein-1 (MCP-1) dimer. *Biochemistry 35*, 6569-6584.

29. Crump, M. P., Rajarathnam, K., Kim, K. S., Clark-Lewis, I., and Sykes, B. D. (1998) Solution structure of eotaxin, a chemokine that selectively recruits eosinophils in allergic inflammation. *J. Biol. Chem. 273*, 22471-22479.

30. Clore, G. M., Appella, E., Yamada, M., Matsushima, K., Gronenborn, A.M. (1990) Three dimensional structure of Interleukin-8 in solution. *Biochemistry 29*, 1689-1696.

31. Crump, M. P., Gong, J. H., Loetscher, P., Rajarathnam, K., Amara, A., Arenzana-Seisdedos, F., Virelizier, J. L., Baggiolini, M., Sykes, B., and Clark-Lewis, I. (1997) Solution structure and the basis for functional activity of stromal cell-derived factor-1; dissociation of CXCR4 activation from binding and inhibition of HIV-1. *EMBO J. 16*, 6996-7007.

32. Skelton, N. J., Aspiras, F., Ogez, J., Schall, T.J. (1995) Proton NMR assignments and solution conformation of RANTES, a chemokine of the C-C type. *Biochemistry 34*, 5329-5342.

33. Meunier, A., Bernassau, J. M., Guillemot, J. C., Ferrara, P., Darbon, H. (1997) Determination of the three-dimensional structure of CC chemokine monocyte chemoattractant protein 3 by ^{1}H two-dimensional NMR spectroscopy. *Biochemistry 36*, 4412-4422.

34. Mayer, K. L., and Stone, M. J. (2000) NMR solution structure and receptor peptide binding of the CC chemokine eotaxin-2. *Biochemistry 39*, 8382-95.

35. Laurence, J. S., Blanpain, C., Parmentier, M., Burgner, J. W., and LiWang, P. J. (2000) The CC chemokine MIP-1β can function as a monomer and depends on Phe13 for receptor binding. *Biochemistry 39*, 3401-3409.

36. Rajarathnam, K., Sykes, B.D., Kay, C.M., Dewald, B., Geiser, T., Baggiolini, M., and Clark-Lewis, I. (1994) Neutrophil activation by monomeric interleukin-8. *Science 264*, 90-92.

37. Paavola, C. D., Hemmerich, S., Grunberger, D., Polsky, I., Bloom, A., Freedman, R., Mulkins, M., Bhakta, S., McCarley, D., Wiesent, L., Wong, B., Jarnagin, K., and Handel, T. M. (1998) Monomeric monocyte chemoattractant protein-1 (MCP-1) binds and activates the MCP-1 receptor CCR2B. *J. Biol. Chem. 273*, 33157-33165.

38. Jin, H., Shen, X., Baggett, B., Kong, X., and LiWang, P. (submitted) The human CC chemokine MIP-1b dimer is not competent to bind the CCR5 receptor. *J. Biol. Chem.*

39. Moser, B., Dewald, B., Barella, L., Schumacher, C., Baggiolini, M., and Clark-Lewis, I. (1993) Interleukin-8 antagonists generated by N-terminal modification. *J. Biol. Chem. 268*, 7125-7128.

40. Clark-Lewis, I., Dewald, B., Loetscher, M., Moser, B., and Baggiolini, M. (1994) Structural requirements for interleukin-8 function identified by design of analogs and CXC chemokine hybrids. *J. Biol. Chem. 269(23)*, 16075-81.

41. Hemmerich, S., Paavola, C., Bloom, A., Bhakta, S., Freedman, R., Grunberger, D., Krstenansky, J., Lee, S., McCarley, D., Mulkins, M., Wong, B., Pease, J., Mizoue, L., Mirzadegan, T., Polsky, I., Thompson, K., Handel, T. M., and Jarnagin, K. (1999) Identification of residues in the monocyte chemotactic protein-1 that contact the MCP-1 receptor, CCR2. *Biochemistry 38*, 13013-25.

42. Jarnagin, K., Grunberger, D., Mulkins, M., Wong, B., Hemmerich, S., Paavola, C., Bloom, A., Bhakta, S., Diehl, F., Freedman, R., McCarley, D., Polsky, I., Ping-Tsou, A., Kosaka, A., and Handel, T. M. (1999) Identification of surface residues of the monocyte chemotactic protein 1 that affect signaling through the receptor CCR2. *Biochemistry 38*, 16167-77.

43. Zhang, Y., and Rollins, B. J. (1995) A dominant negative inhibitor indicates that monocyte chemoattractant protein 1 functions as a dimer. *Mol. Cell. Biol. 15*, 4851-4855.

44. Laurence, J. S., LiWang, A. C., and LiWang, P. J. (1998) The effect of N-terminal truncation and solution conditions on chemokine dimer stability:

Nuclear magnetic resonance structural analysis of macrophage inflammatory protein 1β mutants. *Biochemistry 37*, 9346-9354.

45. Ho, H. H., Du, D., and Gershengorn, M. C. (1999) The N terminus of Kaposi's sarcoma-associated herpesvirus G protein-coupled receptor is necessary for high affinity chemokine binding but not for constitutive activity. *J. Biol. Chem. 274(44)*, 31327-32.

46. Katancik, J. A., Sharma, A., Radel, S. J., and De Nardin, E. (1997) Mapping of the extracellular binding regions of the human interleukin-8 type B receptor. *Biochem Biophys Res Commun. 232(3)*, 663-8.

47. Monteclaro, F. S., and Charo, I. F. (1997) The amino-terminal domain of CCR2 is both necessary and sufficient for high affinity binding of monocyte chemoattractant protein 1. Receptor activation by a pseudo-tethered ligand. *J. Biol. Chem. 272(37)*, 23186-90.

48. Suzuki, H., Prado, G. N., Wilkinson, N., and Navarro, J. (1994) The N terminus of interleukin-8 (IL-8) receptor confers high affinity binding to human IL-8. *J. Biol. Chem. 269(28)*, 18263-6.

49. Wu, L., Ruffing, N., Shi, X., Newman, W., Soler, D., Mackay, C. R., and Qin, S. (1996) Discrete steps in binding and signaling of interleukin-8 with its receptor. *J. Biol. Chem. 271(49)*, 31202-9.

50. Xanthou, G., Williams, T. J., and Pease, J. E. (2003) Molecular characterization of the chemokine receptor CXCR3: Evidence for the involvement of distinct extracellular domains in a multi-step model of ligand binding and receptor activation. *Eur. J. Immunol. 33(10)*, 2927-36.

51. Booth, V., Keizer, D. W., Kamphuis, M. B., Clark-Lewis, I., and Sykes, B. D. (2002) The CXCR3 binding chemokine IP-10/CXCL10: Structure and receptor interactions. *Biochemistry 41(33)*, 10418-25.

52. Booth, V., Slupsky, C. M., Clark-Lewis, I., and Sykes, B. D. (2003) Unmasking ligand binding motifs: Identification of a chemokine receptor motif by NMR studies of antagonist peptides. *J. Mol. Biol. 327(2)*, 329-34.

53. Mizoue, L. S., Bazan, J. F., Johnson, E. C., and Handel, T. M. (1999) Solution structure and dynamics of the CX3C chemokine domain of fractalkine and its interaction with an N-terminal fragment of CX3CR1. *Biochemistry 38*, 1402-1414.

54. Skelton, N. J., Quan, C., Reilly, D., and Lowman, H. (1999) Structure of a CXC chemokine-receptor fragment in complex with interleukin-8. *Structure 7*, 157-68.

55. Ye, J., Kohli, L. L., and Stone, M. J. (2000) Characterization of binding between the chemokine eotaxin and peptides derived from the chemokine receptor CCR3. *J. Biol. Chem. 275*, 27250-7.

56. Duma, L., Haussinger, D., Rogowski, M., Lusso, P., and Grzesiek, S. (2007) Recognition of RANTES by extracellular parts of the CCR5 receptor. *J. Mol. Biol. 365*, 1063-75.

57. Blanpain, C., Doranz, B. J., Vakili, J., Rucker, J., Govaerts, C., Baik, S. S. W., Lorthioir, O., Migeotte, I., Libert, F., Baleux, F., Vassart, G., Doms, R. W., and Parmentier, M. (1999) Multiple charged and aromatic residues in CCR5 amino-terminal domain are involved in high affinity binding of both chemokines and HIV-1 env protein. *J. Biol. Chem. 274*, 34719-34727.

58. Farzan, M., Choe, H., Vaca, L., Martin, K., Sun, Y., Desjardins, E., Ruffing, N., Wu, L., Wyatt, R., Gerard, N., Gerard, C., and Sodroski, J. (1998) A tyrosine-rich region in the N terminus of CCR5 is important for human immunodeficiency virus type 1 entry and mediates an association between gp120 and CCR5. *J.Virol 72*, 1160-4.

59. Fong, A. M., Alam, S. M., Imai, T., Haribabu, B., and Patel, D. D. (2002) CX3CR1 tyrosine sulfation enhances fractalkine-induced cell adhesion. *J. Biol. Chem. 277(22)*, 19418-23.

60. Preobrazhensky, A. A., Dragan, S., Kawano, T., Gavrilin, M. A., Gulina, I. V., Chakravarty, L., and Kolattukudy, P. E. (2000) Monocyte chemotactic protein-1 receptor CCR2B is a glycoprotein that has tyrosine sulfation in a conserved extracellular N-terminal region. *J. Immunol. 165(9)*, 5295-303.

61. Blanpain, C., Doranz, B. J., Bondue, A., Govaerts, C., De Leener, A., Vassart, G., Doms, R. W., Proudfoot, A., and Parmentier, M. (2003) The core domain of chemokines binds CCR5 extracellular domains while their amino terminus interacts with the transmembrane helix bundle. *J. Biol. Chem. 278*, 5179-87.

62. Proudfoot, A. E., Handel, T. M., Johnson, Z., Lau, E. K., LiWang, P., Clark-Lewis, I., Borlat, F., Wells, T. N., and Kosco-Vilbois, M. H. (2003) Glycosaminoglycan binding and oligomerization are essential for the in vivo activity of certain chemokines. *Proc. Natl. Acad. Sci. U.S.A. 100*, 1885-90.

63. McCornack, M. A., Boren, D. M., and LiWang, P. J. (2004) Glycosaminoglycan disaccharide alters the dimer dissociation constant of the chemokine MIP-1 beta. *Biochemistry 43*, 10090-101.

64. Luster, A. D. (2001) Antichemokine immunotherapy for allergic diseases. *Curr. Opin. Allergy Clin. Immunol. 1*, 561-7.

65. Lukacs, N. W., Strieter, R. M., Warmington, K., Lincoln, P., Chensue, S. W., and Kunkel, S. L. (1997) Differential recruitment of leukocyte populations and alteration of airway hyperreactivity by C-C family chemokines in allergic airway inflammation. *J. Immunol. 158*, 4398-404.

66. Gonzalo, J. A., Lloyd, C. M., Wen, D., Albar, J. P., Wells, T. N., Proudfoot, A., Martinez, A. C., Dorf, M., Bjerke, T., Coyle, A. J., and Gutierrez-Ramos, J. C. (1998) The coordinated action of CC chemokines in the lung orchestrates allergic inflammation and airway hyperresponsiveness. *J.Exp. Med. 188*, 157-67.

67. Gonzalo, J. A., Pan, Y., Lloyd, C. M., Jia, G. Q., Yu, G., Dussault, B., Powers, C. A., Proudfoot, A. E., Coyle, A. J., Gearing, D., and Gutierrez-Ramos, J. C. (1999) Mouse monocyte-derived chemokine is involved in airway hyperreactivity and lung inflammation. *J. Immunol. 163*, 403-11.

68. Kawasaki, S., Takizawa, H., Yoneyama, H., Nakayama, T., Fujisawa, R., Izumizaki, M., Imai, T., Yoshie, O., Homma, I., Yamamoto, K., and Matsushima, K. (2001) Intervention of thymus and activation-regulated chemokine attenuates the development of allergic airway inflammation and hyperresponsiveness in mice. *J. Immunol. 166*, 2055-62.

69. Wells, T. N., and Schwartz, T. W. (1997) Plagiarism of the host immune system: Lessons about chemokine immunology from viruses. *Curr. Opin. Biotechnol. 8(6)*, 741-8.

70. McFadden, G., Graham, K., Ellison, K., Barry, M., Macen, J., Schreiber, M., Mossman, K., Nash, P., Lalani, A., and Everett, H. (1995) Interruption of cytokine networks by poxviruses: Lessons from myxoma virus. *J. Leukoc. Biol. 57(5)*, 731-8.

71. Nash, P., Barrett, J., Cao, J., Hota-Mitchell, S., Lalani, A. S., Everett, H., Xu, X., Robichaud, J., Hnatiuk, S., Ainslie, C., Seet, B. T., and McFadden, G. (1999) Immunomodulation by viruses: The myxoma virus story. *Immunol. Rev. 168*, 103-20.

72. Seet, B. T., Johnston, J. B., Brunetti, C. R., Barrett, J. W., Everett, H., Cameron, C., Sypula, J., Nazarian, S. H., Lucas, A., and McFadden, G. (2003) Poxviruses and immune evasion. *Ann. Rev. Immunol. 21*, 377-423.

73. Murphy, P. M. (2001) Viral exploitation and subversion of the immune system through chemokine mimicry. *Nat. Immunol. 2*, 116-122.

74. McFadden, G., Lalani, A., Everett, H., Nash, P., and Xu, X. (1998) Virus-encoded receptors for cytokines and chemokines. *Semin. Cell Dev. Biol. 9(3)*, 359-68.

75. Seet, B. T., and McFadden, G. (2002) Viral chemokine-binding proteins. *J. Leukoc. Biol. 72*, 24-34.

76. Boomker, J. M., de Leij, L. F., The, T. H., and Harmsen, M. C. (2005) Viral chemokine-modulatory proteins: Tools and targets. *Cytokine Growth Factor Rev. 16*, 91-103.

77. Lalani, A. S., Graham, K., Mossman, K., Rajarathnam, K., Clark-Lewis, I., Kelvin, D., and McFadden, G. (1997) The purified myxoma virus gamma interferon receptor homolog M-T7 interacts with the heparin-binding domains of chemokines. *J. Virol. 71*, 4356-63.

78. van Berkel, V., Barrett, J., Tiffany, H. L., Fremont, D. H., Murphy, P. M., McFadden, G., Speck, S. H., and Virgin, H. I. (2000) Identification of a gammaherpesvirus selective chemokine binding protein that inhibits chemokine action. *J. Virol. 74*, 6741-7.

79. Parry, C. M., Simas, J. P., Smith, V. P., Stewart, C. A., Minson, A. C., Efstathiou, S., and Alcami, A. (2000) A broad spectrum secreted chemokine binding protein encoded by a herpesvirus. *J. Exp. Med. 191(3)*, 573-8.

80. Alexander, J. M., Nelson, C. A., van Berkel, V., Lau, E. K., Studts, J. M., Brett, T. J., Speck, S. H., Handel, T. M., Virgin, H. W., and Fremont, D. H. (2002) Structural basis of chemokine sequestration by a herpesvirus decoy receptor. *Cell 111*, 343-56.

81. Graham, K. A., Lalani, A. S., Macen, J. L., Ness, T. L., Barry, M., Liu, L. Y., Lucas, A., Clark-Lewis, I., Moyer, R. W., and McFadden, G. (1997) The T1/35kDa family of poxvirus-secreted proteins bind chemokines and modulate leukocyte influx into virus-infected tissues. *Virology 229*, 12-24.

82. Lalani, A. S., Ness, T. L., Singh, J. K., Harrison, J. K., Seet, B. T., Kelvin, D. J., McFadden, G., and Moyer, R. W. (1998) Functional comparisons among

members of the poxvirus T1/35kDa family of soluble CC-chemokine inhibitor glycoproteins. *Virology 250*, 173-184.

83. Lalani, A. S., Masters, J., Graham, K., Liu, L., Lucas, A., and McFadden, G. (1999) Role of the myxoma virus soluble CC-chemokine inhibitor glycoprotein, M-T1, during myxoma virus pathogenesis. *Virology 256*, 233-45.

84. Martinez-Pomares, L., Thompson, J. P., and Moyer, R. W. (1995) Mapping and investigation of the role in pathogenesis of the major unique secreted 35-kDa protein of rabbitpox virus. *Virology 206(1)*, 591-600.

85. Smith, C. A., Smith, T. D., Smolak, P. J., Friend, D., Hagen, H., Gerhart, M., Parik, L., Pickup, D. J., Torrance, D., Mohler, K., Schooley, K., and Goodwin, R. G. (1997) Poxvirus genomes encode a secreted, soluble protein that preferentially inhibits b chemokine activity yet lacks sequence homology to known chemokine receptors. *Virology 236*, 316-327.

86. Alcami, A., Symons, J. A., Collins, P. D., Williams, T. J., and Smith, G. L. (1998) Blockade of chemokine activity by a soluble chemokine binding protein from vaccinia virus. *J. Immunol. 160*, 624-33.

87. Dabbagh, K., Xiao, Y., Smith, C., Stepick-Biek, P., Kim, S. G., Lamm, W. J., Liggitt, D. H., and Lewis, D. B. (2000) Local blockade of allergic airway hyperreactivity and inflammation by the poxvirus-derived pan-CC-chemokine inhibitor vCCI. *J. Immunol. 165*, 3418-22.

88. Patel, A. H., Gaffney, D. F., Subak-Sharpe, J. H., and Stow, N. D. (1990) DNA sequence of the gene encoding a major secreted protein of vaccinia virus, strain Lister. *J. Gen. Virol. 71*, 2013-2021.

89. Smith, V. P., and Alcami, A. (2000) Expression of secreted cytokine and chemokine inhibitors by ectromelia virus. *J. Virol. 74(18)*, 8460-71.

90. Burns, J. M., Dairaghi, D. J., Deitz, M., Tsang, M., and Schall, T. J. (2002) Comprehensive mapping of poxvirus vCCI chemokine-binding protein. Expanded range of ligand interactions and unusual dissociation kinetics. *J. Biol. Chem. 277*, 2785-9.

91. Carfi, A., Smith, C. A., Smolak, P. J., McGrew, J., and Wiley, D. C. (1999) Structure of a soluble secreted chemokine inhibitor vCCI (p35) from cowpox virus. *Proc. Natl. Acad. Sci. U.S.A. 96*, 12379-12383.

92. Seet, B. T., Singh, R., Paavola, C., Lau, E. K., Handel, T. M., and McFadden, G. (2001) Molecular determinants for CC-chemokine recognition by a poxvirus CC-chemokine inhibitor. *Proc. Natl. Acad. Sci. U.S.A. 98*, 9008-13.

93. Beck, C. G., Studer, C., Zuber, J. F., Demange, B. J., Manning, U., and Urfer, R. (2001) The viral CC chemokine-binding protein vCCI inhibits monocyte chemoattractant protein-1 activity by masking its CCR2B-binding site. *J. Biol. Chem. 276*, 43270-6.

94. McCornack, M. A., Cassidy, C. K., and LiWang, P. J. (2003) The binding surface and affinity of monomeric and dimeric chemokine MIP-1β for various glycosaminoglycan disaccharides. *J. Biol. Chem. 278*, 1946-1956.

95. Shaw, J. P., Johnson, Z., Borlat, F., Zwahlen, C., Kungl, A., Roulin, K., Harrenga, A., Wells, T. N., and Proudfoot, A. E. (2004) The X-ray structure of RANTES: heparin-derived disaccharides allows the rational design of chemokine inhibitors. *Structure 12*, 2081-93.

96. Laurence, J. S., Blanpain, C., De Leener, A., Parmentier, M., and LiWang, P. J. (2001) The importance of basic residues and quaternary structure in the function of MIP-1β: CCR5 binding and cell surface sugar interactions. *Biochemistry 40*, 4990-4999.

97. Kay, L. E. (1995) Pulsed field gradient multi-dimensional NMR methods for the study of protein structure and dynamics in solution. *Prog. Biophys. Mol. Biol. 63*, 277-299.

98. Yamazaki, T., lee, W., Arrowsmith, C. H., Muhandiram, D. R., and Kay, L. E. (1994) A suite of triple resonance NMR experiments for the backbone assignment of 15N, 13C. 2H labeled proteins with high sensitivity. *J. Am. Chem. Soc. 116*, 11655-11666.

99. Delaglio, F., Grzesiek, S., Vuister, G. W., Hu, G., Pfeifer, J., and Bax, A. (1995) NMRPipe: A multidimensional spectral processing system based on UNIX pipes. *J. Biomol. NMR 6*, 277-293.

100. Garrett, D. S., Powers, R., Gronenborn, A. M., and Clore, G. M. (1991) A common sense approach to peak picking in two-, three-, and four-dimensional spectra using automatic computer analysis of contour diagrams. *J. Magn. Reson. 95*, 214-220.

101. Wishart, D. S., Bigam, C. G., Yao, J., Abildgaard, F., Dyson, H. J., Oldfield, E., Markley, J. L., and Sykes, B. D. (1995) ^{1}H, ^{13}C, ^{15}N chemical shift referencing in biomolecular NMR. *J. Biomol. NMR 6*, 135-140.

102. Grzesiek, S., Bax, A., Clore, G. M., Gronenborn, A. M., Hu, J. S., Kaufman, J., Palmer, I., Stahl, S. J., Wingfield, P. T. (1996) The solution structure of HIV-1 Nef reveals an unexpected fold and permits delineation of the binding surface for the SH3 domain of Hck tyrosine protein kinase. *Nat. Struct. Biol. 3(4)*, 340-345.

103. Kay, L. E., Torchia, D. A., and Bax, A. (1989) Backbone dynamics of proteins as studied by 15N inverse detected heteronuclear NMR spectroscopy: Application to staphylococcal nuclease. *Biochemistry 28*, 8972-8979.

104. Gardner, K. H., and Kay, L. E. (1998) The use of 2H, 13C, 15N multidimensional NMR to study the structure and dynamics of proteins. *Annu. Rev. Biophys. Biomol. Struct. 27*, 357-406.

105. Derider, M. L., Zhang, L., and LiWang, P. J. (2006) Resonance assignments and secondary structure of vCCI, a 26 kDa CC chemokine inhibitor from rabbitpox virus. *J. Biomol. NMR. 34(4)*, 229-236.

106. Zhang, L., and LiWang, P. J. (2006) Resonance assignments of the 34 kD rabbitpox vCCI:human MIP-1beta complex. *J. Biomol. NMR 36* Suppl 1:49.

107. Kim, S., Jao, S.-c., Laurence, J. S., and LiWang, P. J. (2001) Structural comparison of monomeric variants of the chemokine MIP-1b having differing ability to bind the receptor CCR5. *Biochemistry 40*, 10782-10791.

108. Wider, G., Weber, C., Traber, R., Widmer, H., and Wuthrich, K. (1990) Use of a Double-Half-Filter in Two-Dimensional 1H NMR Studies of Receptor-Bound Cyclosporin. *J. Am. Chem. Soc. 112*, 9015-9016.

109. Ikura, M., and Bax, A. (1992) Isotope filtered 2D NMR of a protein-peptide complex: Study of a skeletal muscle myosin light chain kinase fragment bound to calmodulin. . *J. Am. Chem. Soc. 114*, 2433-2440.

110. Gemmecker, G., Olejniczak, E. T., and Fesik, S. W. (1992) An improved method for selectively observing protons attached to 12C in the presence of 1H-13C spin pairs. *J. Magn. Reson. 96*, 199-204.

111. Folkers, P. J. M., Folmer, R. H. A., Konings, R. N. H., and Hilbers, C. W. (1993) Overcoming the ambiguity problem encountered in the analysis of nuclear magnetic resonance spectra of symmetric dimer proteins. *J. Am. Chem. Soc. 115*, 3798-3799.

112. Bax, A., Grzesiek, S., Gronenborn, A. M., and Clore, G. M. (1994) Isotope-filtered 2D HOHAHA spectroscopy of a peptide-protein complex using heteronuclear Hartmann-Hahn dephasing. *J. Magn. Reson. 106*, 269-273.

113. Muhandiram, D. R., Xu, G. Y., and Kay, L. E. (1993) An enhanced-sensitivity pure absorption gradient 4D 15N, 13C-edited NOESY experiment. *J. Biomol. NMR 3*, 463-470.

114. Bax, A. (2003) Weak alignment offers new NMR opportunities to study protein structure and dynamics. *Protein Sci. 12*, 1-16.

115. Sanders, C. R., Hare, B. J., Howard, K. P., and Prestegard, J. H. (1994) Magnetically-oriented phospholipid micelles as a tool for the study of membrane-associated molecules. *Prog. Nucl. Magn. Reson. Spectrosc. 26*, 421-444.

116. Sanders, C. R., and Prestegard, J. H. (1990) Magnetically orientable phospholipid-bilayers containing small amounts of a bile-salt analog, chapso. *Biophys. J. 58*, 447-460.

117. Sanders, C. R., and Schwonek, J. P. (1992) Characterization of magnetically orientable bilayers in mixtures of dihexanoylphosphatidylcholine and dimyristoylphosphatidylcholine by solid-state NMR. *Biochemistry 31*, 8898–8905.

118. Ottiger, M., and Bax, A. (1998) Characterization of magnetically oriented phospholipid micelles for measurement of dipolar couplings in macromolecules. *J. Biomol. NMR 12*, 361-372.

119. Ottiger, M., and Bax, A. (1998) Determination of relative N-H, N-C', Ca-C', and C-H effective bond lengths in a protein by NMR in a dilute liquid crystalline phase. *J. Am. Chem. Soc. 120*, 12334-12341.

120. Tjandra, N., and Bax, A. (1997) Direct measurement of distances and angles in biomolecules by NMR in a dilute liquid crystalline medium. *Science 278*, 1111-1114.

121. Bax, A., and Tjandra, N. (1997) High-resolution heteronuclear NMR of human ubiquitin in an aqueous liquid crystalline medium. *J. Biomol. NMR 10*, 289-292.

122. Hansen, M. R., Mueller, L., and Pardi, A. (1998) Tunable alignment of macromolecules by filamentous phage yields dipolar coupling interactions. *Nat. Struct. Biol. 5*, 1065-1074.

123. Zweckstetter, M., and Bax, A. (2001) Characterization of molecular alignment in aqueous suspensions of Pf1 bacteriophage. *J. Biomol. NMR 20*, 365-377.

124. Chou, J. J., Gaemers, S., Howder, B., Louis, J. M., and Bax, A. (2001) A simple apparatus for generating stretched polyacrylamide gels, yielding uniform alignment of proteins and detergent micelles. *J. Biomol. NMR 21*, 377-82.

125. Chou, J. J., Kaufman, J. D., Stahl, S. J., Wingfield, P. T., and Bax, A. (2002) Micelle-induced curvature in a water-insoluble HIV-1 Env peptide revealed by NMR dipolar coupling measurement in stretched polyacrylamide gel. *J. Am. Chem. Soc. 124*, 2450-2451.

126. Sass, H. J., Musco, G., Stahl, S. J., Wingfield, P. T., and Grzesiek, S. (2000) Solution NMR of proteins within polyacrylamide gels: Diffusional properties and residual alignment by mechanical stress or embedding of oriented purple membranes. *J. Biomol. NMR 18*, 303-309.

127. Tycko, R., Blanco, F. J., and Ishii, Y. (2000) Alignment of biopolymers in strained gels: A new way to create detectable dipole-dipole couplings in high-resolution biomolecular NMR. *J. Am. Chem. Soc. 122*, 9340-9341.

128. Zhang, O., Forman-Kay, J. D., Shortle, D., and Kay, L. E. (1997) Triple-resonance NOESY-based experiments with improved spectral resolution: Applications to structural characterization of unfolded, partially folded and folded proteins. *J. Biomol. NMR 9*, 181-200.

129. Hall, J. B., Dayie, K. T., Fushman, D. (2003) Direct measurement of the 15N CSA/dipolar relaxation interference from coupled HSQC spectra. *J. Biomol. NMR 26*, 181-186.

130. Cornilescu, G., Delaglio, F., and Bax, A. (1999) Protein backbone angle restraints from searching a database for chemical shift and sequence homology. *J. Biomol. NMR 13*, 289-302.

131. Fiser, A., Do, R. K., and Sali, A. (2000) Modeling of loops in protein structures. *Protein Sci. 9*, 1753-73.

132. Johnson, Z., Proudfoot, A. E., and Handel, T. M. (2005) Interaction of chemokines and glycosaminoglycans: A new twist in the regulation of chemokine function with opportunities for therapeutic intervention. *Cytokine Growth Factor Rev. 16*, 625-36.

133. Webb, L. M., Smith, V. P., and Alcami, A. (2004) The gammaherpesvirus chemokine binding protein can inhibit the interaction of chemokines with glycosaminoglycans. *FASEB J. 18*, 571-3.

134. Kuschert, G. S., Coulin, F., Power, C. A., Proudfoot, A. E., Hubbard, R. E., Hoogewerf, A. J., and Wells, T. N. (1999) Glycosaminoglycans interact selectively with chemokines and modulate receptor binding and cellular responses. *Biochemistry 38*, 12959-68.

135. Koopmann, W., Ediriwickrema, C., and Krangel, M. S. (1999) Structure and function of the glycosaminoglycan binding site of chemokine macrophage inflammatory protein-1b. *J. Immunol. 163*, 2120-2127.

APPENDIX A

RESONANCE ASSIGNMENTS OF RABBITPOX VIRUS VCCI

BMRB Accession Code 6809 (http://www.bmrb.wisc.edu)

```
_Atom_shift_assign_ID
_Residue_seq_code
_Residue_label
_Atom_name
_Atom_type
_Chem_shift_value
_Chem_shift_value_error
_Chem_shift_ambiguity_code

  1   2 PRO C  C 178.2   0.2  .
  2   2 PRO CA C  62.8   0.2  .
  3   2 PRO CB C  30.88  0.2  .
  4   3 ALA H  H   8.364 0.05 .
  5   3 ALA C  C 174.8   0.2  .
  6   3 ALA CA C  52.54  0.2  .
  7   3 ALA CB C  18.09  0.2  .
  8   3 ALA N  N 123.67  0.2  .
  9   4 SER H  H   8.139 0.05 .
 10   4 SER C  C 174.2   0.2  .
 11   4 SER CA C  58.16  0.2  .
 12   4 SER CB C  63.06  0.2  .
 13   4 SER N  N 113.745 0.2  .
 14   5 LEU H  H   8.058 0.05 .
 15   5 LEU CA C  55.01  0.2  .
 16   5 LEU CB C  41.06  0.2  .
 17   5 LEU N  N 123.251 0.2  .
 18   6 GLN H  H   8.153 0.05 .
 19   6 GLN CA C  55.567 0.2  .
 20   6 GLN CB C  28.29  0.2  .
 21   6 GLN N  N 120.232 0.2  .
 22  16 THR C  C 176.5   0.2  .
 23  16 THR CA C  61.76  0.2  .
 24  16 THR CB C  68.49  0.2  .
 25  17 GLU H  H   8.482 0.05 .
 26  17 GLU C  C 176.4   0.2  .
 27  17 GLU CA C  55.78  0.2  .
 28  17 GLU CB C  29.13  0.2  .
```

```
29  17 GLU N  N 123.697 0.2  .
30  18 GLU H  H   8.273 0.05 .
31  18 GLU C  C 176.5   0.2  .
32  18 GLU CA C  56.17  0.2  .
33  18 GLU CB C  29.67  0.2  .
34  18 GLU N  N 121.933 0.2  .
35  19 GLU H  H   8.477 0.05 .
36  19 GLU C  C 173.9   0.2  .
37  19 GLU CA C  57.15  0.2  .
38  19 GLU CB C  28.94  0.2  .
39  19 GLU N  N 122.531 0.2  .
40  20 ASN H  H   8.654 0.05 .
41  20 ASN C  C 175.3   0.2  .
42  20 ASN CA C  53.54  0.2  .
43  20 ASN CB C  37.55  0.2  .
44  20 ASN N  N 116.126 0.2  .
45  21 LYS H  H   7.157 0.05 .
46  21 LYS C  C 175.2   0.2  .
47  21 LYS CA C  54.34  0.2  .
48  21 LYS CB C  34.54  0.2  .
49  21 LYS N  N 116.318 0.2  .
50  22 HIS H  H   9.243 0.05 .
51  22 HIS C  C 174.5   0.2  .
52  22 HIS CA C  54.5   0.2  .
53  22 HIS CB C  31.86  0.2  .
54  22 HIS N  N 116.744 0.2  .
55  23 HIS H  H   9.935 0.05 .
56  23 HIS C  C 176.6   0.2  .
57  23 HIS CA C  54.56  0.2  .
58  23 HIS CB C  26.15  0.2  .
59  23 HIS N  N 127.945 0.2  .
60  24 MET H  H   7.811 0.05 .
61  24 MET C  C 169.8   0.2  .
62  24 MET CA C  52.7   0.2  .
63  24 MET CB C  29.02  0.2  .
64  24 MET N  N 121.424 0.2  .
65  25 GLY H  H   9.549 0.05 .
66  25 GLY C  C 172.4   0.2  .
67  25 GLY CA C  42.67  0.2  .
68  25 GLY N  N 109.442 0.2  .
69  26 ILE H  H   8.241 0.05 .
70  26 ILE C  C 173.7   0.2  .
71  26 ILE CA C  56.83  0.2  .
72  26 ILE CB C  42.15  0.2  .
73  26 ILE N  N 115.232 0.2  .
```

```
 74  27 ASP H  H   8.872 0.05 .
 75  27 ASP C  C 174.4   0.2  .
 76  27 ASP CA C  54.23  0.2  .
 77  27 ASP CB C  44.94  0.2  .
 78  27 ASP N  N 127.124 0.2  .
 79  28 VAL H  H   9.402 0.05 .
 80  28 VAL C  C 173.8   0.2  .
 81  28 VAL CA C  59.94  0.2  .
 82  28 VAL CB C  32.89  0.2  .
 83  28 VAL N  N 127.881 0.2  .
 84  29 ILE H  H   8.637 0.05 .
 85  29 ILE C  C 171.1   0.2  .
 86  29 ILE CA C  58.93  0.2  .
 87  29 ILE CB C  41.14  0.2  .
 88  29 ILE N  N 118.678 0.2  .
 89  30 ILE H  H   8.853 0.05 .
 90  30 ILE C  C 176.3   0.2  .
 91  30 ILE CA C  58.77  0.2  .
 92  30 ILE CB C  42.32  0.2  .
 93  30 ILE N  N 121.109 0.2  .
 94  31 LYS H  H   8.956 0.05 .
 95  31 LYS C  C 174.2   0.2  .
 96  31 LYS CA C  54.83  0.2  .
 97  31 LYS CB C  35.63  0.2  .
 98  31 LYS N  N 127.149 0.2  .
 99  32 VAL H  H   9.718 0.05 .
100  32 VAL C  C 174.8   0.2  .
101  32 VAL CA C  61.14  0.2  .
102  32 VAL CB C  32.97  0.2  .
103  32 VAL N  N 129.923 0.2  .
104  33 THR H  H   9.087 0.05 .
105  33 THR C  C 176.3   0.2  .
106  33 THR CA C  61.74  0.2  .
107  33 THR CB C  68.44  0.2  .
108  33 THR N  N 123.977 0.2  .
109  34 LYS H  H   9.124 0.05 .
110  34 LYS C  C 176.6   0.2  .
111  34 LYS CA C  56.16  0.2  .
112  34 LYS CB C  32      0.2  .
113  34 LYS N  N 128.151 0.2  .
114  35 GLN H  H   7.395 0.05 .
115  35 GLN C  C 175.5   0.2  .
116  35 GLN CA C  55.68  0.2  .
117  35 GLN CB C  26.91  0.2  .
118  35 GLN N  N 116.253 0.2  .
```

```
119  36 ASP H  H   8.748 0.05 .
120  36 ASP C  C 174.2   0.2  .
121  36 ASP CA C  55.56  0.2  .
122  36 ASP CB C  39.77  0.2  .
123  36 ASP N  N 122.606 0.2  .
124  37 GLN H  H   7.773 0.05 .
125  37 GLN CA C  55.11  0.2  .
126  37 GLN CB C  31.02  0.2  .
127  37 GLN N  N 121.995 0.2  .
128  38 THR H  H   8.325 0.05 .
129  38 THR CA C  58.31  0.2  .
130  38 THR CB C  70.35  0.2  .
131  38 THR N  N 117.429 0.2  .
132  39 PRO C  C 173.8   0.2  .
133  39 PRO CA C  62.44  0.2  .
134  39 PRO CB C  33.51  0.2  .
135  40 THR H  H   8.376 0.05 .
136  40 THR C  C 173     0.2  .
137  40 THR CA C  62.26  0.2  .
138  40 THR CB C  68.73  0.2  .
139  40 THR N  N 114.886 0.2  .
140  41 ASN H  H   8.392 0.05 .
141  41 ASN CA C  53.65  0.2  .
142  41 ASN CB C  37.98  0.2  .
143  41 ASN N  N 123.575 0.2  .
144  42 ASP H  H   8.286 0.05 .
145  42 ASP C  C 176.7   0.2  .
146  42 ASP CA C  51.8   0.2  .
147  42 ASP CB C  39.99  0.2  .
148  42 ASP N  N 122.521 0.2  .
149  43 LYS H  H   8.332 0.05 .
150  43 LYS C  C 176.5   0.2  .
151  43 LYS CA C  55.95  0.2  .
152  43 LYS CB C  29.53  0.2  .
153  43 LYS N  N 121.354 0.2  .
154  44 ILE H  H   7.493 0.05 .
155  44 ILE C  C 175.7   0.2  .
156  44 ILE CA C  60.15  0.2  .
157  44 ILE CB C  38.34  0.2  .
158  44 ILE N  N 115.523 0.2  .
159  45 CYS H  H   8.704 0.05 .
160  45 CYS C  C 177.8   0.2  .
161  45 CYS CA C  52.5   0.2  .
162  45 CYS CB C  34.17  0.2  .
163  45 CYS N  N 109.713 0.2  .
```

```
164  46 GLN H  H   9.026 0.05 .
165  46 GLN C  C 172.8   0.2  .
166  46 GLN CA C  59.7   0.2  .
167  46 GLN CB C  28.33  0.2  .
168  46 GLN N  N 119.744 0.2  .
169  47 SER H  H   7.695 0.05 .
170  47 SER C  C 175.5   0.2  .
171  47 SER CA C  58.14  0.2  .
172  47 SER CB C  63.97  0.2  .
173  47 SER N  N 108.69  0.2  .
174  48 VAL H  H   8.494 0.05 .
175  48 VAL C  C 172.2   0.2  .
176  48 VAL CA C  61.06  0.2  .
177  48 VAL CB C  33.7   0.2  .
178  48 VAL N  N 124.911 0.2  .
179  49 THR H  H   8.691 0.05 .
180  49 THR C  C 175.2   0.2  .
181  49 THR CA C  60.51  0.2  .
182  49 THR CB C  70.9   0.2  .
183  49 THR N  N 120.578 0.2  .
184  50 GLU H  H   8.515 0.05 .
185  50 GLU C  C 174.9   0.2  .
186  50 GLU CA C  54.22  0.2  .
187  50 GLU CB C  31.44  0.2  .
188  50 GLU N  N 125.909 0.2  .
189  51 ILE H  H   8.882 0.05 .
190  51 ILE C  C 174.4   0.2  .
191  51 ILE CA C  60.08  0.2  .
192  51 ILE CB C  40.19  0.2  .
193  51 ILE N  N 126.522 0.2  .
194  52 THR H  H   8.473 0.05 .
195  52 THR C  C 175.7   0.2  .
196  52 THR CA C  60.77  0.2  .
197  52 THR CB C  69.48  0.2  .
198  52 THR N  N 119.512 0.2  .
199  53 GLU H  H   8.561 0.05 .
200  53 GLU C  C 174.4   0.2  .
201  53 GLU CA C  55.83  0.2  .
202  53 GLU CB C  30.36  0.2  .
203  53 GLU N  N 124.239 0.2  .
204  54 SER H  H   8.391 0.05 .
205  54 SER CA C  57.67  0.2  .
206  54 SER CB C  63.59  0.2  .
207  54 SER N  N 117.086 0.2  .
208  55 GLU H  H   8.546 0.05 .
```

```
209  55 GLU C  C 173     0.2  .
210  55 GLU CA C  56.24  0.2  .
211  55 GLU CB C  29.35  0.2  .
212  55 GLU N  N 122.991 0.2  .
213  56 SER H  H   8.173 0.05 .
214  56 SER CA C  57.75  0.2  .
215  56 SER CB C  63.55  0.2  .
216  56 SER N  N 116.8   0.2  .
217  57 ASP H  H   8.349 0.05 .
218  57 ASP CA C  52.41  0.2  .
219  57 ASP CB C  40.13  0.2  .
220  57 ASP N  N 123.634 0.2  .
221  58 PRO CA C  62.63  0.2  .
222  58 PRO CB C  31     0.2  .
223  59 ASP H  H   8.366 0.05 .
224  59 ASP CA C  51.93  0.2  .
225  59 ASP CB C  40.43  0.2  .
226  59 ASP N  N 121.845 0.2  .
227  60 PRO C  C 176.7   0.2  .
228  60 PRO CA C  63.13  0.2  .
229  60 PRO CB C  31.17  0.2  .
230  61 GLU H  H   8.441 0.05 .
231  61 GLU C  C 176     0.2  .
232  61 GLU CA C  56.34  0.2  .
233  61 GLU CB C  28.92  0.2  .
234  61 GLU N  N 119.426 0.2  .
235  62 VAL H  H   7.763 0.05 .
236  62 VAL C  C 176.4   0.2  .
237  62 VAL CA C  61.64  0.2  .
238  62 VAL CB C  31.94  0.2  .
239  62 VAL N  N 119.486 0.2  .
240  63 GLU H  H   8.39  0.05 .
241  63 GLU C  C 174.6   0.2  .
242  63 GLU CA C  56.15  0.2  .
243  63 GLU CB C  29.29  0.2  .
244  63 GLU N  N 124.407 0.2  .
245  64 SER H  H   8.258 0.05 .
246  64 SER C  C 176.3   0.2  .
247  64 SER CA C  57.7   0.2  .
248  64 SER CB C  63.57  0.2  .
249  64 SER N  N 116.788 0.2  .
250  65 GLU H  H   8.511 0.05 .
251  65 GLU C  C 176     0.2  .
252  65 GLU CA C  56.3   0.2  .
253  65 GLU CB C  29.24  0.2  .
```

```
254  65 GLU N  N 122.871 0.2  .
255  66 ASP H  H   8.226 0.05 .
256  66 ASP C  C 176.7   0.2  .
257  66 ASP CA C  54.04  0.2  .
258  66 ASP CB C  40.75  0.2  .
259  66 ASP N  N 120.556 0.2  .
260  67 ASP H  H   8.249 0.05 .
261  67 ASP C  C 175.1   0.2  .
262  67 ASP CA C  54     0.2  .
263  67 ASP CB C  40.31  0.2  .
264  67 ASP N  N 120.909 0.2  .
265  68 SER H  H   8.312 0.05 .
266  68 SER C  C 174.7   0.2  .
267  68 SER CA C  58.6   0.2  .
268  68 SER CB C  63.18  0.2  .
269  68 SER N  N 116.15  0.2  .
270  69 THR H  H   8.131 0.05 .
271  69 THR C  C 174.6   0.2  .
272  69 THR CA C  61.8   0.2  .
273  69 THR CB C  68.93  0.2  .
274  69 THR N  N 115.452 0.2  .
275  70 SER H  H   8.252 0.05 .
276  70 SER C  C 176.1   0.2  .
277  70 SER CA C  57.81  0.2  .
278  70 SER CB C  63.24  0.2  .
279  70 SER N  N 118.407 0.2  .
280  71 VAL H  H   8.12  0.05 .
281  71 VAL C  C 176     0.2  .
282  71 VAL CA C  61.83  0.2  .
283  71 VAL CB C  31.6   0.2  .
284  71 VAL N  N 121.416 0.2  .
285  72 GLU H  H   8.313 0.05 .
286  72 GLU C  C 175.8   0.2  .
287  72 GLU CA C  56.09  0.2  .
288  72 GLU CB C  29.5   0.2  .
289  72 GLU N  N 123.335 0.2  .
290  73 ASP H  H   8.239 0.05 .
291  73 ASP C  C 175.8   0.2  .
292  73 ASP CA C  54.08  0.2  .
293  73 ASP CB C  40.46  0.2  .
294  73 ASP N  N 121.357 0.2  .
295  74 VAL H  H   7.899 0.05 .
296  74 VAL C  C 176.9   0.2  .
297  74 VAL CA C  61.13  0.2  .
298  74 VAL CB C  32.2   0.2  .
```

```
299  74 VAL N  N 119.061 0.2  .
300  75 ASP H  H   8.346 0.05 .
301  75 ASP CA C  52.4   0.2  .
302  75 ASP CB C  39.75  0.2  .
303  75 ASP N  N 125.157 0.2  .
304  77 PRO C  C 173.5   0.2  .
305  77 PRO CA C  62.53  0.2  .
306  77 PRO CB C  31.1   0.2  .
307  78 THR H  H   8.231 0.05 .
308  78 THR C  C 172.6   0.2  .
309  78 THR CA C  62.35  0.2  .
310  78 THR CB C  70.28  0.2  .
311  78 THR N  N 119.195 0.2  .
312  79 THR H  H   8.637 0.05 .
313  79 THR C  C 175.6   0.2  .
314  79 THR CA C  61.97  0.2  .
315  79 THR CB C  69.97  0.2  .
316  79 THR N  N 122.914 0.2  .
317  80 TYR H  H   9.144 0.05 .
318  80 TYR C  C 175.6   0.2  .
319  80 TYR CA C  56.05  0.2  .
320  80 TYR CB C  40.1   0.2  .
321  80 TYR N  N 125.245 0.2  .
322  81 TYR H  H   9.348 0.05 .
323  81 TYR C  C 175     0.2  .
324  81 TYR CA C  56.85  0.2  .
325  81 TYR CB C  41.83  0.2  .
326  81 TYR N  N 118.775 0.2  .
327  82 SER H  H   8.889 0.05 .
328  82 SER C  C 176.6   0.2  .
329  82 SER CA C  56.29  0.2  .
330  82 SER CB C  63.87  0.2  .
331  82 SER N  N 116.874 0.2  .
332  83 ILE H  H   9.542 0.05 .
333  83 ILE C  C 175.4   0.2  .
334  83 ILE CA C  60.18  0.2  .
335  83 ILE CB C  39.46  0.2  .
336  83 ILE N  N 126.848 0.2  .
337  84 ILE H  H   9.412 0.05 .
338  84 ILE C  C 176     0.2  .
339  84 ILE CA C  60.38  0.2  .
340  84 ILE CB C  37.1   0.2  .
341  84 ILE N  N 133.167 0.2  .
342  85 GLY H  H   8.731 0.05 .
343  85 GLY C  C 175.4   0.2  .
```

```
344  85 GLY CA C  45.74  0.2  .
345  85 GLY N  N 116.138 0.2  .
346  86 GLY H  H   8.264 0.05 .
347  86 GLY C  C 174.5   0.2  .
348  86 GLY CA C  45.99  0.2  .
349  86 GLY N  N 112.39  0.2  .
350  87 GLY H  H   8.656 0.05 .
351  87 GLY C  C 174.7   0.2  .
352  87 GLY CA C  44.51  0.2  .
353  87 GLY N  N 106.942 0.2  .
354  88 LEU H  H   7.584 0.05 .
355  88 LEU C  C 174.6   0.2  .
356  88 LEU CA C  52.44  0.2  .
357  88 LEU CB C  45.34  0.2  .
358  88 LEU N  N 119.34  0.2  .
359  89 ARG H  H   8.807 0.05 .
360  89 ARG CA C  54.76  0.2  .
361  89 ARG CB C  30.93  0.2  .
362  89 ARG N  N 121.938 0.2  .
363  90 MET H  H   8.833 0.05 .
364  90 MET C  C 174.2   0.2  .
365  90 MET CA C  55.23  0.2  .
366  90 MET CB C  34.37  0.2  .
367  90 MET N  N 124.939 0.2  .
368  91 ASN H  H   8.631 0.05 .
369  91 ASN C  C 174.7   0.2  .
370  91 ASN CA C  51.39  0.2  .
371  91 ASN CB C  39.26  0.2  .
372  91 ASN N  N 122.904 0.2  .
373  92 PHE H  H   9.38  0.05 .
374  92 PHE C  C 172.1   0.2  .
375  92 PHE CA C  55.74  0.2  .
376  92 PHE CB C  43.24  0.2  .
377  92 PHE N  N 123.05  0.2  .
378  93 GLY H  H   8.627 0.05 .
379  93 GLY C  C 175.5   0.2  .
380  93 GLY CA C  44.45  0.2  .
381  93 GLY N  N 110.528 0.2  .
382  94 PHE H  H   8.987 0.05 .
383  94 PHE C  C 171.6   0.2  .
384  94 PHE CA C  56.89  0.2  .
385  94 PHE CB C  41.88  0.2  .
386  94 PHE N  N 121.804 0.2  .
387  95 THR H  H   9.028 0.05 .
388  95 THR C  C 174.5   0.2  .
```

```
389  95 THR CA C  61.7   0.2  .
390  95 THR CB C  69.58  0.2  .
391  95 THR N  N 123.731 0.2  .
392  96 LYS H  H   9.116 0.05 .
393  96 LYS C  C 174.1   0.2  .
394  96 LYS CA C  57.42  0.2  .
395  96 LYS CB C  27.45  0.2  .
396  96 LYS N  N 120.258 0.2  .
397  97 CYS H  H   8.002 0.05 .
398  97 CYS CA C  53.56  0.2  .
399  97 CYS CB C  43.35  0.2  .
400  97 CYS N  N 113.366 0.2  .
401  98 PRO C  C 176.4   0.2  .
402  98 PRO CA C  62.18  0.2  .
403  98 PRO CB C  30.89  0.2  .
404  99 GLN H  H   8.23  0.05 .
405  99 GLN C  C 181.2   0.2  .
406  99 GLN CA C  56.06  0.2  .
407  99 GLN CB C  28.58  0.2  .
408  99 GLN N  N 117.156 0.2  .
409 100 ILE H  H   8.267 0.05 .
410 100 ILE C  C 174.4   0.2  .
411 100 ILE CA C  58.4   0.2  .
412 100 ILE CB C  35.31  0.2  .
413 100 ILE N  N 124.872 0.2  .
414 101 LYS H  H   7.997 0.05 .
415 101 LYS C  C 173.7   0.2  .
416 101 LYS CA C  54.79  0.2  .
417 101 LYS CB C  35.68  0.2  .
418 101 LYS N  N 122.661 0.2  .
419 102 SER H  H   7.949 0.05 .
420 102 SER C  C 174     0.2  .
421 102 SER CA C  56.12  0.2  .
422 102 SER CB C  63.07  0.2  .
423 102 SER N  N 115.163 0.2  .
424 103 ILE H  H   8.209 0.05 .
425 103 ILE C  C 173.1   0.2  .
426 103 ILE CA C  61.36  0.2  .
427 103 ILE CB C  40.39  0.2  .
428 103 ILE N  N 126.709 0.2  .
429 104 SER H  H   9.101 0.05 .
430 104 SER C  C 174.8   0.2  .
431 104 SER CA C  57.44  0.2  .
432 104 SER CB C  66.51  0.2  .
433 104 SER N  N 123.631 0.2  .
```

```
434 105 GLU H  H   8.636 0.05 .
435 105 GLU C  C 171.8   0.2  .
436 105 GLU CA C  54.78  0.2  .
437 105 GLU CB C  35.13  0.2  .
438 105 GLU N  N 116.114 0.2  .
439 106 SER H  H   9.083 0.05 .
440 106 SER C  C 176     0.2  .
441 106 SER CA C  57.7   0.2  .
442 106 SER CB C  66.33  0.2  .
443 106 SER N  N 113.7   0.2  .
444 107 ALA H  H   8.829 0.05 .
445 107 ALA CA C  51.41  0.2  .
446 107 ALA CB C  20.84  0.2  .
447 107 ALA N  N 121.942 0.2  .
448 108 ASP H  H   8.265 0.05 .
449 108 ASP CA C  53.39  0.2  .
450 108 ASP CB C  42.26  0.2  .
451 108 ASP N  N 120.541 0.2  .
452 110 ASN C  C 174.3   0.2  .
453 110 ASN CA C  51.85  0.2  .
454 110 ASN CB C  37.91  0.2  .
455 111 THR H  H   8.267 0.05 .
456 111 THR C  C 173.3   0.2  .
457 111 THR CA C  60.95  0.2  .
458 111 THR CB C  70.83  0.2  .
459 111 THR N  N 114.48  0.2  .
460 112 VAL H  H   9.24  0.05 .
461 112 VAL C  C 174.5   0.2  .
462 112 VAL CA C  61.38  0.2  .
463 112 VAL CB C  33.91  0.2  .
464 112 VAL N  N 125.843 0.2  .
465 113 ASN H  H   9.188 0.05 .
466 113 ASN C  C 174.5   0.2  .
467 113 ASN CA C  50.54  0.2  .
468 113 ASN CB C  41.16  0.2  .
469 113 ASN N  N 124.921 0.2  .
470 114 ALA H  H   9.073 0.05 .
471 114 ALA C  C 175.1   0.2  .
472 114 ALA CA C  50.93  0.2  .
473 114 ALA CB C  22.06  0.2  .
474 114 ALA N  N 119.83  0.2  .
475 115 ARG H  H   8.348 0.05 .
476 115 ARG C  C 175.2   0.2  .
477 115 ARG CA C  54.38  0.2  .
478 115 ARG CB C  33.89  0.2  .
```

```
479 115 ARG N  N 118.494 0.2  .
480 116 LEU H  H   9.095 0.05 .
481 116 LEU C  C 176.1   0.2  .
482 116 LEU CA C  54.62  0.2  .
483 116 LEU CB C  42.76  0.2  .
484 116 LEU N  N 129.319 0.2  .
485 117 SER H  H   9.4   0.05 .
486 117 SER C  C 171.3   0.2  .
487 117 SER CA C  57.4   0.2  .
488 117 SER CB C  69.65  0.2  .
489 117 SER N  N 115.539 0.2  .
490 118 SER H  H   8.889 0.05 .
491 118 SER C  C 174.7   0.2  .
492 118 SER CA C  58.52  0.2  .
493 118 SER CB C  63.45  0.2  .
494 118 SER N  N 118.064 0.2  .
495 119 VAL H  H   8.087 0.05 .
496 119 VAL C  C 176.6   0.2  .
497 119 VAL CA C  59.89  0.2  .
498 119 VAL CB C  33.34  0.2  .
499 119 VAL N  N 119.304 0.2  .
500 120 SER H  H   8.445 0.05 .
501 120 SER CA C  56.25  0.2  .
502 120 SER CB C  61.44  0.2  .
503 120 SER N  N 123.23  0.2  .
504 121 PRO C  C 175.5   0.2  .
505 121 PRO CA C  62.65  0.2  .
506 121 PRO CB C  31.47  0.2  .
507 122 GLY H  H   8.779 0.05 .
508 122 GLY CA C  45.13  0.2  .
509 122 GLY N  N 108.944 0.2  .
510 123 GLN H  H   8.509 0.05 .
511 123 GLN C  C 173.9   0.2  .
512 123 GLN CA C  54.51  0.2  .
513 123 GLN CB C  30.19  0.2  .
514 123 GLN N  N 118.117 0.2  .
515 124 GLY H  H   8.492 0.05 .
516 124 GLY CA C  44.98  0.2  .
517 124 GLY N  N 107.569 0.2  .
518 125 LYS H  H   7.408 0.05 .
519 125 LYS CA C  52.85  0.2  .
520 125 LYS CB C  32.63  0.2  .
521 125 LYS N  N 117.839 0.2  .
522 126 ASP C  C 176.6   0.2  .
523 126 ASP CA C  55.01  0.2  .
```

```
524 126 ASP CB C  40.74  0.2  .
525 127 SER H  H   8.412 0.05 .
526 127 SER CA C  55.2   0.2  .
527 127 SER CB C  62.98  0.2  .
528 127 SER N  N 116.401 0.2  .
529 128 PRO C  C 177     0.2  .
530 128 PRO CA C  62.82  0.2  .
531 128 PRO CB C  31.51  0.2  .
532 129 ALA H  H   8.479 0.05 .
533 129 ALA C  C 176     0.2  .
534 129 ALA CA C  50.31  0.2  .
535 129 ALA CB C  17.99  0.2  .
536 129 ALA N  N 125.335 0.2  .
537 130 ILE H  H   8.52  0.05 .
538 130 ILE C  C 175.6   0.2  .
539 130 ILE CA C  59.21  0.2  .
540 130 ILE CB C  39.22  0.2  .
541 130 ILE N  N 115.415 0.2  .
542 131 THR H  H   8.646 0.05 .
543 131 THR C  C 176.3   0.2  .
544 131 THR CA C  61.56  0.2  .
545 131 THR CB C  70.65  0.2  .
546 131 THR N  N 110.526 0.2  .
547 132 HIS H  H   8.727 0.05 .
548 132 HIS CA C  60.88  0.2  .
549 132 HIS CB C  29.28  0.2  .
550 132 HIS N  N 120.001 0.2  .
551 133 GLU H  H   8.979 0.05 .
552 133 GLU C  C 179.5   0.2  .
553 133 GLU CA C  60.03  0.2  .
554 133 GLU CB C  28.15  0.2  .
555 133 GLU N  N 116.07  0.2  .
556 134 GLU H  H   7.73  0.05 .
557 134 GLU C  C 178.1   0.2  .
558 134 GLU CA C  58.55  0.2  .
559 134 GLU CB C  29.07  0.2  .
560 134 GLU N  N 120.095 0.2  .
561 135 ALA H  H   8.782 0.05 .
562 135 ALA C  C 179.2   0.2  .
563 135 ALA CA C  55.28  0.2  .
564 135 ALA CB C  17.97  0.2  .
565 135 ALA N  N 124.798 0.2  .
566 136 LEU H  H   7.99  0.05 .
567 136 LEU C  C 179.2   0.2  .
568 136 LEU CA C  56.92  0.2  .
```

```
569 136 LEU CB C  40.93  0.2  .
570 136 LEU N  N 116.978 0.2  .
571 137 ALA H  H   7.137 0.05 .
572 137 ALA C  C 178     0.2  .
573 137 ALA CA C  53.97  0.2  .
574 137 ALA CB C  17.05  0.2  .
575 137 ALA N  N 119.144 0.2  .
576 138 MET H  H   7.869 0.05 .
577 138 MET C  C 175.9   0.2  .
578 138 MET CA C  58.82  0.2  .
579 138 MET CB C  31.15  0.2  .
580 138 MET N  N 118.918 0.2  .
581 139 ILE H  H   7.813 0.05 .
582 139 ILE C  C 178.1   0.2  .
583 139 ILE CA C  65.09  0.2  .
584 139 ILE CB C  36.35  0.2  .
585 139 ILE N  N 113.393 0.2  .
586 140 LYS H  H   6.709 0.05 .
587 140 LYS C  C 176.6   0.2  .
588 140 LYS CA C  55.8   0.2  .
589 140 LYS CB C  31.47  0.2  .
590 140 LYS N  N 114.734 0.2  .
591 141 ASP H  H   7.851 0.05 .
592 141 ASP C  C 173.8   0.2  .
593 141 ASP CA C  54.97  0.2  .
594 141 ASP CB C  41.88  0.2  .
595 141 ASP N  N 119.178 0.2  .
596 142 CYS H  H   7.919 0.05 .
597 142 CYS C  C 175.1   0.2  .
598 142 CYS CA C  55.96  0.2  .
599 142 CYS CB C  37.2   0.2  .
600 142 CYS N  N 118.569 0.2  .
601 143 GLU H  H   8.882 0.05 .
602 143 GLU C  C 174.6   0.2  .
603 143 GLU CA C  54.06  0.2  .
604 143 GLU CB C  33     0.2  .
605 143 GLU N  N 129.484 0.2  .
606 144 VAL H  H   7.986 0.05 .
607 144 VAL C  C 176.7   0.2  .
608 144 VAL CA C  59.12  0.2  .
609 144 VAL CB C  34.27  0.2  .
610 144 VAL N  N 124.652 0.2  .
611 145 SER H  H   9.249 0.05 .
612 145 SER CA C  55.69  0.2  .
613 145 SER CB C  65.9   0.2  .
```

```
614 145 SER N  N 122.614 0.2  .
615 150 CYS H  H   8.049 0.05 .
616 150 CYS CA C  54.54  0.2  .
617 150 CYS CB C  40.15  0.2  .
618 150 CYS N  N 124.927 0.2  .
619 151 SER H  H   8.017 0.05 .
620 151 SER CA C  58.29  0.2  .
621 151 SER CB C  63.24  0.2  .
622 151 SER N  N 114.755 0.2  .
623 152 GLU C  C 176.9   0.2  .
624 152 GLU CA C  54.87  0.2  .
625 152 GLU CB C  28.32  0.2  .
626 153 GLU H  H   7.751 0.05 .
627 153 GLU C  C 176.7   0.2  .
628 153 GLU CA C  56.93  0.2  .
629 153 GLU CB C  29.45  0.2  .
630 153 GLU N  N 122.029 0.2  .
631 154 GLU H  H   8.442 0.05 .
632 154 GLU C  C 174.6   0.2  .
633 154 GLU CA C  55.38  0.2  .
634 154 GLU CB C  30.21  0.2  .
635 154 GLU N  N 126.284 0.2  .
636 155 LYS H  H   8.599 0.05 .
637 155 LYS C  C 176.9   0.2  .
638 155 LYS CA C  56.33  0.2  .
639 155 LYS CB C  30.6   0.2  .
640 155 LYS N  N 121.711 0.2  .
641 156 ASP H  H   8.16  0.05 .
642 156 ASP C  C 173.1   0.2  .
643 156 ASP CA C  54.49  0.2  .
644 156 ASP CB C  40.64  0.2  .
645 156 ASP N  N 117.447 0.2  .
646 157 SER H  H   8.478 0.05 .
647 157 SER C  C 174     0.2  .
648 157 SER CA C  60.73  0.2  .
649 157 SER CB C  64.46  0.2  .
650 157 SER N  N 114.896 0.2  .
651 158 ASP H  H   8.084 0.05 .
652 158 ASP C  C 177.3   0.2  .
653 158 ASP CA C  52.37  0.2  .
654 158 ASP CB C  39.69  0.2  .
655 158 ASP N  N 127.456 0.2  .
656 159 ILE H  H   7.465 0.05 .
657 159 ILE CA C  60.17  0.2  .
658 159 ILE CB C  38.88  0.2  .
```

```
659 159 ILE N  N 118.338 0.2  .
660 160 LYS H  H   8.621 0.05 .
661 160 LYS C  C 174.9   0.2  .
662 160 LYS CA C  52.69  0.2  .
663 160 LYS CB C  30.59  0.2  .
664 160 LYS N  N 124.908 0.2  .
665 161 THR H  H   8.378 0.05 .
666 161 THR CA C  61.1   0.2  .
667 161 THR CB C  67.5   0.2  .
668 161 THR N  N 111.995 0.2  .
669 162 HIS H  H   7.039 0.05 .
670 162 HIS CA C  52.43  0.2  .
671 162 HIS CB C  28.03  0.2  .
672 162 HIS N  N 118.193 0.2  .
673 163 PRO C  C 176.5   0.2  .
674 163 PRO CA C  62.09  0.2  .
675 163 PRO CB C  31.24  0.2  .
676 164 VAL H  H   8.605 0.05 .
677 164 VAL C  C 177.6   0.2  .
678 164 VAL CA C  62.97  0.2  .
679 164 VAL CB C  30.45  0.2  .
680 164 VAL N  N 122.908 0.2  .
681 165 LEU H  H   8.502 0.05 .
682 165 LEU C  C 173.6   0.2  .
683 165 LEU CA C  54.05  0.2  .
684 165 LEU CB C  41.76  0.2  .
685 165 LEU N  N 130.336 0.2  .
686 166 GLY H  H   8.749 0.05 .
687 166 GLY C  C 174.5   0.2  .
688 166 GLY CA C  43.93  0.2  .
689 166 GLY N  N 109.499 0.2  .
690 167 SER H  H   8.563 0.05 .
691 167 SER C  C 174.5   0.2  .
692 167 SER CA C  58.5   0.2  .
693 167 SER CB C  64.68  0.2  .
694 167 SER N  N 114.73  0.2  .
695 168 ASN H  H   8.227 0.05 .
696 168 ASN C  C 175.4   0.2  .
697 168 ASN CA C  54.65  0.2  .
698 168 ASN CB C  38.19  0.2  .
699 168 ASN N  N 115.214 0.2  .
700 169 ILE H  H   8.073 0.05 .
701 169 ILE C  C 173.6   0.2  .
702 169 ILE CA C  60.76  0.2  .
703 169 ILE CB C  37.56  0.2  .
```

```
704 169 ILE N  N 120.203 0.2  .
705 170 SER H  H   8.705 0.05 .
706 170 SER CA C  55.64  0.2  .
707 170 SER CB C  64.65  0.2  .
708 170 SER N  N 120.618 0.2  .
709 171 HIS C  C 173.6   0.2  .
710 171 HIS CA C  57.78  0.2  .
711 171 HIS CB C  28.16  0.2  .
712 172 LYS H  H   6.889 0.05 .
713 172 LYS C  C 176     0.2  .
714 172 LYS CA C  55.1   0.2  .
715 172 LYS CB C  31.49  0.2  .
716 172 LYS N  N 118.113 0.2  .
717 173 LYS H  H   8.033 0.05 .
718 173 LYS C  C 174.7   0.2  .
719 173 LYS CA C  58.22  0.2  .
720 173 LYS CB C  31.06  0.2  .
721 173 LYS N  N 118.001 0.2  .
722 174 VAL H  H   6.593 0.05 .
723 174 VAL C  C 176     0.2  .
724 174 VAL CA C  59.56  0.2  .
725 174 VAL CB C  31.96  0.2  .
726 174 VAL N  N 118.605 0.2  .
727 175 SER H  H   7.59  0.05 .
728 175 SER C  C 175.7   0.2  .
729 175 SER CA C  59.81  0.2  .
730 175 SER CB C  63.14  0.2  .
731 175 SER N  N 115.789 0.2  .
732 176 TYR H  H   8.509 0.05 .
733 176 TYR C  C 175.6   0.2  .
734 176 TYR CA C  58.94  0.2  .
735 176 TYR CB C  38.82  0.2  .
736 176 TYR N  N 124.507 0.2  .
737 177 GLU H  H   7.198 0.05 .
738 177 GLU C  C 177.3   0.2  .
739 177 GLU CA C  53.94  0.2  .
740 177 GLU CB C  32.64  0.2  .
741 177 GLU N  N 128.627 0.2  .
742 178 ASP H  H   7.787 0.05 .
743 178 ASP CA C  53.25  0.2  .
744 178 ASP CB C  40.27  0.2  .
745 178 ASP N  N 122.378 0.2  .
746 179 ILE C  C 177.2   0.2  .
747 179 ILE CA C  61.88  0.2  .
748 179 ILE CB C  41.34  0.2  .
```

```
749 180 ILE H  H   8.937 0.05 .
750 180 ILE CA C  61.44  0.2  .
751 180 ILE CB C  37.97  0.2  .
752 180 ILE N  N 120.972 0.2  .
753 181 GLY H  H   9.173 0.05 .
754 181 GLY CA C  44.23  0.2  .
755 181 GLY N  N 118.284 0.2  .
756 190 VAL C  C 174.5   0.2  .
757 191 LYS H  H   8.973 0.05 .
758 191 LYS C  C 173.7   0.2  .
759 191 LYS N  N 128.509 0.2  .
760 192 ASN H  H   7.859 0.05 .
761 192 ASN CA C  50.75  0.2  .
762 192 ASN CB C  42.14  0.2  .
763 192 ASN N  N 110.211 0.2  .
764 193 LEU H  H   9.633 0.05 .
765 193 LEU C  C 173.7   0.2  .
766 193 LEU CA C  55.05  0.2  .
767 193 LEU CB C  45.47  0.2  .
768 193 LEU N  N 121.711 0.2  .
769 194 GLU H  H   9.104 0.05 .
770 194 GLU CA C  55.77  0.2  .
771 194 GLU CB C  34.17  0.2  .
772 194 GLU N  N 124.21  0.2  .
773 195 PHE H  H   9.431 0.05 .
774 195 PHE C  C 172.8   0.2  .
775 195 PHE CA C  55.35  0.2  .
776 195 PHE CB C  43.08  0.2  .
777 195 PHE N  N 123.696 0.2  .
778 196 SER H  H   8.892 0.05 .
779 196 SER C  C 172.8   0.2  .
780 196 SER CA C  56.91  0.2  .
781 196 SER CB C  61.65  0.2  .
782 196 SER N  N 122.66  0.2  .
783 197 VAL H  H   8.717 0.05 .
784 197 VAL C  C 174.9   0.2  .
785 197 VAL CA C  59.75  0.2  .
786 197 VAL CB C  33.91  0.2  .
787 197 VAL N  N 125.661 0.2  .
788 198 ARG H  H   8.897 0.05 .
789 198 ARG C  C 174.3   0.2  .
790 198 ARG CA C  52.42  0.2  .
791 198 ARG CB C  34.36  0.2  .
792 198 ARG N  N 124.976 0.2  .
793 199 ILE H  H   7.738 0.05 .
```

```
794 199 ILE C  C 170.8   0.2  .
795 199 ILE CA C  59.76  0.2  .
796 199 ILE CB C  39.25  0.2  .
797 199 ILE N  N 119.059 0.2  .
798 200 GLY H  H   8.285 0.05 .
799 200 GLY C  C 177.7   0.2  .
800 200 GLY CA C  45.55  0.2  .
801 200 GLY N  N 111.191 0.2  .
802 201 ASP H  H   9.493 0.05 .
803 201 ASP C  C 176.4   0.2  .
804 201 ASP CA C  53.78  0.2  .
805 201 ASP CB C  42.38  0.2  .
806 201 ASP N  N 122.13  0.2  .
807 202 MET H  H   8.732 0.05 .
808 202 MET C  C 174.5   0.2  .
809 202 MET CA C  58.26  0.2  .
810 202 MET CB C  34.38  0.2  .
811 202 MET N  N 123.499 0.2  .
812 203 CYS H  H   9.359 0.05 .
813 203 CYS C  C 173.8   0.2  .
814 203 CYS CA C  57.17  0.2  .
815 203 CYS CB C  43.28  0.2  .
816 203 CYS N  N 116.482 0.2  .
817 204 LYS H  H   7.871 0.05 .
818 204 LYS C  C 177.3   0.2  .
819 204 LYS CA C  55.55  0.2  .
820 204 LYS CB C  32.79  0.2  .
821 204 LYS N  N 121.69  0.2  .
822 205 GLU H  H   8.299 0.05 .
823 205 GLU C  C 175.4   0.2  .
824 205 GLU CA C  57.21  0.2  .
825 205 GLU CB C  29.21  0.2  .
826 205 GLU N  N 123.802 0.2  .
827 206 SER H  H   8.96  0.05 .
828 206 SER CA C  57.03  0.2  .
829 206 SER CB C  63.96  0.2  .
830 206 SER N  N 121.059 0.2  .
831 207 SER C  C 175.9   0.2  .
832 207 SER CA C  61.22  0.2  .
833 207 SER CB C  62.7   0.2  .
834 208 GLU H  H   8.965 0.05 .
835 208 GLU C  C 173.4   0.2  .
836 208 GLU CA C  57.71  0.2  .
837 208 GLU CB C  28.79  0.2  .
838 208 GLU N  N 120.112 0.2  .
```

```
839 209 LEU H  H   7.99  0.05 .
840 209 LEU C  C 177     0.2  .
841 209 LEU CA C  53.25  0.2  .
842 209 LEU CB C  41.55  0.2  .
843 209 LEU N  N 117.609 0.2  .
844 210 GLU H  H   6.763 0.05 .
845 210 GLU C  C 177.4   0.2  .
846 210 GLU CA C  53.7   0.2  .
847 210 GLU CB C  28.41  0.2  .
848 210 GLU N  N 112.162 0.2  .
849 211 VAL H  H   8.445 0.05 .
850 211 VAL C  C 173.4   0.2  .
851 211 VAL CA C  58.62  0.2  .
852 211 VAL CB C  36.42  0.2  .
853 211 VAL N  N 113.5   0.2  .
854 212 LYS H  H   8.664 0.05 .
855 212 LYS C  C 175.5   0.2  .
856 212 LYS CA C  54.58  0.2  .
857 212 LYS CB C  37.29  0.2  .
858 212 LYS N  N 124.212 0.2  .
859 213 ASP H  H   9.085 0.05 .
860 213 ASP C  C 170.8   0.2  .
861 213 ASP CA C  51.53  0.2  .
862 213 ASP CB C  44.93  0.2  .
863 213 ASP N  N 124.619 0.2  .
864 214 GLY H  H   9.839 0.05 .
865 214 GLY C  C 173.4   0.2  .
866 214 GLY CA C  45.89  0.2  .
867 214 GLY N  N 111.77  0.2  .
868 215 PHE H  H   8.648 0.05 .
869 215 PHE CA C  56.43  0.2  .
870 215 PHE CB C  43.15  0.2  .
871 215 PHE N  N 119.97  0.2  .
872 216 LYS H  H   8.428 0.05 .
873 216 LYS C  C 174.4   0.2  .
874 216 LYS CA C  54.83  0.2  .
875 216 LYS CB C  34.7   0.2  .
876 216 LYS N  N 124.924 0.2  .
877 217 TYR H  H   9.327 0.05 .
878 217 TYR N  N 126.306 0.2  .
879 221 SER CA C  57.19  0.2  .
880 221 SER CB C  63.34  0.2  .
881 222 ALA H  H   8.152 0.05 .
882 222 ALA C  C 173.2   0.2  .
883 222 ALA CA C  52.46  0.2  .
```

```
884 222 ALA CB C  18.58  0.2  .
885 222 ALA N  N 123.712 0.2  .
886 223 SER H  H   8.541 0.05 .
887 223 SER C  C 177     0.2  .
888 223 SER CA C  57.7   0.2  .
889 223 SER CB C  65.13  0.2  .
890 223 SER N  N 114.777 0.2  .
891 224 LYS H  H   8.555 0.05 .
892 224 LYS C  C 172.2   0.2  .
893 224 LYS CA C  55.82  0.2  .
894 224 LYS CB C  33.91  0.2  .
895 224 LYS N  N 121.24  0.2  .
896 225 GLY H  H   7.929 0.05 .
897 225 GLY C  C 175.7   0.2  .
898 225 GLY CA C  44.88  0.2  .
899 225 GLY N  N 105.921 0.2  .
900 226 ALA H  H   8.545 0.05 .
901 226 ALA C  C 172.8   0.2  .
902 226 ALA CA C  50.94  0.2  .
903 226 ALA CB C  18.15  0.2  .
904 226 ALA N  N 124.859 0.2  .
905 227 THR H  H   8.427 0.05 .
906 227 THR CA C  59.35  0.2  .
907 227 THR CB C  70.44  0.2  .
908 227 THR N  N 115.376 0.2  .
909 228 ASP H  H   8.446 0.05 .
910 228 ASP C  C 176.8   0.2  .
911 228 ASP CA C  53.8   0.2  .
912 228 ASP CB C  40.8   0.2  .
913 228 ASP N  N 119.104 0.2  .
914 229 ASP H  H   8.446 0.05 .
915 229 ASP C  C 174.4   0.2  .
916 229 ASP CA C  53.98  0.2  .
917 229 ASP CB C  42.46  0.2  .
918 229 ASP N  N 126.778 0.2  .
919 230 THR H  H   8.427 0.05 .
920 230 THR CA C  65.77  0.2  .
921 230 THR CB C  68.79  0.2  .
922 230 THR N  N 114.088 0.2  .
923 231 SER C  C 177.2   0.2  .
924 231 SER CA C  56.8   0.2  .
925 231 SER CB C  62.72  0.2  .
926 232 LEU H  H   7.16  0.05 .
927 232 LEU CA C  58.18  0.2  .
928 232 LEU CB C  41.68  0.2  .
```

```
929 232 LEU N  N 123.454 0.2  .
930 233 ILE H  H   7.673 0.05 .
931 233 ILE CA C  57.88  0.2  .
932 233 ILE CB C  40.96  0.2  .
933 233 ILE N  N 106.389 0.2  .
934 234 ASP H  H   8.218 0.05 .
935 234 ASP CA C  51.6   0.2  .
936 234 ASP CB C  39.01  0.2  .
937 234 ASP N  N 120.061 0.2  .
938 235 SER C  C 176.1   0.2  .
939 235 SER CA C  61.26  0.2  .
940 235 SER CB C  62.05  0.2  .
941 236 THR H  H   8.349 0.05 .
942 236 THR C  C 176.6   0.2  .
943 236 THR CA C  63.95  0.2  .
944 236 THR CB C  68.18  0.2  .
945 236 THR N  N 112.692 0.2  .
946 237 LYS H  H   6.907 0.05 .
947 237 LYS C  C 176.4   0.2  .
948 237 LYS CA C  54.81  0.2  .
949 237 LYS CB C  32.05  0.2  .
950 237 LYS N  N 117.724 0.2  .
951 238 LEU H  H   6.77  0.05 .
952 238 LEU C  C 175.1   0.2  .
953 238 LEU CA C  55.46  0.2  .
954 238 LEU CB C  41.39  0.2  .
955 238 LEU N  N 116.92  0.2  .
956 239 LYS H  H   8.637 0.05 .
957 239 LYS C  C 176.8   0.2  .
958 239 LYS CA C  53.37  0.2  .
959 239 LYS CB C  33.66  0.2  .
960 239 LYS N  N 119.987 0.2  .
961 240 ALA H  H   8.655 0.05 .
962 240 ALA C  C 175.3   0.2  .
963 240 ALA CA C  52.92  0.2  .
964 240 ALA CB C  18.15  0.2  .
965 240 ALA N  N 123.45  0.2  .
966 241 CYS H  H   9.184 0.05 .
967 241 CYS CA C  52.32  0.2  .
968 241 CYS CB C  35.19  0.2  .
969 241 CYS N  N 116.929 0.2  .
970 242 VAL H  H   7.625 0.05 .
971 242 VAL CA C  62.23  0.2  .
972 242 VAL CB C  33.89  0.2  .
973 242 VAL N  N 118.701 0.2  .
```

APPENDIX B

RESONANCE ASSIGNMENTS OF THE 34 KD RABBITPOX VCCI:HUMAN MIP-1B COMPLEX

BMRB Accession Code 7024 (http://www.bmrb.wisc.edu)

```
Mol_system_component_name       "human MIP-1b"
      _Atom_shift_assign_ID
      _Residue_author_seq_code
      _Residue_seq_code
      _Residue_label
      _Atom_name
      _Atom_type
      _Chem_shift_value
      _Chem_shift_value_error
      _Chem_shift_ambiguity_code

        1  1  1 ALA HB   H   1.501  0.028 .
        2  1  1 ALA CB   C  18.200  0.12  .
        3  2  2 PRO HA   H   4.475  0.028 .
        4  2  2 PRO HB2  H   1.900  0.028 .
        5  2  2 PRO HB3  H   2.312  0.028 .
        6  2  2 PRO HG2  H   1.973  0.028 .
        7  2  2 PRO HG3  H   2.036  0.028 .
        8  2  2 PRO HD2  H   3.582  0.028 .
        9  2  2 PRO HD3  H   3.690  0.028 .
       10  2  2 PRO CA   C  63.0985 0.12  .
       11  2  2 PRO CB   C  32.0035 0.12  .
       12  2  2 PRO CG   C  27.507  0.12  .
       13  2  2 PRO CD   C  50.447  0.12  .
       14  3  3 MET H    H   8.5273 0.028 .
       15  3  3 MET HA   H   4.451  0.028 .
       16  3  3 MET HB2  H   2.050  0.028 .
       17  3  3 MET HB3  H   2.092  0.028 .
       18  3  3 MET HG2  H   2.588  0.028 .
       19  3  3 MET HG3  H   2.641  0.028 .
       20  3  3 MET HE   H   2.098  0.028 .
       21  3  3 MET CA   C  55.8967 0.12  .
       22  3  3 MET CB   C  33.0430 0.12  .
```

```
23  3  3 MET CG   C  32.035  0.12  .
24  3  3 MET CE   C  17.004  0.12  .
25  3  3 MET N    N 121.2883 0.113 .
26  4  4 GLY H    H   8.4210 0.028 .
27  4  4 GLY HA2  H   3.996  0.028 .
28  4  4 GLY HA3  H   3.996  0.028 .
29  4  4 GLY CA   C  45.4120 0.12  .
30  4  4 GLY N    N 110.6100 0.113 .
31  5  5 SER H    H   8.0800 0.028 .
32  5  5 SER HA   H   4.447  0.028 .
33  5  5 SER HB2  H   3.818  0.028 .
34  5  5 SER HB3  H   3.818  0.028 .
35  5  5 SER CA   C  58.2420 0.12  .
36  5  5 SER CB   C  64.0040 0.12  .
37  5  5 SER N    N 115.1140 0.113 .
38  6  6 ASP H    H   8.2080 0.028 .
39  6  6 ASP HA   H   4.837  0.028 .
40  6  6 ASP HB2  H   2.363  0.028 .
41  6  6 ASP HB3  H   2.556  0.028 .
42  6  6 ASP CA   C  52.7790 0.12  .
43  6  6 ASP CB   C  40.5670 0.12  .
44  6  6 ASP N    N 122.7560 0.113 .
45  8  8 PRO HA   H   4.536  0.028 .
46  8  8 PRO HB2  H   2.016  0.028 .
47  8  8 PRO HB3  H   2.218  0.028 .
48  8  8 PRO HG2  H   2.023  0.028 .
49  8  8 PRO HG3  H   2.023  0.028 .
50  8  8 PRO CA   C  63.3290 0.12  .
51  8  8 PRO CB   C  32.0220 0.12  .
52  8  8 PRO CG   C  26.968  0.12  .
53  9  9 THR H    H   7.8390 0.028 .
54  9  9 THR HA   H   4.408  0.028 .
55  9  9 THR HB   H   4.578  0.028 .
56  9  9 THR HG2  H   1.156  0.028 .
57  9  9 THR CA   C  60.8610 0.12  .
58  9  9 THR CB   C  69.3060 0.12  .
59  9  9 THR CG2  C  21.868  0.12  .
60  9  9 THR N    N 109.7970 0.113 .
61 10 10 ALA H    H   7.6090 0.028 .
62 10 10 ALA HA   H   5.148  0.028 .
63 10 10 ALA HB   H   1.347  0.028 .
64 10 10 ALA CA   C  52.0950 0.12  .
65 10 10 ALA CB   C  19.6620 0.12  .
66 10 10 ALA N    N 124.7880 0.113 .
67 11 11 CYS H    H   8.2230 0.028 .
```

```
 68 11 11 CYS HA   H   5.234  0.028 .
 69 11 11 CYS HB2  H   2.043  0.028 .
 70 11 11 CYS HB3  H   2.997  0.028 .
 71 11 11 CYS CA   C  51.6360 0.12  .
 72 11 11 CYS CB   C  40.7930 0.12  .
 73 11 11 CYS N    N 115.877  0.113 .
 74 12 12 CYS H    H   9.1890 0.028 .
 75 12 12 CYS HA   H   5.300  0.028 .
 76 12 12 CYS HB2  H   2.391  0.028 .
 77 12 12 CYS HB3  H   2.965  0.028 .
 78 12 12 CYS CA   C  55.6260 0.12  .
 79 12 12 CYS CB   C  45.3720 0.12  .
 80 12 12 CYS N    N 119.3210 0.113 .
 81 13 13 PHE H    H   8.5770 0.028 .
 82 13 13 PHE HA   H   4.481  0.028 .
 83 13 13 PHE HB2  H   3.360  0.028 .
 84 13 13 PHE HB3  H   3.360  0.028 .
 85 13 13 PHE HD1  H   6.910  0.028 .
 86 13 13 PHE HD2  H   6.910  0.028 .
 87 13 13 PHE HE1  H   6.670  0.028 .
 88 13 13 PHE HE2  H   6.670  0.028 .
 89 13 13 PHE CA   C  57.4950 0.12  .
 90 13 13 PHE CB   C  42.9420 0.12  .
 91 13 13 PHE CD1  C 131.0000 0.12  .
 92 13 13 PHE CE1  C 129.3200 0.12  .
 93 13 13 PHE N    N 117.7070 0.113 .
 94 14 14 SER H    H   7.3300 0.028 .
 95 14 14 SER HA   H   4.124  0.028 .
 96 14 14 SER HB2  H   3.639  0.028 .
 97 14 14 SER HB3  H   3.757  0.028 .
 98 14 14 SER CA   C  57.2900 0.12  .
 99 14 14 SER CB   C  63.1830 0.12  .
100 14 14 SER N    N 112.2940 0.113 .
101 15 15 TYR H    H   8.3870 0.028 .
102 15 15 TYR HA   H   4.943  0.028 .
103 15 15 TYR HB2  H   2.830  0.028 .
104 15 15 TYR HB3  H   3.337  0.028 .
105 15 15 TYR HD1  H   6.890  0.028 .
106 15 15 TYR HD2  H   6.890  0.028 .
107 15 15 TYR HE1  H   6.820  0.028 .
108 15 15 TYR HE2  H   6.820  0.028 .
109 15 15 TYR CA   C  55.2900 0.12  .
110 15 15 TYR CB   C  41.7520 0.12  .
111 15 15 TYR CD1  C 133.1000 0.12  .
112 15 15 TYR CE1  C 117.4000 0.12  .
```

```
113 15 15 TYR N    N 123.4350 0.113 .
114 16 16 THR H    H   8.3490 0.028 .
115 16 16 THR HA   H   4.363  0.028 .
116 16 16 THR HB   H   4.417  0.028 .
117 16 16 THR HG2  H   1.646  0.028 .
118 16 16 THR CA   C  62.5210 0.12  .
119 16 16 THR CB   C  69.0640 0.12  .
120 16 16 THR CG2  C  19.116  0.12  .
121 16 16 THR N    N 112.8730 0.113 .
122 17 17 ALA H    H   9.4430 0.028 .
123 17 17 ALA HA   H   4.710  0.028 .
124 17 17 ALA HB   H   1.524  0.028 .
125 17 17 ALA CA   C  52.4740 0.12  .
126 17 17 ALA CB   C  19.7610 0.12  .
127 17 17 ALA N    N 131.9760 0.113 .
128 18 18 ARG H    H   8.2200 0.028 .
129 18 18 ARG HA   H   4.420  0.028 .
130 18 18 ARG HB2  H   1.553  0.028 .
131 18 18 ARG HB3  H   1.668  0.028 .
132 18 18 ARG HG2  H   1.471  0.028 .
133 18 18 ARG HG3  H   1.471  0.028 .
134 18 18 ARG HD2  H   3.074  0.028 .
135 18 18 ARG HD3  H   3.189  0.028 .
136 18 18 ARG CA   C  54.4390 0.12  .
137 18 18 ARG CB   C  33.0010 0.12  .
138 18 18 ARG CG   C  27.386  0.12  .
139 18 18 ARG CD   C  43.310  0.12  .
140 18 18 ARG N    N 119.6700 0.113 .
141 19 19 LYS H    H   7.7320 0.028 .
142 19 19 LYS HA   H   2.252  0.028 .
143 19 19 LYS HB2  H   0.594  0.028 .
144 19 19 LYS HB3  H   0.919  0.028 .
145 19 19 LYS HG2  H  -0.132  0.028 .
146 19 19 LYS HG3  H   0.207  0.028 .
147 19 19 LYS HD2  H   1.193  0.028 .
148 19 19 LYS HD3  H   1.283  0.028 .
149 19 19 LYS HE2  H   2.758  0.028 .
150 19 19 LYS HE3  H   2.791  0.028 .
151 19 19 LYS CA   C  55.8280 0.12  .
152 19 19 LYS CB   C  32.0870 0.12  .
153 19 19 LYS CG   C  23.422  0.12  .
154 19 19 LYS CD   C  29.572  0.12  .
155 19 19 LYS CE   C  41.852  0.12  .
156 19 19 LYS N    N 120.5930 0.113 .
157 20 20 LEU H    H   5.049  0.028 .
```

```
158 20 20 LEU HA   H   4.304  0.028 .
159 20 20 LEU HB2  H   1.408  0.028 .
160 20 20 LEU HB3  H   1.408  0.028 .
161 20 20 LEU HG   H   1.686  0.028 .
162 20 20 LEU HD1  H   1.051  0.028 .
163 20 20 LEU HD2  H   0.939  0.028 .
164 20 20 LEU CA   C  52.507  0.12  .
165 20 20 LEU CB   C  43.742  0.12  .
166 20 20 LEU CG   C  26.829  0.12  .
167 20 20 LEU CD1  C  25.506  0.12  .
168 20 20 LEU CD2  C  25.805  0.12  .
169 20 20 LEU N    N 129.067  0.113 .
170 21 21 PRO HA   H   4.110  0.028 .
171 21 21 PRO HB2  H   1.105  0.028 .
172 21 21 PRO HB3  H   1.977  0.028 .
173 21 21 PRO CA   C  63.2190 0.12  .
174 21 21 PRO CB   C  31.2730 0.12  .
175 22 22 ARG H    H   8.3590 0.028 .
176 22 22 ARG HA   H   3.459  0.028 .
177 22 22 ARG HB2  H   1.552  0.028 .
178 22 22 ARG HB3  H   1.552  0.028 .
179 22 22 ARG CA   C  57.8990 0.12  .
180 22 22 ARG CB   C  28.5420 0.12  .
181 22 22 ARG N    N 127.0300 0.113 .
182 23 23 ASN H    H   8.6710 0.028 .
183 23 23 ASN HA   H   4.457  0.028 .
184 23 23 ASN HB2  H   2.696  0.028 .
185 23 23 ASN HB3  H   2.696  0.028 .
186 23 23 ASN CA   C  54.6700 0.12  .
187 23 23 ASN CB   C  37.0040 0.12  .
188 23 23 ASN N    N 113.4150 0.113 .
189 24 24 PHE H    H   7.4821 0.028 .
190 24 24 PHE HA   H   4.855  0.028 .
191 24 24 PHE HB2  H   3.097  0.028 .
192 24 24 PHE HB3  H   3.429  0.028 .
193 24 24 PHE HD1  H   7.095  0.028 .
194 24 24 PHE HD2  H   7.095  0.028 .
195 24 24 PHE HE1  H   7.260  0.028 .
196 24 24 PHE HE2  H   7.260  0.028 .
197 24 24 PHE CA   C  56.0529 0.12  .
198 24 24 PHE CB   C  39.0468 0.12  .
199 24 24 PHE N    N 116.6377 0.113 .
200 25 25 VAL H    H   7.4334 0.028 .
201 25 25 VAL HA   H   3.961  0.028 .
202 25 25 VAL HB   H   2.068  0.028 .
```

```
203 25 25 VAL HG1  H   0.844  0.028 .
204 25 25 VAL HG2  H   1.069  0.028 .
205 25 25 VAL CA   C  64.1621 0.12  .
206 25 25 VAL CB   C  32.8526 0.12  .
207 25 25 VAL CG1  C  22.371  0.12  .
208 25 25 VAL CG2  C  23.695  0.12  .
209 25 25 VAL N    N 118.3007 0.113 .
210 26 26 VAL H    H   8.8590 0.028 .
211 26 26 VAL HA   H   4.584  0.028 .
212 26 26 VAL HB   H   2.192  0.028 .
213 26 26 VAL HG1  H   0.876  0.028 .
214 26 26 VAL HG2  H   0.678  0.028 .
215 26 26 VAL CA   C  61.2329 0.12  .
216 26 26 VAL CB   C  33.5565 0.12  .
217 26 26 VAL CG1  C  21.151  0.12  .
218 26 26 VAL CG2  C  18.818  0.12  .
219 26 26 VAL N    N 119.0764 0.113 .
220 27 27 ASP H    H   8.2318 0.028 .
221 27 27 ASP HA   H   4.981  0.028 .
222 27 27 ASP HB2  H   2.717  0.028 .
223 27 27 ASP HB3  H   2.819  0.028 .
224 27 27 ASP CA   C  53.5463 0.12  .
225 27 27 ASP CB   C  43.4975 0.12  .
226 27 27 ASP N    N 118.7743 0.113 .
227 28 28 TYR H    H   9.5247 0.028 .
228 28 28 TYR HA   H   5.873  0.028 .
229 28 28 TYR HB2  H   2.922  0.028 .
230 28 28 TYR HB3  H   2.492  0.028 .
231 28 28 TYR HD1  H   6.7760 0.028 .
232 28 28 TYR HE1  H   6.7200 0.028 .
233 28 28 TYR CA   C  56.5261 0.12  .
234 28 28 TYR CB   C  42.7351 0.12  .
235 28 28 TYR CD1  C 133.0000 0.12  .
236 28 28 TYR CE1  C 118.2000 0.12  .
237 28 28 TYR N    N 119.1694 0.113 .
238 29 29 TYR H    H   8.5831 0.028 .
239 29 29 TYR HA   H   4.251  0.028 .
240 29 29 TYR HB2  H   2.886  0.028 .
241 29 29 TYR HB3  H   2.886  0.028 .
242 29 29 TYR HD1  H   6.7400 0.028 .
243 29 29 TYR HE1  H   6.4570 0.028 .
244 29 29 TYR CA   C  56.8635 0.12  .
245 29 29 TYR CB   C  40.0260 0.12  .
246 29 29 TYR CD1  C 134.0000 0.12  .
247 29 29 TYR CE1  C 117.3000 0.12  .
```

```
248 29 29 TYR N    N 114.8540 0.113 .
249 30 30 GLU H    H   8.6517 0.028 .
250 30 30 GLU HA   H   5.119  0.028 .
251 30 30 GLU HB2  H   1.983  0.028 .
252 30 30 GLU HB3  H   2.186  0.028 .
253 30 30 GLU HG2  H   2.339  0.028 .
254 30 30 GLU HG3  H   2.371  0.028 .
255 30 30 GLU CA   C  54.9777 0.12  .
256 30 30 GLU CB   C  32.2517 0.12  .
257 30 30 GLU CG   C  37.700  0.12  .
258 30 30 GLU N    N 119.3211 0.113 .
259 31 31 THR H    H   7.9020 0.028 .
260 31 31 THR HA   H   4.470  0.028 .
261 31 31 THR HB   H   4.877  0.028 .
262 31 31 THR HG2  H   1.204  0.028 .
263 31 31 THR CA   C  62.2392 0.12  .
264 31 31 THR CB   C  70.5225 0.12  .
265 31 31 THR CG2  C  23.059  0.12  .
266 31 31 THR N    N 111.7390 0.113 .
267 32 32 SER H    H   9.0470 0.028 .
268 32 32 SER HA   H   4.493  0.028 .
269 32 32 SER HB2  H   3.965  0.028 .
270 32 32 SER HB3  H   4.284  0.028 .
271 32 32 SER CA   C  58.2990 0.12  .
272 32 32 SER CB   C  64.8500 0.12  .
273 32 32 SER N    N 115.2920 0.113 .
274 33 33 SER HA   H   4.381  0.028 .
275 33 33 SER HB2  H   4.092  0.028 .
276 33 33 SER HB3  H   4.007  0.028 .
277 33 33 SER CA   C  60.6660 0.12  .
278 33 33 SER CB   C  62.8580 0.12  .
279 34 34 LEU H    H   8.0750 0.028 .
280 34 34 LEU HA   H   4.259  0.028 .
281 34 34 LEU HB2  H   1.634  0.028 .
282 34 34 LEU HB3  H   1.634  0.028 .
283 34 34 LEU HG   H   1.648  0.028 .
284 34 34 LEU HD1  H   0.870  0.028 .
285 34 34 LEU HD2  H   0.866  0.028 .
286 34 34 LEU CA   C  56.2690 0.12  .
287 34 34 LEU CB   C  41.9090 0.12  .
288 34 34 LEU CG   C  27.315  0.12  .
289 34 34 LEU CD1  C  25.045  0.12  .
290 34 34 LEU CD2  C  23.363  0.12  .
291 34 34 LEU N    N 120.5170 0.113 .
292 35 35 CYS H    H   7.5770 0.028 .
```

```
293 35 35 CYS HA   H   4.728  0.028 .
294 35 35 CYS HB2  H   2.772  0.028 .
295 35 35 CYS HB3  H   3.700  0.028 .
296 35 35 CYS CA   C  53.9320 0.12  .
297 35 35 CYS CB   C  37.7310 0.12  .
298 35 35 CYS N    N 118.5510 0.113 .
299 36 36 SER H    H   8.6790 0.028 .
300 36 36 SER HA   H   4.207  0.028 .
301 36 36 SER HB2  H   4.113  0.028 .
302 36 36 SER HB3  H   4.113  0.028 .
303 36 36 SER CA   C  60.9320 0.12  .
304 36 36 SER CB   C  63.5290 0.12  .
305 36 36 SER N    N 117.9860 0.113 .
306 37 37 GLN H    H   8.1150 0.028 .
307 37 37 GLN HA   H   4.975  0.028 .
308 37 37 GLN HB2  H   1.914  0.028 .
309 37 37 GLN HB3  H   2.028  0.028 .
310 37 37 GLN HG2  H   2.122  0.028 .
311 37 37 GLN HG3  H   2.288  0.028 .
312 37 37 GLN HE21 H   6.3960 0.028 .
313 37 37 GLN HE22 H   6.2370 0.028 .
314 37 37 GLN CA   C  52.4970 0.12  .
315 37 37 GLN CB   C  29.7370 0.12  .
316 37 37 GLN CG   C  33.317  0.12  .
317 37 37 GLN N    N 120.0630 0.113 .
318 37 37 GLN NE2  N 107.3180 0.113 .
319 38 38 PRO HA   H   4.590  0.028 .
320 38 38 PRO HB2  H   1.814  0.028 .
321 38 38 PRO HB3  H   2.232  0.028 .
322 38 38 PRO HG2  H   2.006  0.028 .
323 38 38 PRO HG3  H   2.006  0.028 .
324 38 38 PRO HD2  H   3.834  0.028 .
325 38 38 PRO HD3  H   3.834  0.028 .
326 38 38 PRO CA   C  62.0990 0.12  .
327 38 38 PRO CB   C  32.8310 0.12  .
328 38 38 PRO CG   C  27.253  0.12  .
329 38 38 PRO CD   C  50.534  0.12  .
330 39 39 ALA H    H   8.1250 0.028 .
331 39 39 ALA HA   H   4.621  0.028 .
332 39 39 ALA HB   H   1.552  0.028 .
333 39 39 ALA CA   C  53.4680 0.12  .
334 39 39 ALA CB   C  24.3640 0.12  .
335 39 39 ALA N    N 120.4190 0.113 .
336 40 40 VAL H    H   7.8250 0.028 .
337 40 40 VAL HA   H   3.999  0.028 .
```

```
338 40 40 VAL HB   H   1.122  0.028 .
339 40 40 VAL HG1  H  -0.187  0.028 .
340 40 40 VAL HG2  H   0.596  0.028 .
341 40 40 VAL CA   C  62.1540 0.12  .
342 40 40 VAL CB   C  33.6470 0.12  .
343 40 40 VAL CG1  C  20.969  0.12  .
344 40 40 VAL CG2  C  21.955  0.12  .
345 40 40 VAL N    N 121.3990 0.113 .
346 41 41 VAL H    H   8.8650 0.028 .
347 41 41 VAL HA   H   4.291  0.028 .
348 41 41 VAL HB   H   0.385  0.028 .
349 41 41 VAL HG1  H   0.372  0.028 .
350 41 41 VAL HG2  H   0.349  0.028 .
351 41 41 VAL CA   C  60.3060 0.12  .
352 41 41 VAL CB   C  31.4650 0.12  .
353 41 41 VAL CG1  C  22.565  0.12  .
354 41 41 VAL CG2  C  22.318  0.12  .
355 41 41 VAL N    N 127.0090 0.113 .
356 42 42 PHE H    H   8.9700 0.028 .
357 42 42 PHE HA   H   5.138  0.028 .
358 42 42 PHE HB2  H   3.071  0.028 .
359 42 42 PHE HB3  H   2.776  0.028 .
360 42 42 PHE HD2  H   7.2760 0.028 .
361 42 42 PHE CA   C  57.9240 0.12  .
362 42 42 PHE CB   C  41.0290 0.12  .
363 42 42 PHE CD1  C 131.6000 0.12  .
364 42 42 PHE N    N 123.3600 0.113 .
365 43 43 GLN H    H   8.7480 0.028 .
366 43 43 GLN HA   H   5.249  0.028 .
367 43 43 GLN HB2  H   1.890  0.028 .
368 43 43 GLN HB3  H   2.058  0.028 .
369 43 43 GLN HG2  H   2.229  0.028 .
370 43 43 GLN HG3  H   2.277  0.028 .
371 43 43 GLN CA   C  54.0890 0.12  .
372 43 43 GLN CB   C  30.8400 0.12  .
373 43 43 GLN CG   C  34.538  0.12  .
374 43 43 GLN N    N 121.9430 0.113 .
375 44 44 THR H    H   8.4360 0.028 .
376 44 44 THR HA   H   5.671  0.028 .
377 44 44 THR HB   H   4.731  0.028 .
378 44 44 THR HG2  H   1.046  0.028 .
379 44 44 THR CA   C  59.9610 0.12  .
380 44 44 THR CB   C  70.8820 0.12  .
381 44 44 THR CG2  C  21.318  0.12  .
382 44 44 THR N    N 115.2720 0.113 .
```

```
383 45 45 ALA H    H   8.7110 0.028 .
384 45 45 ALA HA   H   4.060  0.028 .
385 45 45 ALA HB   H   1.498  0.028 .
386 45 45 ALA CA   C  54.7010 0.12  .
387 45 45 ALA CB   C  17.7590 0.12  .
388 45 45 ALA N    N 125.8790 0.113 .
389 46 46 ALA H    H   8.2720 0.028 .
390 46 46 ALA HA   H   4.341  0.028 .
391 46 46 ALA HB   H   1.109  0.028 .
392 46 46 ALA CA   C  52.0140 0.12  .
393 46 46 ALA CB   C  17.7890 0.12  .
394 46 46 ALA N    N 120.4530 0.113 .
395 47 47 SER H    H   8.0780 0.028 .
396 47 47 SER HA   H   3.904  0.028 .
397 47 47 SER HB2  H   4.019  0.028 .
398 47 47 SER HB3  H   4.019  0.028 .
399 47 47 SER CA   C  59.9260 0.12  .
400 47 47 SER CB   C  61.781  0.12  .
401 47 47 SER N    N 111.8340 0.113 .
402 48 48 ALA H    H   6.9790 0.028 .
403 48 48 ALA HA   H   4.060  0.028 .
404 48 48 ALA HB   H   0.744  0.028 .
405 48 48 ALA CA   C  51.1250 0.12  .
406 48 48 ALA CB   C  20.2620 0.12  .
407 48 48 ALA N    N 122.0140 0.113 .
408 49 49 GLN H    H   8.1840 0.028 .
409 49 49 GLN HA   H   5.160  0.028 .
410 49 49 GLN HB2  H   1.835  0.028 .
411 49 49 GLN HB3  H   1.638  0.028 .
412 49 49 GLN CA   C  55.1030 0.12  .
413 49 49 GLN CB   C  31.5740 0.12  .
414 49 49 GLN N    N 118.5200 0.113 .
415 50 50 VAL H    H   9.0050 0.028 .
416 50 50 VAL HA   H   4.162  0.028 .
417 50 50 VAL HB   H   2.109  0.028 .
418 50 50 VAL HG1  H   1.225  0.028 .
419 50 50 VAL HG2  H   0.969  0.028 .
420 50 50 VAL CA   C  61.6270 0.12  .
421 50 50 VAL CB   C  35.8810 0.12  .
422 50 50 VAL CG1  C  21.701  0.12  .
423 50 50 VAL CG2  C  20.272  0.12  .
424 50 50 VAL N    N 122.8400 0.113 .
425 51 51 CYS H    H   9.7580 0.028 .
426 51 51 CYS HA   H   4.739  0.028 .
427 51 51 CYS HB2  H   2.737  0.028 .
```

```
428 51 51 CYS HB3  H   2.737  0.028 .
429 51 51 CYS CA   C  57.4240 0.12  .
430 51 51 CYS CB   C  46.6530 0.12  .
431 51 51 CYS N    N 124.9820 0.113 .
432 52 52 ALA H    H   9.8880 0.028 .
433 52 52 ALA HA   H   4.914  0.028 .
434 52 52 ALA HB   H   1.237  0.028 .
435 52 52 ALA CA   C  50.5190 0.12  .
436 52 52 ALA CB   C  24.4080 0.12  .
437 52 52 ALA N    N 128.4850 0.113 .
438 53 53 ASP H    H   8.1690 0.028 .
439 53 53 ASP HA   H   4.893  0.028 .
440 53 53 ASP CA   C  52.8630 0.12  .
441 53 53 ASP CB   C  41.9240 0.12  .
442 53 53 ASP N    N 122.7730 0.113 .
443 54 54 PRO HA   H   3.906  0.028 .
444 54 54 PRO HB2  H   1.845  0.028 .
445 54 54 PRO HB3  H   2.135  0.028 .
446 54 54 PRO HG2  H   1.718  0.028 .
447 54 54 PRO HG3  H   1.787  0.028 .
448 54 54 PRO HD2  H   3.620  0.028 .
449 54 54 PRO HD3  H   4.095  0.028 .
450 54 54 PRO CA   C  63.4400 0.12  .
451 54 54 PRO CB   C  32.3230 0.12  .
452 54 54 PRO CG   C  27.078  0.12  .
453 54 54 PRO CD   C  50.693  0.12  .
454 55 55 SER H    H   8.3780 0.028 .
455 55 55 SER HA   H   4.099  0.028 .
456 55 55 SER HB2  H   3.815  0.028 .
457 55 55 SER HB3  H   3.815  0.028 .
458 55 55 SER CA   C  59.4360 0.12  .
459 55 55 SER CB   C  64.0670 0.12  .
460 55 55 SER N    N 111.8480 0.113 .
461 56 56 GLU H    H   7.5290 0.028 .
462 56 56 GLU HA   H   4.187  0.028 .
463 56 56 GLU HB2  H   1.664  0.028 .
464 56 56 GLU HB3  H   1.773  0.028 .
465 56 56 GLU HG2  H   2.104  0.028 .
466 56 56 GLU HG3  H   2.249  0.028 .
467 56 56 GLU CA   C  56.2080 0.12  .
468 56 56 GLU CB   C  30.4640 0.12  .
469 56 56 GLU CG   C  36.873  0.12  .
470 56 56 GLU N    N 123.0430 0.113 .
471 57 57 SER H    H   8.8200 0.028 .
472 57 57 SER HA   H   3.989  0.028 .
```

```
473 57 57 SER HB2  H   3.989  0.028 .
474 57 57 SER HB3  H   3.989  0.028 .
475 57 57 SER CA   C  62.268  0.12  .
476 57 57 SER CB   C  62.2680 0.12  .
477 57 57 SER N    N 120.4770 0.113 .
478 58 58 TRP H    H   8.1530 0.028 .
479 58 58 TRP HA   H   4.343  0.028 .
480 58 58 TRP HB2  H   2.9900 0.028 .
481 58 58 TRP HB3  H   3.0800 0.028 .
482 58 58 TRP HD1  H   7.5360 0.028 .
483 58 58 TRP HE1  H  10.2300 0.028 .
484 58 58 TRP HE3  H   5.7970 0.028 .
485 58 58 TRP HZ2  H   7.3640 0.028 .
486 58 58 TRP HZ3  H   6.2800 0.028 .
487 58 58 TRP HH2  H   6.7740 0.028 .
488 58 58 TRP CA   C  59.1940 0.12  .
489 58 58 TRP CB   C  26.9200 0.12  .
490 58 58 TRP CD1  C 128.3000 0.12  .
491 58 58 TRP CE3  C 121.5000 0.12  .
492 58 58 TRP CZ2  C 115.9400 0.12  .
493 58 58 TRP CZ3  C 121.9000 0.12  .
494 58 58 TRP CH2  C 122.4000 0.12  .
495 58 58 TRP N    N 119.5500 0.113 .
496 58 58 TRP NE1  N 130.3610 0.113 .
497 59 59 VAL H    H   5.5950 0.028 .
498 59 59 VAL HA   H   2.656  0.028 .
499 59 59 VAL HB   H   1.723  0.028 .
500 59 59 VAL HG1  H   0.373  0.028 .
501 59 59 VAL HG2  H  -0.708  0.028 .
502 59 59 VAL CA   C  65.7730 0.12  .
503 59 59 VAL CB   C  30.9260 0.12  .
504 59 59 VAL CG1  C  20.371  0.12  .
505 59 59 VAL CG2  C  22.139  0.12  .
506 59 59 VAL N    N 122.4190 0.113 .
507 60 60 GLN H    H   6.9330 0.028 .
508 60 60 GLN HA   H   3.756  0.028 .
509 60 60 GLN HB2  H   1.976  0.028 .
510 60 60 GLN HB3  H   2.044  0.028 .
511 60 60 GLN HG2  H   2.369  0.028 .
512 60 60 GLN HG3  H   2.369  0.028 .
513 60 60 GLN CA   C  58.2740 0.12  .
514 60 60 GLN CB   C  27.7960 0.12  .
515 60 60 GLN CG   C  33.422  0.12  .
516 60 60 GLN N    N 116.1850 0.113 .
517 61 61 GLU H    H   8.2090 0.028 .
```

```
518 61 61 GLU HA   H   4.071  0.028 .
519 61 61 GLU HB2  H   2.314  0.028 .
520 61 61 GLU HB3  H   2.314  0.028 .
521 61 61 GLU HG2  H   2.310  0.028 .
522 61 61 GLU HG3  H   2.528  0.028 .
523 61 61 GLU CA   C  59.4280 0.12  .
524 61 61 GLU CB   C  29.5110 0.12  .
525 61 61 GLU CG   C  36.514  0.12  .
526 61 61 GLU N    N 119.6170 0.113 .
527 62 62 TYR H    H   8.6640 0.028 .
528 62 62 TYR HA   H   4.410  0.028 .
529 62 62 TYR HB2  H   3.570  0.028 .
530 62 62 TYR HB3  H   2.773  0.028 .
531 62 62 TYR HD1  H   6.7360 0.028 .
532 62 62 TYR HE1  H   6.7120 0.028 .
533 62 62 TYR CA   C  59.6930 0.12  .
534 62 62 TYR CB   C  37.4550 0.12  .
535 62 62 TYR CD1  C 130.6000 0.12  .
536 62 62 TYR CE1  C 117.3000 0.12  .
537 62 62 TYR N    N 122.1140 0.113 .
538 63 63 VAL H    H   8.1770 0.028 .
539 63 63 VAL HA   H   3.090  0.028 .
540 63 63 VAL HB   H   1.803  0.028 .
541 63 63 VAL HG1  H   0.416  0.028 .
542 63 63 VAL HG2  H   0.474  0.028 .
543 63 63 VAL CA   C  67.4060 0.12  .
544 63 63 VAL CB   C  31.5740 0.12  .
545 63 63 VAL CG1  C  22.869  0.12  .
546 63 63 VAL CG2  C  20.768  0.12  .
547 63 63 VAL N    N 118.7630 0.113 .
548 64 64 TYR H    H   7.7770 0.028 .
549 64 64 TYR HA   H   4.169  0.028 .
550 64 64 TYR HB2  H   3.111  0.028 .
551 64 64 TYR HB3  H   3.185  0.028 .
552 64 64 TYR HD1  H   7.1970 0.028 .
553 64 64 TYR HE1  H   6.8170 0.028 .
554 64 64 TYR CA   C  60.9580 0.12  .
555 64 64 TYR CB   C  38.0920 0.12  .
556 64 64 TYR CD1  C 133.5000 0.12  .
557 64 64 TYR CE1  C 118.2000 0.12  .
558 64 64 TYR N    N 117.6540 0.113 .
559 65 65 ASP H    H   7.9520 0.028 .
560 65 65 ASP HA   H   4.419  0.028 .
561 65 65 ASP HB2  H   2.725  0.028 .
562 65 65 ASP HB3  H   2.913  0.028 .
```

```
563 65 65 ASP CA   C  57.4360 0.12  .
564 65 65 ASP CB   C  42.9580 0.12  .
565 65 65 ASP N    N 118.3930 0.113 .
566 66 66 LEU H    H   8.4450 0.028 .
567 66 66 LEU HA   H   4.099  0.028 .
568 66 66 LEU HB2  H   1.738  0.028 .
569 66 66 LEU HB3  H   2.061  0.028 .
570 66 66 LEU HG   H   1.798  0.028 .
571 66 66 LEU HD1  H   0.950  0.028 .
572 66 66 LEU CA   C  57.2640 0.12  .
573 66 66 LEU CB   C  42.7040 0.12  .
574 66 66 LEU CG   C  27.585  0.12  .
575 66 66 LEU CD1  C  26.959  0.12  .
576 66 66 LEU N    N 119.5930 0.113 .
577 67 67 GLU H    H   7.9050 0.028 .
578 67 67 GLU HA   H   4.319  0.028 .
579 67 67 GLU HB2  H   2.057  0.028 .
580 67 67 GLU HB3  H   2.149  0.028 .
581 67 67 GLU HG2  H   2.455  0.028 .
582 67 67 GLU HG3  H   2.499  0.028 .
583 67 67 GLU CA   C  57.4360 0.12  .
584 67 67 GLU CB   C  30.1490 0.12  .
585 67 67 GLU CG   C  36.302  0.12  .
586 67 67 GLU N    N 118.2670 0.113 .
587 68 68 LEU H    H   7.5720 0.028 .
588 68 68 LEU HA   H   4.243  0.028 .
589 68 68 LEU HB2  H   1.569  0.028 .
590 68 68 LEU HB3  H   1.667  0.028 .
591 68 68 LEU HG   H   1.664  0.028 .
592 68 68 LEU HD1  H   0.817  0.028 .
593 68 68 LEU CA   C  55.8060 0.12  .
594 68 68 LEU CB   C  42.5310 0.12  .
595 68 68 LEU CG   C  26.594  0.12  .
596 68 68 LEU CD1  C  23.539  0.12  .
597 68 68 LEU N    N 120.9570 0.113 .
598 69 69 ASN H    H   7.6670 0.028 .
599 69 69 ASN CA   C  54.9240 0.12  .
600 69 69 ASN CB   C  41.0150 0.12  .
601 69 69 ASN N    N 124.0200 0.113 .
STOP
```

```
Mol_system_component_name       "rabbitpox vCCI"
      _Atom_shift_assign_ID
      _Residue_author_seq_code
      _Residue_seq_code
      _Residue_label
      _Atom_name
      _Atom_type
      _Chem_shift_value
      _Chem_shift_value_error
      _Chem_shift_ambiguity_code

        1  17  17 GLU H  H   8.4772 0.011 .
        2  17  17 GLU C  C 176.464  0.325 .
        3  17  17 GLU CA C  55.8785 0.325 .
        4  17  17 GLU CB C  29.4452 0.325 .
        5  17  17 GLU N  N 123.7010 0.113 .
        6  18  18 GLU H  H   8.2705 0.011 .
        7  18  18 GLU C  C 176.401  0.325 .
        8  18  18 GLU CA C  56.061  0.325 .
        9  18  18 GLU CB C  30.0149 0.325 .
       10  18  18 GLU N  N 121.9503 0.113 .
       11  19  19 GLU H  H   8.4774 0.011 .
       12  19  19 GLU C  C 172.990  0.325 .
       13  19  19 GLU CA C  57.201  0.325 .
       14  19  19 GLU CB C  29.399  0.325 .
       15  19  19 GLU N  N 122.5482 0.113 .
       16  20  20 ASN H  H   8.6478 0.011 .
       17  20  20 ASN C  C 173.870  0.325 .
       18  20  20 ASN CA C  53.550  0.325 .
       19  20  20 ASN CB C  37.888  0.325 .
       20  20  20 ASN N  N 116.2207 0.113 .
       21  21  21 LYS H  H   7.1588 0.011 .
       22  21  21 LYS C  C 175.273  0.325 .
       23  21  21 LYS CA C  54.3963 0.325 .
       24  21  21 LYS CB C  34.855  0.325 .
       25  21  21 LYS N  N 116.3596 0.113 .
       26  22  22 HIS H  H   9.2475 0.011 .
       27  22  22 HIS C  C 175.137  0.325 .
       28  22  22 HIS CA C  54.573  0.325 .
       29  22  22 HIS CB C  32.1460 0.325 .
       30  22  22 HIS N  N 116.7666 0.113 .
       31  23  23 HIS H  H   9.9487 0.011 .
       32  23  23 HIS C  C 174.437  0.325 .
       33  23  23 HIS CA C  54.636  0.325 .
       34  23  23 HIS CB C  26.4697 0.325 .
```

```
35  23  23 HIS N  N 127.9639 0.113 .
36  24  24 MET H  H   7.8325 0.011 .
37  24  24 MET C  C 176.539  0.325 .
38  24  24 MET CA C  52.802  0.325 .
39  24  24 MET CB C  29.345  0.325 .
40  24  24 MET N  N 121.4663 0.113 .
41  25  25 GLY H  H   9.5646 0.011 .
42  25  25 GLY C  C 169.811  0.325 .
43  25  25 GLY CA C  42.74   0.325 .
44  25  25 GLY N  N 109.5229 0.113 .
45  26  26 ILE H  H   8.2662 0.011 .
46  26  26 ILE C  C 172.390  0.325 .
47  26  26 ILE CA C  56.8748 0.325 .
48  26  26 ILE CB C  42.165  0.325 .
49  26  26 ILE N  N 115.2975 0.113 .
50  27  27 ASP H  H   8.8485 0.011 .
51  27  27 ASP C  C 173.635  0.325 .
52  27  27 ASP CA C  54.233  0.325 .
53  27  27 ASP CB C  45.1676 0.325 .
54  27  27 ASP N  N 127.0619 0.113 .
55  28  28 VAL H  H   9.4421 0.011 .
56  28  28 VAL N  N 128.4793 0.113 .
57  30  30 ILE H  H   8.777  0.011 .
58  30  30 ILE C  C 170.920  0.325 .
59  30  30 ILE CA C  58.869  0.325 .
60  30  30 ILE CB C  42.335  0.325 .
61  30  30 ILE N  N 120.386  0.113 .
62  31  31 LYS H  H   9.0110 0.011 .
63  31  31 LYS C  C 176.217  0.325 .
64  31  31 LYS CA C  54.978  0.325 .
65  31  31 LYS CB C  36.074  0.325 .
66  31  31 LYS N  N 127.0718 0.113 .
67  32  32 VAL H  H   9.7599 0.011 .
68  32  32 VAL C  C 175.007  0.325 .
69  32  32 VAL N  N 130.0904 0.113 .
70  33  33 THR H  H   9.0244 0.011 .
71  33  33 THR C  C 174.789  0.325 .
72  33  33 THR CA C  61.7372 0.325 .
73  33  33 THR CB C  68.7893 0.325 .
74  33  33 THR N  N 123.6228 0.113 .
75  34  34 LYS H  H   9.1496 0.011 .
76  34  34 LYS C  C 176.183  0.325 .
77  34  34 LYS CA C  56.3639 0.325 .
78  34  34 LYS CB C  32.2347 0.325 .
79  34  34 LYS N  N 128.3265 0.113 .
```

```
 80  35  35 GLN H  H   7.3971 0.011 .
 81  35  35 GLN C  C 176.421  0.325 .
 82  35  35 GLN CA C  55.888  0.325 .
 83  35  35 GLN CB C  27.3182 0.325 .
 84  35  35 GLN N  N 116.2795 0.113 .
 85  36  36 ASP H  H   8.7181 0.011 .
 86  36  36 ASP C  C 171.654  0.325 .
 87  36  36 ASP CA C  55.574  0.325 .
 88  36  36 ASP CB C  40.1024 0.325 .
 89  36  36 ASP N  N 122.4009 0.113 .
 90  37  37 GLN H  H   7.7876 0.011 .
 91  37  37 GLN C  C 174.193  0.325 .
 92  37  37 GLN CA C  55.203  0.325 .
 93  37  37 GLN CB C  31.272  0.325 .
 94  37  37 GLN N  N 121.9198 0.113 .
 95  38  38 THR H  H   8.3128 0.011 .
 96  38  38 THR CA C  58.398  0.325 .
 97  38  38 THR CB C  70.607  0.325 .
 98  38  38 THR N  N 117.2693 0.113 .
 99  40  40 THR H  H   8.3759 0.011 .
100  40  40 THR C  C 173.812  0.325 .
101  40  40 THR CA C  62.2130 0.325 .
102  40  40 THR CB C  69.0553 0.325 .
103  40  40 THR N  N 114.8970 0.113 .
104  41  41 ASN H  H   8.394  0.011 .
105  41  41 ASN C  C 173.047  0.325 .
106  41  41 ASN CA C  53.687  0.325 .
107  41  41 ASN CB C  38.381  0.325 .
108  41  41 ASN N  N 123.632  0.113 .
109  42  42 ASP H  H   8.2946 0.011 .
110  42  42 ASP C  C 177.020  0.325 .
111  42  42 ASP CA C  51.9358 0.325 .
112  42  42 ASP CB C  40.2930 0.325 .
113  42  42 ASP N  N 122.6210 0.113 .
114  43  43 LYS H  H   8.2959 0.011 .
115  43  43 LYS C  C 176.756  0.325 .
116  43  43 LYS CA C  56.004  0.325 .
117  43  43 LYS CB C  29.957  0.325 .
118  43  43 LYS N  N 121.2271 0.113 .
119  44  44 ILE H  H   7.5065 0.011 .
120  44  44 ILE C  C 176.428  0.325 .
121  44  44 ILE CA C  60.2073 0.325 .
122  44  44 ILE CB C  38.7746 0.325 .
123  44  44 ILE N  N 115.5853 0.113 .
124  45  45 CYS H  H   8.6911 0.011 .
```

```
125  45  45 CYS C  C 175.723  0.325 .
126  45  45 CYS CA C  52.584  0.325 .
127  45  45 CYS CB C  34.458  0.325 .
128  45  45 CYS N  N 109.6962 0.113 .
129  46  46 GLN H  H   9.0894 0.011 .
130  46  46 GLN C  C 177.761  0.325 .
131  46  46 GLN CA C  59.737  0.325 .
132  46  46 GLN CB C  28.521  0.325 .
133  46  46 GLN N  N 119.7933 0.113 .
134  47  47 SER H  H   7.6621 0.011 .
135  47  47 SER C  C 172.834  0.325 .
136  47  47 SER CA C  58.2220 0.325 .
137  47  47 SER CB C  64.2935 0.325 .
138  47  47 SER N  N 108.6086 0.113 .
139  48  48 VAL H  H   8.4310 0.011 .
140  48  48 VAL C  C 175.627  0.325 .
141  48  48 VAL CA C  61.0005 0.325 .
142  48  48 VAL CB C  34.0859 0.325 .
143  48  48 VAL N  N 124.7000 0.113 .
144  49  49 THR H  H   8.7091 0.011 .
145  49  49 THR C  C 176.544  0.325 .
146  49  49 THR CA C  60.490  0.325 .
147  49  49 THR CB C  71.467  0.325 .
148  49  49 THR N  N 120.1580 0.113 .
149  50  50 GLU H  H   8.4857 0.011 .
150  50  50 GLU C  C 175.011  0.325 .
151  50  50 GLU CA C  54.103  0.325 .
152  50  50 GLU CB C  32.001  0.325 .
153  50  50 GLU N  N 125.3885 0.113 .
154  51  51 ILE H  H   8.9360 0.011 .
155  51  51 ILE C  C 173.848  0.325 .
156  51  51 ILE CA C  59.9726 0.325 .
157  51  51 ILE CB C  41.3623 0.325 .
158  51  51 ILE N  N 126.4737 0.113 .
159  52  52 THR H  H   8.4675 0.011 .
160  52  52 THR C  C 173.838  0.325 .
161  52  52 THR CA C  60.871  0.325 .
162  52  52 THR CB C  69.9709 0.325 .
163  52  52 THR N  N 120.7241 0.113 .
164  53  53 GLU H  H   8.748  0.011 .
165  53  53 GLU C  C 174.309  0.325 .
166  53  53 GLU CA C  55.9512 0.325 .
167  53  53 GLU CB C  29.7614 0.325 .
168  53  53 GLU N  N 127.524  0.113 .
169  54  54 SER H  H   8.0463 0.011 .
```

```
170  54  54 SER C  C 173.940  0.325 .
171  54  54 SER CA C  57.1573 0.325 .
172  54  54 SER CB C  64.8258 0.325 .
173  54  54 SER N  N 117.5771 0.113 .
174  55  55 GLU H  H   8.858  0.011 .
175  55  55 GLU C  C 176.470  0.325 .
176  55  55 GLU CA C  56.444  0.325 .
177  55  55 GLU CB C  29.8328 0.325 .
178  55  55 GLU N  N 122.977  0.113 .
179  56  56 SER H  H   8.3421 0.011 .
180  56  56 SER C  C 173.812  0.325 .
181  56  56 SER CA C  57.913  0.325 .
182  56  56 SER CB C  63.761  0.325 .
183  56  56 SER N  N 116.7604 0.113 .
184  57  57 ASP H  H   8.3942 0.011 .
185  57  57 ASP CA C  52.428  0.325 .
186  57  57 ASP CB C  40.474  0.325 .
187  57  57 ASP N  N 123.6324 0.113 .
188  59  59 ASP H  H   8.3637 0.011 .
189  59  59 ASP CA C  51.990  0.325 .
190  59  59 ASP CB C  40.802  0.325 .
191  59  59 ASP N  N 121.7651 0.113 .
192  61  61 GLU H  H   8.4445 0.011 .
193  61  61 GLU C  C 176.665  0.325 .
194  61  61 GLU CA C  56.4354 0.325 .
195  61  61 GLU CB C  29.1987 0.325 .
196  61  61 GLU N  N 119.3849 0.113 .
197  62  62 VAL H  H   7.7475 0.011 .
198  62  62 VAL C  C 175.969  0.325 .
199  62  62 VAL CA C  61.7157 0.325 .
200  62  62 VAL CB C  32.2348 0.325 .
201  62  62 VAL N  N 119.4117 0.113 .
202  63  63 GLU H  H   8.3856 0.011 .
203  63  63 GLU C  C 176.326  0.325 .
204  63  63 GLU CA C  56.232  0.325 .
205  63  63 GLU CB C  29.596  0.325 .
206  63  63 GLU N  N 124.3502 0.113 .
207  64  64 SER H  H   8.2522 0.011 .
208  64  64 SER C  C 174.608  0.325 .
209  64  64 SER CA C  57.7238 0.325 .
210  64  64 SER CB C  63.858  0.325 .
211  64  64 SER N  N 116.7822 0.113 .
212  65  65 GLU H  H   8.5110 0.011 .
213  65  65 GLU C  C 176.270  0.325 .
214  65  65 GLU CA C  56.406  0.325 .
```

```
215  65  65 GLU CB C  29.494  0.325 .
216  65  65 GLU N  N 122.8446 0.113 .
217  66  66 ASP H  H   8.2120 0.011 .
218  66  66 ASP C  C 175.967  0.325 .
219  66  66 ASP CA C  54.155  0.325 .
220  66  66 ASP CB C  41.056  0.325 .
221  66  66 ASP N  N 120.4522 0.113 .
222  67  67 ASP H  H   8.2365 0.011 .
223  67  67 ASP C  C 176.615  0.325 .
224  67  67 ASP CA C  54.0956 0.325 .
225  67  67 ASP CB C  40.724  0.325 .
226  67  67 ASP N  N 120.8361 0.113 .
227  68  68 SER H  H   8.3040 0.011 .
228  68  68 SER C  C 175.042  0.325 .
229  68  68 SER CA C  58.663  0.325 .
230  68  68 SER CB C  63.488  0.325 .
231  68  68 SER N  N 116.1157 0.113 .
232  69  69 THR H  H   8.1235 0.011 .
233  69  69 THR C  C 174.670  0.325 .
234  69  69 THR CA C  61.8696 0.325 .
235  69  69 THR CB C  69.1982 0.325 .
236  69  69 THR N  N 115.4643 0.113 .
237  70  70 SER H  H   8.2450 0.011 .
238  70  70 SER C  C 174.581  0.325 .
239  70  70 SER CA C  57.8596 0.325 .
240  70  70 SER CB C  63.530  0.325 .
241  70  70 SER N  N 118.4007 0.113 .
242  71  71 VAL H  H   8.1144 0.011 .
243  71  71 VAL C  C 176.133  0.325 .
244  71  71 VAL CA C  61.906  0.325 .
245  71  71 VAL CB C  31.866  0.325 .
246  71  71 VAL N  N 121.4130 0.113 .
247  72  72 GLU H  H   8.2878 0.011 .
248  72  72 GLU C  C 176.017  0.325 .
249  72  72 GLU CA C  56.1477 0.325 .
250  72  72 GLU CB C  29.8051 0.325 .
251  72  72 GLU N  N 123.2380 0.113 .
252  73  73 ASP H  H   8.2264 0.011 .
253  73  73 ASP C  C 175.738  0.325 .
254  73  73 ASP CA C  54.025  0.325 .
255  73  73 ASP CB C  40.727  0.325 .
256  73  73 ASP N  N 121.2519 0.113 .
257  74  74 VAL H  H   7.8492 0.011 .
258  74  74 VAL C  C 174.943  0.325 .
259  74  74 VAL CA C  61.180  0.325 .
```

```
260  74  74 VAL CB C  32.507  0.325 .
261  74  74 VAL N  N 119.0652 0.113 .
262  75  75 ASP H  H   8.3659 0.011 .
263  75  75 ASP CA C  61.182  0.325 .
264  75  75 ASP CB C  40.318  0.325 .
265  75  75 ASP N  N 124.9996 0.113 .
266  78  78 THR H  H   8.1177 0.011 .
267  78  78 THR C  C 173.246  0.325 .
268  78  78 THR CA C  62.398  0.325 .
269  78  78 THR CB C  70.611  0.325 .
270  78  78 THR N  N 118.3739 0.113 .
271  79  79 THR H  H   8.4481 0.011 .
272  79  79 THR C  C 172.345  0.325 .
273  79  79 THR CA C  62.163  0.325 .
274  79  79 THR CB C  70.375  0.325 .
275  79  79 THR N  N 123.2056 0.113 .
276  80  80 TYR H  H   9.4095 0.011 .
277  80  80 TYR C  C 175.556  0.325 .
278  80  80 TYR CA C  56.1117 0.325 .
279  80  80 TYR CB C  40.3217 0.325 .
280  80  80 TYR N  N 124.8459 0.113 .
281  81  81 TYR H  H   9.4257 0.011 .
282  81  81 TYR C  C 175.311  0.325 .
283  81  81 TYR CA C  56.878  0.325 .
284  81  81 TYR CB C  41.431  0.325 .
285  81  81 TYR N  N 119.3582 0.113 .
286  82  82 SER H  H   8.9513 0.011 .
287  82  82 SER C  C 175.136  0.325 .
288  82  82 SER CA C  56.0344 0.325 .
289  82  82 SER CB C  64.0842 0.325 .
290  82  82 SER N  N 117.3608 0.113 .
291  83  83 ILE H  H   9.611  0.011 .
292  83  83 ILE C  C 176.746  0.325 .
293  83  83 ILE CA C  60.314  0.325 .
294  83  83 ILE CB C  39.846  0.325 .
295  83  83 ILE N  N 126.596  0.113 .
296  84  84 ILE H  H   9.360  0.011 .
297  84  84 ILE C  C 175.302  0.325 .
298  84  84 ILE CA C  60.419  0.325 .
299  84  84 ILE CB C  37.3660 0.325 .
300  84  84 ILE N  N 132.999  0.113 .
301  85  85 GLY H  H   8.757  0.011 .
302  85  85 GLY C  C 176.133  0.325 .
303  85  85 GLY CA C  45.8266 0.325 .
304  85  85 GLY N  N 116.161  0.113 .
```

```
305  86  86 GLY H  H   8.2698 0.011 .
306  86  86 GLY C  C 174.314  0.325 .
307  86  86 GLY CA C  46.035  0.325 .
308  86  86 GLY N  N 112.1875 0.113 .
309  87  87 GLY H  H   8.654  0.011 .
310  87  87 GLY C  C 174.382  0.325 .
311  87  87 GLY CA C  44.659  0.325 .
312  87  87 GLY N  N 107.022  0.113 .
313  88  88 LEU H  H   7.6049 0.011 .
314  88  88 LEU C  C 173.790  0.325 .
315  88  88 LEU CA C  52.5020 0.325 .
316  88  88 LEU CB C  45.6223 0.325 .
317  88  88 LEU N  N 119.2881 0.113 .
318  89  89 ARG H  H   8.613  0.011 .
319  89  89 ARG C  C 172.566  0.325 .
320  89  89 ARG CA C  54.823  0.325 .
321  89  89 ARG CB C  30.029  0.325 .
322  89  89 ARG N  N 122.099  0.113 .
323  90  90 MET H  H   8.797  0.011 .
324  90  90 MET CA C  54.861  0.325 .
325  90  90 MET CB C  35.098  0.325 .
326  90  90 MET N  N 125.433  0.113 .
327  91  91 ASN H  H   9.0244 0.011 .
328  91  91 ASN C  C 174.467  0.325 .
329  91  91 ASN CA C  51.358  0.325 .
330  91  91 ASN CB C  40.186  0.325 .
331  91  91 ASN N  N 123.6228 0.113 .
332  92  92 PHE H  H   9.3895 0.011 .
333  92  92 PHE C  C 174.581  0.325 .
334  92  92 PHE CA C  55.959  0.325 .
335  92  92 PHE CB C  42.992  0.325 .
336  92  92 PHE N  N 124.4245 0.113 .
337  93  93 GLY H  H   8.652  0.011 .
338  93  93 GLY C  C 172.194  0.325 .
339  93  93 GLY CA C  44.624  0.325 .
340  93  93 GLY N  N 110.572  0.113 .
341  94  94 PHE H  H   8.8727 0.011 .
342  94  94 PHE C  C 175.471  0.325 .
343  94  94 PHE CA C  57.1436 0.325 .
344  94  94 PHE CB C  42.4735 0.325 .
345  94  94 PHE N  N 120.2636 0.113 .
346  95  95 THR H  H   8.7522 0.011 .
347  95  95 THR C  C 171.563  0.325 .
348  95  95 THR CA C  61.8216 0.325 .
349  95  95 THR CB C  69.9100 0.325 .
```

```
350  95  95 THR N  N 123.4455 0.113 .
351  96  96 LYS H  H   9.3386 0.011 .
352  96  96 LYS C  C 174.169  0.325 .
353  96  96 LYS CA C  57.254  0.325 .
354  96  96 LYS CB C  27.7490 0.325 .
355  96  96 LYS N  N 121.0152 0.113 .
356  97  97 CYS H  H   7.9481 0.011 .
357  97  97 CYS CA C  53.5132 0.325 .
358  97  97 CYS CB C  43.890  0.325 .
359  97  97 CYS N  N 113.0842 0.113 .
360  99  99 GLN H  H   8.2069 0.011 .
361  99  99 GLN C  C 176.217  0.325 .
362  99  99 GLN CA C  56.074  0.325 .
363  99  99 GLN CB C  28.9396 0.325 .
364  99  99 GLN N  N 116.9809 0.113 .
365 100 100 ILE H  H   8.1148 0.011 .
366 100 100 ILE C  C 175.518  0.325 .
367 100 100 ILE CA C  58.2494 0.325 .
368 100 100 ILE CB C  35.4674 0.325 .
369 100 100 ILE N  N 124.3754 0.113 .
370 101 101 LYS H  H   8.0003 0.011 .
371 101 101 LYS C  C 174.377  0.325 .
372 101 101 LYS CA C  54.2026 0.325 .
373 101 101 LYS CB C  36.1026 0.325 .
374 101 101 LYS N  N 122.5799 0.113 .
375 102 102 SER H  H   7.9511 0.011 .
376 102 102 SER C  C 173.651  0.325 .
377 102 102 SER CA C  56.2213 0.325 .
378 102 102 SER CB C  63.4292 0.325 .
379 102 102 SER N  N 115.1674 0.113 .
380 103 103 ILE H  H   8.1830 0.011 .
381 103 103 ILE C  C 174.018  0.325 .
382 103 103 ILE CA C  61.3513 0.325 .
383 103 103 ILE CB C  40.7572 0.325 .
384 103 103 ILE N  N 126.6591 0.113 .
385 104 104 SER H  H   9.1171 0.011 .
386 104 104 SER C  C 176.508  0.325 .
387 104 104 SER CA C  57.5765 0.325 .
388 104 104 SER CB C  66.7729 0.325 .
389 104 104 SER N  N 123.6521 0.113 .
390 105 105 GLU H  H   8.6478 0.011 .
391 105 105 GLU C  C 174.707  0.325 .
392 105 105 GLU CA C  54.911  0.325 .
393 105 105 GLU CB C  35.364  0.325 .
394 105 105 GLU N  N 116.2207 0.113 .
```

```
395 106 106 SER H  H   9.0981 0.011 .
396 106 106 SER C  C 171.790  0.325 .
397 106 106 SER CA C  57.8282 0.325 .
398 106 106 SER CB C  66.5891 0.325 .
399 106 106 SER N  N 113.9075 0.113 .
400 107 107 ALA H  H   8.8157 0.011 .
401 107 107 ALA C  C 176.104  0.325 .
402 107 107 ALA CA C  51.5106 0.325 .
403 107 107 ALA CB C  21.2273 0.325 .
404 107 107 ALA N  N 121.8496 0.113 .
405 108 108 ASP H  H   8.2926 0.011 .
406 108 108 ASP CA C  53.4460 0.325 .
407 108 108 ASP CB C  42.5741 0.325 .
408 108 108 ASP N  N 120.5204 0.113 .
409 111 111 THR H  H   8.288  0.011 .
410 111 111 THR C  C 174.193  0.325 .
411 111 111 THR CA C  61.045  0.325 .
412 111 111 THR CB C  71.060  0.325 .
413 111 111 THR N  N 114.705  0.113 .
414 112 112 VAL H  H   9.260  0.011 .
415 112 112 VAL C  C 173.326  0.325 .
416 112 112 VAL CA C  61.369  0.325 .
417 112 112 VAL CB C  34.289  0.325 .
418 112 112 VAL N  N 125.966  0.113 .
419 113 113 ASN H  H   9.1996 0.011 .
420 113 113 ASN C  C 174.433  0.325 .
421 113 113 ASN CA C  50.6406 0.325 .
422 113 113 ASN CB C  41.408  0.325 .
423 113 113 ASN N  N 124.9551 0.113 .
424 114 114 ALA H  H   9.062  0.011 .
425 114 114 ALA C  C 174.405  0.325 .
426 114 114 ALA CA C  50.996  0.325 .
427 114 114 ALA CB C  22.343  0.325 .
428 114 114 ALA N  N 119.799  0.113 .
429 115 115 ARG H  H   8.324  0.011 .
430 115 115 ARG C  C 175.136  0.325 .
431 115 115 ARG CA C  54.422  0.325 .
432 115 115 ARG CB C  34.107  0.325 .
433 115 115 ARG N  N 118.329  0.113 .
434 116 116 LEU H  H   9.1133 0.011 .
435 116 116 LEU C  C 175.133  0.325 .
436 116 116 LEU CA C  54.5865 0.325 .
437 116 116 LEU CB C  43.2755 0.325 .
438 116 116 LEU N  N 129.1430 0.113 .
439 117 117 SER H  H   9.3940 0.011 .
```

```
440 117 117 SER C  C 176.078  0.325 .
441 117 117 SER CA C  57.4654 0.325 .
442 117 117 SER CB C  70.0237 0.325 .
443 117 117 SER N  N 115.3913 0.113 .
444 118 118 SER H  H   8.8745 0.011 .
445 118 118 SER C  C 171.288  0.325 .
446 118 118 SER CA C  58.5145 0.325 .
447 118 118 SER CB C  63.6756 0.325 .
448 118 118 SER N  N 118.0411 0.113 .
449 119 119 VAL H  H   8.0572 0.011 .
450 119 119 VAL C  C 174.734  0.325 .
451 119 119 VAL CA C  59.9343 0.325 .
452 119 119 VAL CB C  33.6890 0.325 .
453 119 119 VAL N  N 119.2793 0.113 .
454 120 120 SER H  H   8.4481 0.011 .
455 120 120 SER CA C  57.655  0.325 .
456 120 120 SER CB C  61.791  0.325 .
457 120 120 SER N  N 123.2056 0.113 .
458 122 122 GLY H  H   8.7581 0.011 .
459 122 122 GLY C  C 175.434  0.325 .
460 122 122 GLY CA C  45.2536 0.325 .
461 122 122 GLY N  N 108.9700 0.113 .
462 123 123 GLN H  H   8.5035 0.011 .
463 123 123 GLN C  C 175.868  0.325 .
464 123 123 GLN CA C  54.5999 0.325 .
465 123 123 GLN CB C  30.4626 0.325 .
466 123 123 GLN N  N 118.1177 0.113 .
467 124 124 GLY H  H   8.5017 0.011 .
468 124 124 GLY C  C 173.900  0.325 .
469 124 124 GLY CA C  45.1914 0.325 .
470 124 124 GLY N  N 107.6244 0.113 .
471 125 125 LYS H  H   7.4052 0.011 .
472 125 125 LYS CA C  52.9633 0.325 .
473 125 125 LYS CB C  32.9762 0.325 .
474 125 125 LYS N  N 117.7862 0.113 .
475 127 127 SER H  H   8.4126 0.011 .
476 127 127 SER CA C  55.258  0.325 .
477 127 127 SER CB C  63.713  0.325 .
478 127 127 SER N  N 116.3866 0.113 .
479 129 129 ALA H  H   8.486  0.011 .
480 129 129 ALA C  C 176.895  0.325 .
481 129 129 ALA CA C  50.390  0.325 .
482 129 129 ALA CB C  18.320  0.325 .
483 129 129 ALA N  N 125.388  0.113 .
484 130 130 ILE H  H   8.5207 0.011 .
```

```
485 130 130 ILE C  C 175.925  0.325 .
486 130 130 ILE CA C  59.2364 0.325 .
487 130 130 ILE CB C  39.5720 0.325 .
488 130 130 ILE N  N 115.4118 0.113 .
489 131 131 THR H  H   8.6525 0.011 .
490 131 131 THR C  C 175.585  0.325 .
491 131 131 THR CA C  61.611  0.325 .
492 131 131 THR CB C  70.932  0.325 .
493 131 131 THR N  N 110.5718 0.113 .
494 132 132 HIS H  H   8.736  0.011 .
495 132 132 HIS C  C 176.317  0.325 .
496 132 132 HIS CA C  60.801  0.325 .
497 132 132 HIS CB C  29.532  0.325 .
498 132 132 HIS N  N 120.021  0.113 .
499 133 133 GLU H  H   8.9838 0.011 .
500 133 133 GLU C  C 180.001  0.325 .
501 133 133 GLU CA C  60.0880 0.325 .
502 133 133 GLU CB C  28.4840 0.325 .
503 133 133 GLU N  N 116.0832 0.113 .
504 134 134 GLU H  H   7.7352 0.011 .
505 134 134 GLU C  C 179.496  0.325 .
506 134 134 GLU CA C  58.610  0.325 .
507 134 134 GLU CB C  29.450  0.325 .
508 134 134 GLU N  N 120.1308 0.113 .
509 135 135 ALA H  H   8.7832 0.011 .
510 135 135 ALA C  C 178.058  0.325 .
511 135 135 ALA CA C  55.367  0.325 .
512 135 135 ALA CB C  18.283  0.325 .
513 135 135 ALA N  N 124.7941 0.113 .
514 136 136 LEU H  H   7.9966 0.011 .
515 136 136 LEU C  C 179.160  0.325 .
516 136 136 LEU CA C  56.988  0.325 .
517 136 136 LEU CB C  41.2327 0.325 .
518 136 136 LEU N  N 117.0016 0.113 .
519 137 137 ALA H  H   7.1475 0.011 .
520 137 137 ALA C  C 179.187  0.325 .
521 137 137 ALA CA C  54.0407 0.325 .
522 137 137 ALA CB C  17.3585 0.325 .
523 137 137 ALA N  N 119.1213 0.113 .
524 138 138 MET H  H   7.882  0.011 .
525 138 138 MET C  C 177.934  0.325 .
526 138 138 MET CA C  58.907  0.325 .
527 138 138 MET CB C  31.557  0.325 .
528 138 138 MET N  N 119.036  0.113 .
529 139 139 ILE H  H   7.8280 0.011 .
```

```
530 139 139 ILE C  C 175.900  0.325 .
531 139 139 ILE CA C  65.1685 0.325 .
532 139 139 ILE CB C  36.7227 0.325 .
533 139 139 ILE N  N 113.5047 0.113 .
534 140 140 LYS H  H   6.7058 0.011 .
535 140 140 LYS C  C 178.042  0.325 .
536 140 140 LYS CA C  55.8075 0.325 .
537 140 140 LYS CB C  31.7785 0.325 .
538 140 140 LYS N  N 114.6417 0.113 .
539 141 141 ASP H  H   7.867  0.011 .
540 141 141 ASP C  C 176.706  0.325 .
541 141 141 ASP CA C  55.0034 0.325 .
542 141 141 ASP CB C  42.3305 0.325 .
543 141 141 ASP N  N 119.192  0.113 .
544 142 142 CYS H  H   7.9201 0.011 .
545 142 142 CYS C  C 173.953  0.325 .
546 142 142 CYS CA C  56.012  0.325 .
547 142 142 CYS CB C  37.667  0.325 .
548 142 142 CYS N  N 118.5531 0.113 .
549 143 143 GLU H  H   8.8283 0.011 .
550 143 143 GLU C  C 175.085  0.325 .
551 143 143 GLU CA C  54.2461 0.325 .
552 143 143 GLU CB C  32.8681 0.325 .
553 143 143 GLU N  N 129.8800 0.113 .
554 144 144 VAL H  H   8.0574 0.011 .
555 144 144 VAL C  C 174.410  0.325 .
556 144 144 VAL CA C  59.0721 0.325 .
557 144 144 VAL CB C  34.4841 0.325 .
558 144 144 VAL N  N 126.3821 0.113 .
559 145 145 SER H  H   9.4100 0.011 .
560 145 145 SER C  C 173.753  0.325 .
561 145 145 SER CA C  55.249  0.325 .
562 145 145 SER CB C  66.283  0.325 .
563 145 145 SER N  N 121.8108 0.113 .
564 146 146 ILE H  H   8.7964 0.011 .
565 146 146 ILE C  C 175.162  0.325 .
566 146 146 ILE CA C  59.9745 0.325 .
567 146 146 ILE CB C  41.1324 0.325 .
568 146 146 ILE N  N 118.0337 0.113 .
569 148 148 ILE H  H   8.6284 0.011 .
570 148 148 ILE CA C  59.0825 0.325 .
571 148 148 ILE CB C  36.8061 0.325 .
572 148 148 ILE N  N 124.2178 0.113 .
573 149 149 ARG H  H   8.944  0.011 .
574 149 149 ARG C  C 175.247  0.325 .
```

```
575 149 149 ARG N  N 127.438  0.113 .
576 150 150 CYS H  H   9.1773 0.011 .
577 150 150 CYS C  C 174.714  0.325 .
578 150 150 CYS CA C  54.2887 0.325 .
579 150 150 CYS CB C  32.511  0.325 .
580 150 150 CYS N  N 120.3950 0.113 .
581 151 151 SER H  H   7.8878 0.011 .
582 151 151 SER CA C  56.5805 0.325 .
583 151 151 SER CB C  64.3593 0.325 .
584 151 151 SER N  N 115.4293 0.113 .
585 153 153 GLU H  H   7.7522 0.011 .
586 153 153 GLU C  C 176.893  0.325 .
587 153 153 GLU CA C  57.0218 0.325 .
588 153 153 GLU CB C  29.723  0.325 .
589 153 153 GLU N  N 122.0409 0.113 .
590 154 154 GLU H  H   8.4590 0.011 .
591 154 154 GLU C  C 176.621  0.325 .
592 154 154 GLU CA C  55.402  0.325 .
593 154 154 GLU CB C  30.434  0.325 .
594 154 154 GLU N  N 126.3730 0.113 .
595 155 155 LYS H  H   8.5713 0.011 .
596 155 155 LYS C  C 174.612  0.325 .
597 155 155 LYS CA C  56.377  0.325 .
598 155 155 LYS CB C  30.859  0.325 .
599 155 155 LYS N  N 121.6960 0.113 .
600 156 156 ASP H  H   8.1487 0.011 .
601 156 156 ASP C  C 176.874  0.325 .
602 156 156 ASP CA C  54.5624 0.325 .
603 156 156 ASP CB C  40.9564 0.325 .
604 156 156 ASP N  N 117.3912 0.113 .
605 157 157 SER H  H   8.4793 0.011 .
606 157 157 SER C  C 173.104  0.325 .
607 157 157 SER CA C  60.7015 0.325 .
608 157 157 SER CB C  64.7062 0.325 .
609 157 157 SER N  N 114.9318 0.113 .
610 158 158 ASP H  H   8.0861 0.011 .
611 158 158 ASP C  C 173.983  0.325 .
612 158 158 ASP CA C  52.4334 0.325 .
613 158 158 ASP CB C  39.9978 0.325 .
614 158 158 ASP N  N 127.5108 0.113 .
615 159 159 ILE H  H   7.4673 0.011 .
616 159 159 ILE C  C 177.315  0.325 .
617 159 159 ILE CA C  60.2700 0.325 .
618 159 159 ILE CB C  39.3496 0.325 .
619 159 159 ILE N  N 118.3522 0.113 .
```

```
620 160 160 LYS H  H   8.6230 0.011 .
621 160 160 LYS C  C 177.150  0.325 .
622 160 160 LYS CA C  52.7827 0.325 .
623 160 160 LYS CB C  30.8906 0.325 .
624 160 160 LYS N  N 124.9340 0.113 .
625 161 161 THR H  H   8.3647 0.011 .
626 161 161 THR C  C 174.860  0.325 .
627 161 161 THR CA C  61.2002 0.325 .
628 161 161 THR CB C  67.7821 0.325 .
629 161 161 THR N  N 112.0385 0.113 .
630 162 162 HIS H  H   7.0484 0.011 .
631 162 162 HIS CA C  52.4543 0.325 .
632 162 162 HIS CB C  28.3280 0.325 .
633 162 162 HIS N  N 118.1933 0.113 .
634 164 164 VAL H  H   8.6041 0.011 .
635 164 164 VAL C  C 176.468  0.325 .
636 164 164 VAL CA C  63.015  0.325 .
637 164 164 VAL CB C  30.7626 0.325 .
638 164 164 VAL N  N 122.9180 0.113 .
639 165 165 LEU H  H   8.5128 0.011 .
640 165 165 LEU C  C 177.597  0.325 .
641 165 165 LEU CA C  54.1456 0.325 .
642 165 165 LEU CB C  42.0489 0.325 .
643 165 165 LEU N  N 130.3650 0.113 .
644 166 166 GLY H  H   8.7542 0.011 .
645 166 166 GLY C  C 173.548  0.325 .
646 166 166 GLY CA C  43.9678 0.325 .
647 166 166 GLY N  N 109.5407 0.113 .
648 167 167 SER H  H   8.5683 0.011 .
649 167 167 SER C  C 174.525  0.325 .
650 167 167 SER CA C  58.526  0.325 .
651 167 167 SER CB C  64.971  0.325 .
652 167 167 SER N  N 114.7093 0.113 .
653 168 168 ASN H  H   8.223  0.011 .
654 168 168 ASN C  C 174.488  0.325 .
655 168 168 ASN CA C  54.727  0.325 .
656 168 168 ASN CB C  38.476  0.325 .
657 168 168 ASN N  N 115.224  0.113 .
658 169 169 ILE H  H   8.0655 0.011 .
659 169 169 ILE C  C 175.255  0.325 .
660 169 169 ILE CA C  60.8467 0.325 .
661 169 169 ILE CB C  37.9408 0.325 .
662 169 169 ILE N  N 120.1736 0.113 .
663 170 170 SER H  H   8.6783 0.011 .
664 170 170 SER CA C  55.6818 0.325 .
```

```
665 170 170 SER CB C  64.9600 0.325 .
666 170 170 SER N  N 120.5152 0.113 .
667 172 172 LYS H  H   6.8838 0.011 .
668 172 172 LYS C  C 173.560  0.325 .
669 172 172 LYS CA C  55.2128 0.325 .
670 172 172 LYS CB C  31.7113 0.325 .
671 172 172 LYS N  N 118.1298 0.113 .
672 173 173 LYS H  H   8.0378 0.011 .
673 173 173 LYS C  C 175.950  0.325 .
674 173 173 LYS CA C  58.3632 0.325 .
675 173 173 LYS CB C  31.606  0.325 .
676 173 173 LYS N  N 117.9487 0.113 .
677 174 174 VAL H  H   6.5762 0.011 .
678 174 174 VAL C  C 174.746  0.325 .
679 174 174 VAL CA C  59.5824 0.325 .
680 174 174 VAL CB C  32.3720 0.325 .
681 174 174 VAL N  N 118.5562 0.113 .
682 175 175 SER H  H   7.6114 0.011 .
683 175 175 SER C  C 172.058  0.325 .
684 175 175 SER CA C  59.852  0.325 .
685 175 175 SER CB C  63.4840 0.325 .
686 175 175 SER N  N 115.7821 0.113 .
687 176 176 TYR H  H   8.5054 0.011 .
688 176 176 TYR C  C 175.549  0.325 .
689 176 176 TYR CA C  58.939  0.325 .
690 176 176 TYR CB C  39.159  0.325 .
691 176 176 TYR N  N 124.6117 0.113 .
692 177 177 GLU H  H   7.2527 0.011 .
693 177 177 GLU C  C 175.500  0.325 .
694 177 177 GLU CA C  54.0020 0.325 .
695 177 177 GLU CB C  33.0809 0.325 .
696 177 177 GLU N  N 129.0926 0.113 .
697 178 178 ASP H  H   7.7876 0.011 .
698 178 178 ASP C  C 173.800  0.325 .
699 178 178 ASP CA C  53.3464 0.325 .
700 178 178 ASP CB C  40.0229 0.325 .
701 178 178 ASP N  N 121.9198 0.113 .
702 179 179 ILE H  H   8.7743 0.011 .
703 179 179 ILE C  C 177.296  0.325 .
704 179 179 ILE CA C  62.2035 0.325 .
705 179 179 ILE CB C  41.5030 0.325 .
706 179 179 ILE N  N 127.6588 0.113 .
707 180 180 ILE H  H   8.9641 0.011 .
708 180 180 ILE C  C 176.830  0.325 .
709 180 180 ILE CA C  62.256  0.325 .
```

```
710 180 180 ILE CB C  38.425  0.325 .
711 180 180 ILE N  N 121.0661 0.113 .
712 181 181 GLY H  H   9.2213 0.011 .
713 181 181 GLY C  C 173.781  0.325 .
714 181 181 GLY CA C  44.1100 0.325 .
715 181 181 GLY N  N 118.4363 0.113 .
716 182 182 SER H  H   8.875  0.011 .
717 182 182 SER C  C 174.462  0.325 .
718 182 182 SER CA C  58.608  0.325 .
719 182 182 SER CB C  61.150  0.325 .
720 182 182 SER N  N 121.824  0.113 .
721 183 183 THR H  H   7.4590 0.011 .
722 183 183 THR C  C 171.346  0.325 .
723 183 183 THR CA C  61.5830 0.325 .
724 183 183 THR CB C  71.2064 0.325 .
725 183 183 THR N  N 123.7048 0.113 .
726 184 184 ILE H  H   8.5701 0.011 .
727 184 184 ILE C  C 173.599  0.325 .
728 184 184 ILE CA C  58.4004 0.325 .
729 184 184 ILE CB C  40.4652 0.325 .
730 184 184 ILE N  N 127.4845 0.113 .
731 185 185 VAL H  H   8.4186 0.011 .
732 185 185 VAL C  C 174.275  0.325 .
733 185 185 VAL CA C  59.071  0.325 .
734 185 185 VAL CB C  35.810  0.325 .
735 185 185 VAL N  N 120.3748 0.113 .
736 186 186 ASP H  H   7.7798 0.011 .
737 186 186 ASP C  C 177.156  0.325 .
738 186 186 ASP CA C  53.443  0.325 .
739 186 186 ASP CB C  40.865  0.325 .
740 186 186 ASP N  N 122.2819 0.113 .
741 187 187 THR H  H   8.3368 0.011 .
742 187 187 THR C  C 175.178  0.325 .
743 187 187 THR CA C  63.516  0.325 .
744 187 187 THR CB C  68.711  0.325 .
745 187 187 THR N  N 118.8856 0.113 .
746 188 188 LYS H  H   8.7502 0.011 .
747 188 188 LYS C  C 177.667  0.325 .
748 188 188 LYS CA C  58.5547 0.325 .
749 188 188 LYS CB C  31.1372 0.325 .
750 188 188 LYS N  N 122.0989 0.113 .
751 189 189 CYS H  H   7.095  0.011 .
752 189 189 CYS C  C 174.202  0.325 .
753 189 189 CYS CA C  55.987  0.325 .
754 189 189 CYS N  N 106.980  0.113 .
```

```
755 190 190 VAL H  H   8.058  0.011 .
756 190 190 VAL C  C 173.137  0.325 .
757 190 190 VAL N  N 123.665  0.113 .
758 191 191 LYS H  H   9.0419 0.011 .
759 191 191 LYS C  C 174.184  0.325 .
760 191 191 LYS CA C  57.775  0.325 .
761 191 191 LYS CB C  33.9130 0.325 .
762 191 191 LYS N  N 128.7566 0.113 .
763 192 192 ASN H  H   7.7655 0.011 .
764 192 192 ASN C  C 173.706  0.325 .
765 192 192 ASN CA C  50.7272 0.325 .
766 192 192 ASN CB C  42.6636 0.325 .
767 192 192 ASN N  N 109.4968 0.113 .
768 193 193 LEU H  H   9.6271 0.011 .
769 193 193 LEU C  C 173.997  0.325 .
770 193 193 LEU CA C  55.0419 0.325 .
771 193 193 LEU CB C  45.9579 0.325 .
772 193 193 LEU N  N 121.2978 0.113 .
773 194 194 GLU H  H   9.086  0.011 .
774 194 194 GLU C  C 173.681  0.325 .
775 194 194 GLU CA C  55.640  0.325 .
776 194 194 GLU CB C  34.819  0.325 .
777 194 194 GLU N  N 124.020  0.113 .
778 195 195 PHE H  H   9.530  0.011 .
779 195 195 PHE C  C 171.826  0.325 .
780 195 195 PHE CA C  55.810  0.325 .
781 195 195 PHE CB C  43.0223 0.325 .
782 195 195 PHE N  N 122.1845 0.113 .
783 196 196 SER H  H   8.844  0.011 .
784 196 196 SER C  C 174.425  0.325 .
785 196 196 SER CA C  56.925  0.325 .
786 196 196 SER CB C  62.016  0.325 .
787 196 196 SER N  N 122.129  0.113 .
788 197 197 VAL H  H   8.7975 0.011 .
789 197 197 VAL C  C 172.543  0.325 .
790 197 197 VAL CA C  59.4183 0.325 .
791 197 197 VAL CB C  33.8688 0.325 .
792 197 197 VAL N  N 125.4334 0.113 .
793 198 198 ARG H  H   8.929  0.011 .
794 198 198 ARG C  C 174.951  0.325 .
795 198 198 ARG CA C  52.505  0.325 .
796 198 198 ARG CB C  34.746  0.325 .
797 198 198 ARG N  N 125.221  0.113 .
798 199 199 ILE H  H   7.7609 0.011 .
799 199 199 ILE C  C 174.266  0.325 .
```

```
800 199 199 ILE CA C  59.8615 0.325 .
801 199 199 ILE CB C  39.5784 0.325 .
802 199 199 ILE N  N 119.0198 0.113 .
803 200 200 GLY H  H   8.2923 0.011 .
804 200 200 GLY C  C 170.851  0.325 .
805 200 200 GLY CA C  45.6485 0.325 .
806 200 200 GLY N  N 111.2167 0.113 .
807 201 201 ASP H  H   9.5116 0.011 .
808 201 201 ASP C  C 177.708  0.325 .
809 201 201 ASP CA C  53.8410 0.325 .
810 201 201 ASP CB C  42.730  0.325 .
811 201 201 ASP N  N 122.1845 0.113 .
812 202 202 MET H  H   8.7272 0.011 .
813 202 202 MET C  C 176.370  0.325 .
814 202 202 MET CA C  58.313  0.325 .
815 202 202 MET CB C  34.686  0.325 .
816 202 202 MET N  N 123.5533 0.113 .
817 203 203 CYS H  H   9.3591 0.011 .
818 203 203 CYS C  C 174.454  0.325 .
819 203 203 CYS CA C  57.2268 0.325 .
820 203 203 CYS CB C  43.5100 0.325 .
821 203 203 CYS N  N 116.4927 0.113 .
822 204 204 LYS H  H   7.8699 0.011 .
823 204 204 LYS C  C 173.837  0.325 .
824 204 204 LYS CA C  55.613  0.325 .
825 204 204 LYS CB C  33.115  0.325 .
826 204 204 LYS N  N 121.7202 0.113 .
827 205 205 GLU H  H   8.300  0.011 .
828 205 205 GLU C  C 177.296  0.325 .
829 205 205 GLU CA C  57.273  0.325 .
830 205 205 GLU CB C  29.410  0.325 .
831 205 205 GLU N  N 123.810  0.113 .
832 206 206 SER H  H   8.964  0.011 .
833 206 206 SER CA C  57.102  0.325 .
834 206 206 SER CB C  64.277  0.325 .
835 206 206 SER N  N 121.066  0.113 .
836 208 208 GLU H  H   8.9739 0.011 .
837 208 208 GLU C  C 175.831  0.325 .
838 208 208 GLU CA C  57.7422 0.325 .
839 208 208 GLU CB C  29.1114 0.325 .
840 208 208 GLU N  N 120.1478 0.113 .
841 209 209 LEU H  H   7.996  0.011 .
842 209 209 LEU C  C 173.421  0.325 .
843 209 209 LEU CA C  53.313  0.325 .
844 209 209 LEU CB C  41.808  0.325 .
```

```
845 209 209 LEU N  N 117.5771 0.113 .
846 210 210 GLU H  H   6.7626 0.011 .
847 210 210 GLU C  C 176.979  0.325 .
848 210 210 GLU CA C  53.798  0.325 .
849 210 210 GLU CB C  28.6984 0.325 .
850 210 210 GLU N  N 112.2086 0.113 .
851 211 211 VAL H  H   8.4606 0.011 .
852 211 211 VAL C  C 177.470  0.325 .
853 211 211 VAL CA C  58.717  0.325 .
854 211 211 VAL CB C  36.754  0.325 .
855 211 211 VAL N  N 113.5448 0.113 .
856 212 212 LYS H  H   8.680  0.011 .
857 212 212 LYS C  C 173.260  0.325 .
858 212 212 LYS CA C  54.711  0.325 .
859 212 212 LYS CB C  37.521  0.325 .
860 212 212 LYS N  N 124.149  0.113 .
861 213 213 ASP H  H   9.1119 0.011 .
862 213 213 ASP C  C 175.615  0.325 .
863 213 213 ASP CA C  51.6875 0.325 .
864 213 213 ASP CB C  45.292  0.325 .
865 213 213 ASP N  N 124.6814 0.113 .
866 214 214 GLY H  H   9.9779 0.011 .
867 214 214 GLY C  C 170.596  0.325 .
868 214 214 GLY CA C  46.0989 0.325 .
869 214 214 GLY N  N 111.7888 0.113 .
870 215 215 PHE H  H   8.5322 0.011 .
871 215 215 PHE C  C 173.028  0.325 .
872 215 215 PHE CA C  56.5000 0.325 .
873 215 215 PHE CB C  43.4268 0.325 .
874 215 215 PHE N  N 120.0228 0.113 .
875 216 216 LYS H  H   8.2224 0.011 .
876 216 216 LYS C  C 173.162  0.325 .
877 216 216 LYS CA C  55.0558 0.325 .
878 216 216 LYS CB C  35.4611 0.325 .
879 216 216 LYS N  N 125.0919 0.113 .
880 217 217 TYR H  H   9.2222 0.011 .
881 217 217 TYR C  C 173.268  0.325 .
882 217 217 TYR CA C  54.893  0.325 .
883 217 217 TYR CB C  38.938  0.325 .
884 217 217 TYR N  N 125.9488 0.113 .
885 218 218 VAL H  H   7.9551 0.011 .
886 218 218 VAL C  C 175.880  0.325 .
887 218 218 VAL CA C  60.0015 0.325 .
888 218 218 VAL CB C  34.6994 0.325 .
889 218 218 VAL N  N 123.2761 0.113 .
```

```
890 219 219 ASP H  H   8.2832 0.011 .
891 219 219 ASP C  C 176.144  0.325 .
892 219 219 ASP CA C  55.1475 0.325 .
893 219 219 ASP CB C  38.9957 0.325 .
894 219 219 ASP N  N 125.9951 0.113 .
895 220 220 GLY H  H   8.4819 0.011 .
896 220 220 GLY C  C 174.098  0.325 .
897 220 220 GLY CA C  45.176  0.325 .
898 220 220 GLY N  N 103.550  0.113 .
899 221 221 SER H  H   7.5454 0.011 .
900 221 221 SER C  C 172.504  0.325 .
901 221 221 SER CA C  57.0865 0.325 .
902 221 221 SER CB C  64.5500 0.325 .
903 221 221 SER N  N 116.0842 0.113 .
904 222 222 ALA H  H   8.8741 0.011 .
905 222 222 ALA C  C 176.998  0.325 .
906 222 222 ALA CA C  49.8674 0.325 .
907 222 222 ALA CB C  22.0453 0.325 .
908 222 222 ALA N  N 128.8788 0.113 .
909 223 223 SER H  H   8.5380 0.011 .
910 223 223 SER C  C 173.146  0.325 .
911 223 223 SER CA C  57.8788 0.325 .
912 223 223 SER CB C  65.511  0.325 .
913 223 223 SER N  N 114.5000 0.113 .
914 224 224 LYS H  H   8.5443 0.011 .
915 224 224 LYS C  C 177.115  0.325 .
916 224 224 LYS CA C  55.557  0.325 .
917 224 224 LYS CB C  34.789  0.325 .
918 224 224 LYS N  N 121.5518 0.113 .
919 225 225 GLY H  H   7.9533 0.011 .
920 225 225 GLY C  C 171.987  0.325 .
921 225 225 GLY CA C  45.1924 0.325 .
922 225 225 GLY N  N 105.9825 0.113 .
923 226 226 ALA H  H   8.581  0.011 .
924 226 226 ALA C  C 175.484  0.325 .
925 226 226 ALA CA C  50.919  0.325 .
926 226 226 ALA CB C  18.503  0.325 .
927 226 226 ALA N  N 124.853  0.113 .
928 227 227 THR H  H   8.4196 0.011 .
929 227 227 THR C  C 172.865  0.325 .
930 227 227 THR CA C  59.3781 0.325 .
931 227 227 THR CB C  70.7408 0.325 .
932 227 227 THR N  N 115.2927 0.113 .
933 228 228 ASP H  H   8.483  0.011 .
934 228 228 ASP C  C 175.948  0.325 .
```

```
935 228 228 ASP CA C  53.900  0.325 .
936 228 228 ASP CB C  41.032  0.325 .
937 228 228 ASP N  N 119.323  0.113 .
938 229 229 ASP H  H   8.4430 0.011 .
939 229 229 ASP C  C 176.776  0.325 .
940 229 229 ASP CA C  54.030  0.325 .
941 229 229 ASP CB C  42.7808 0.325 .
942 229 229 ASP N  N 126.9781 0.113 .
943 230 230 THR H  H   8.4188 0.011 .
944 230 230 THR C  C 174.341  0.325 .
945 230 230 THR CA C  65.798  0.325 .
946 230 230 THR CB C  69.0420 0.325 .
947 230 230 THR N  N 114.0551 0.113 .
948 232 232 LEU H  H   7.1539 0.011 .
949 232 232 LEU C  C 177.125  0.325 .
950 232 232 LEU CA C  58.2431 0.325 .
951 232 232 LEU CB C  41.9319 0.325 .
952 232 232 LEU N  N 123.5194 0.113 .
953 233 233 ILE H  H   7.6644 0.011 .
954 233 233 ILE C  C 174.423  0.325 .
955 233 233 ILE CA C  58.025  0.325 .
956 233 233 ILE CB C  41.477  0.325 .
957 233 233 ILE N  N 106.2956 0.113 .
958 234 234 ASP H  H   8.2373 0.011 .
959 234 234 ASP CA C  51.683  0.325 .
960 234 234 ASP CB C  39.3227 0.325 .
961 234 234 ASP N  N 120.0399 0.113 .
962 236 236 THR H  H   8.3517 0.011 .
963 236 236 THR C  C 176.066  0.325 .
964 236 236 THR CA C  63.9668 0.325 .
965 236 236 THR CB C  68.4410 0.325 .
966 236 236 THR N  N 112.7161 0.113 .
967 237 237 LYS H  H   6.9082 0.011 .
968 237 237 LYS C  C 176.572  0.325 .
969 237 237 LYS CA C  55.074  0.325 .
970 237 237 LYS CB C  32.4250 0.325 .
971 237 237 LYS N  N 117.7439 0.113 .
972 238 238 LEU H  H   6.7691 0.011 .
973 238 238 LEU C  C 176.357  0.325 .
974 238 238 LEU CA C  55.503  0.325 .
975 238 238 LEU CB C  41.7043 0.325 .
976 238 238 LEU N  N 116.9173 0.113 .
977 239 239 LYS H  H   8.6275 0.011 .
978 239 239 LYS C  C 175.138  0.325 .
979 239 239 LYS CA C  53.4406 0.325 .
```

```
980 239 239 LYS CB C  33.9051 0.325 .
981 239 239 LYS N  N 119.9793 0.113 .
982 240 240 ALA H  H   8.6598 0.011 .
983 240 240 ALA C  C 176.721  0.325 .
984 240 240 ALA CA C  52.985  0.325 .
985 240 240 ALA CB C  18.4467 0.325 .
986 240 240 ALA N  N 123.4698 0.113 .
987 241 241 CYS H  H   9.166  0.011 .
988 241 241 CYS C  C 175.244  0.325 .
989 241 241 CYS CA C  52.436  0.325 .
990 241 241 CYS CB C  35.559  0.325 .
991 241 241 CYS N  N 116.972  0.113 .
992 242 242 VAL H  H   7.6320 0.011 .
993 242 242 VAL CA C  62.316  0.325 .
994 242 242 VAL CB C  34.190  0.325 .
995 242 242 VAL N  N 118.7385 0.113 .
STOP
```

VITA

Name: Li Zhang

Address: Department of Biochemistry and Biophysics
c/o Dr. Patricia LiWang
Texas A&M University
2128 TAMU
College Station, TX 77843

Email Address: zlnev@hotmail.com

Education: B.S., Biochemistry, Sichuan University, 2000
Ph.D., Biochemistry, Texas A&M University, 2008

Peer reviewed pulications:

Zhang, L., Derider, M., McCornack, M. A., Jao, S.C., Isern, N., Ness, T., Moyer, R., LiWang, P. J. (2006) Solution structure of the complex between poxvirus-encoded CC chemokine inhibitor vCCI and human MIP-1beta. *Proc. Natl. Acad. Sci. U.S.A.* 1*03(38)*:13985-90.

Zhang, L., LiWang, P. J. (2006) Resonance assignments of the 34 kD rabbitpox vCCI:human MIP-1beta complex. *J. Biomol. NMR, 36*

Derider, M. L., Zhang, L., LiWang, P. J. (2006) Resonance assignments and secondary structure of vCCI, a 26 kDa CC chemokine inhibitor from rabbitpox virus. *J. Biomol. NMR, 36*